# GW astrophysics with LIGO/VIRGO data

**March 2021**

**Matias Zaldarriaga**

# GW @ IAS



**Barak Zackay**

**Tejaswi Venumadhav**

**Javier Roulet**

**Liang Dai**

**Horng-Sheng Chia**
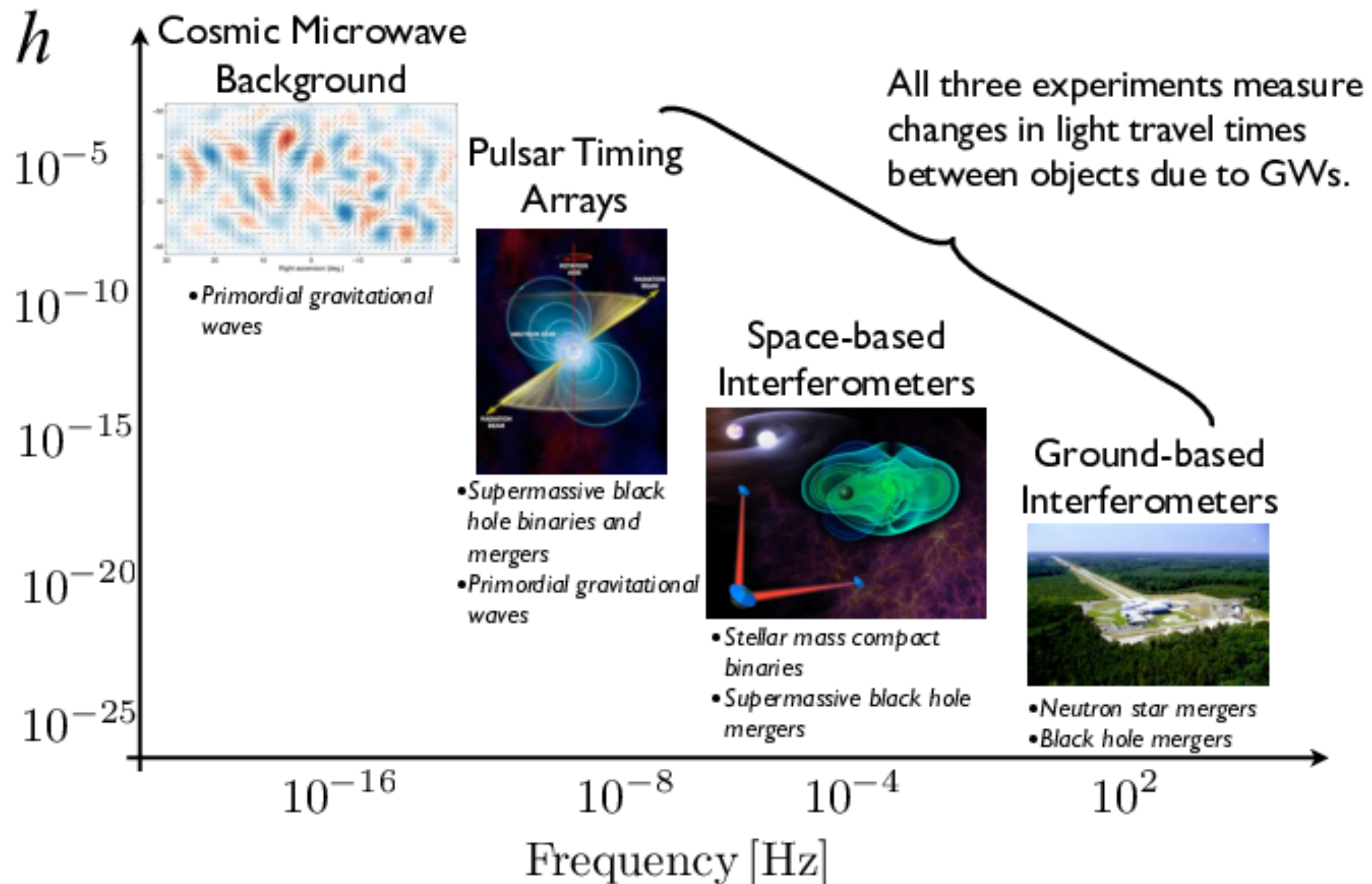
**Seth Olsen**

**Matias Zaldarriaga**

# Outline

- Introduction

- Status of observations and outstanding questions

- The IAS O2 search

The spectrum of gravitational wave astronomy

# Binary system



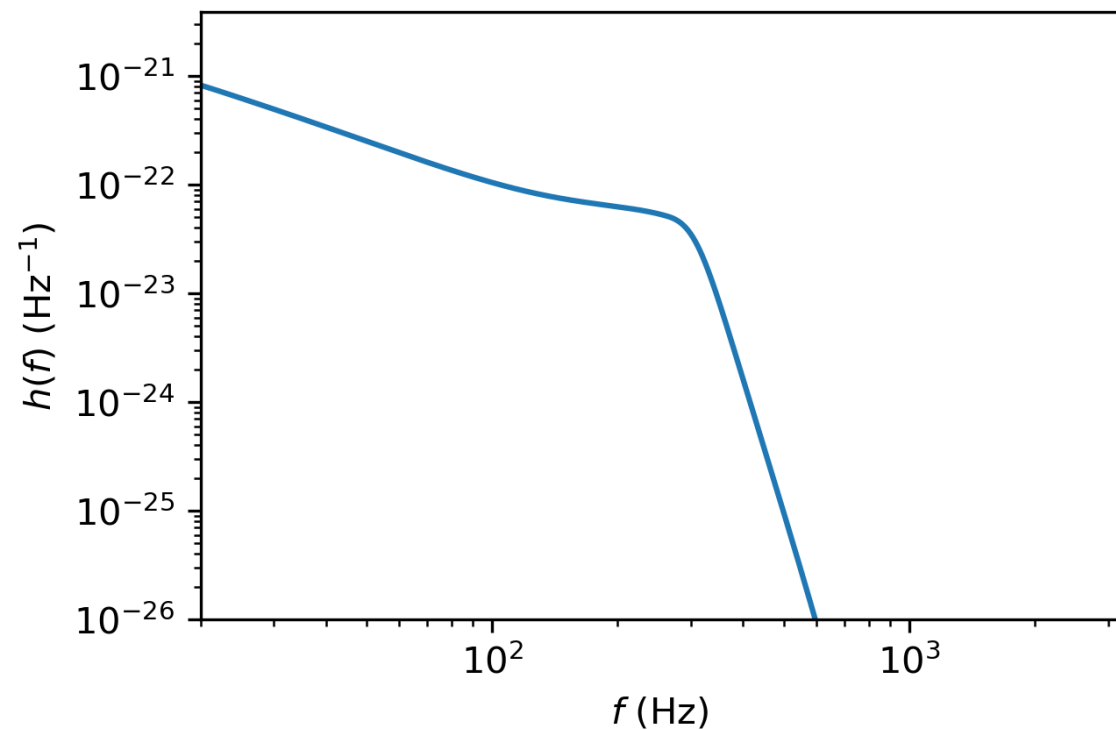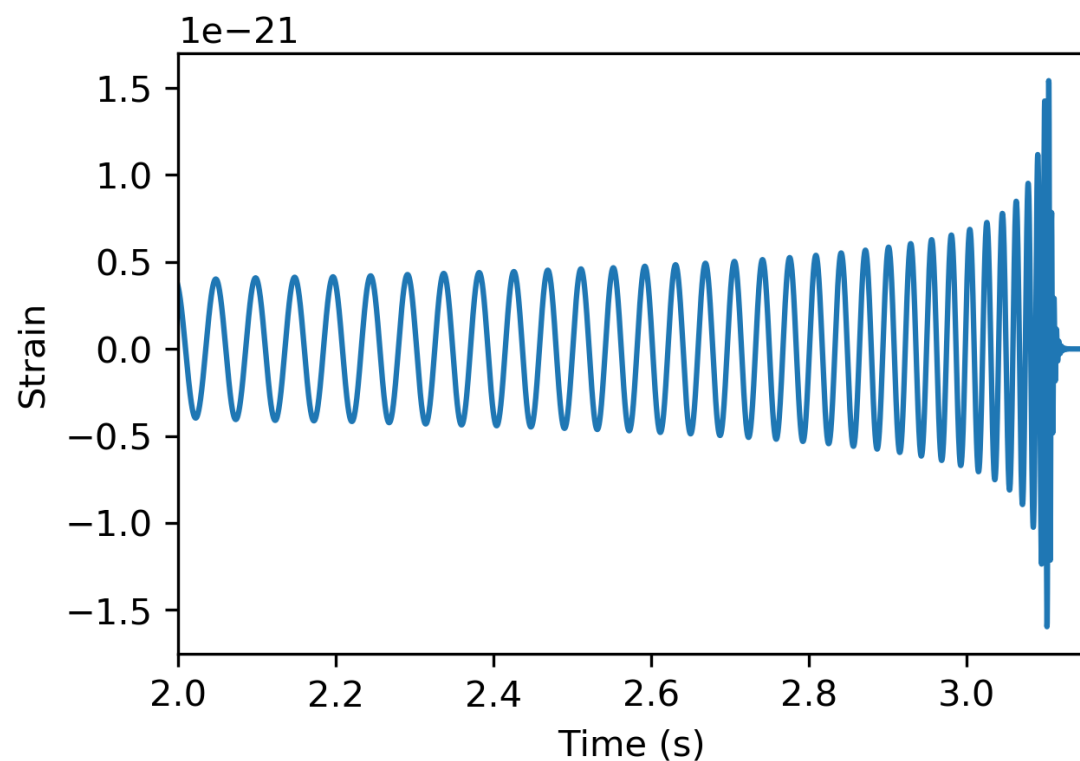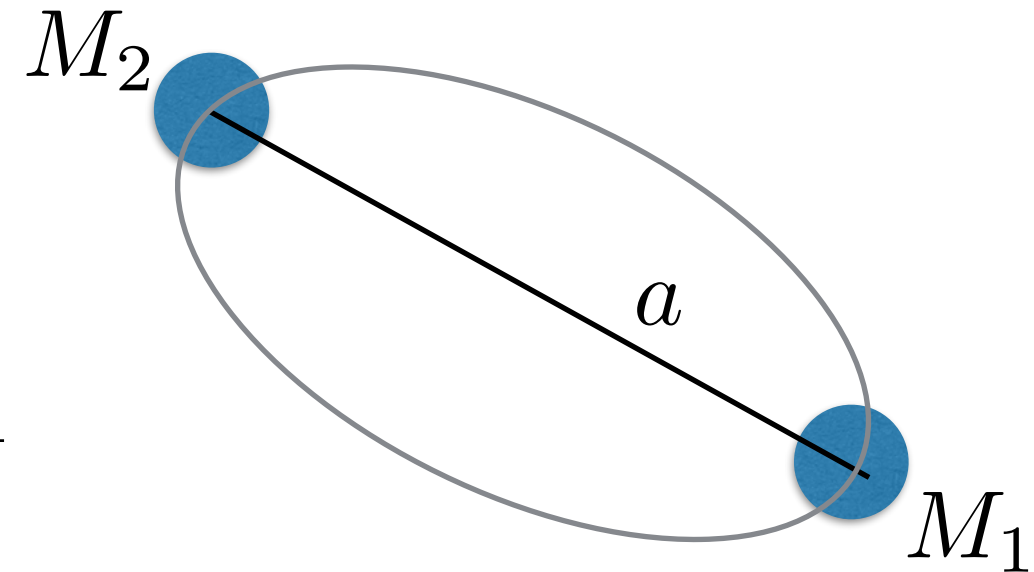$$M = m_1 + m_2 \qquad \eta = \frac{m_1 m_2}{(m_1 + m_2)^2} \qquad q = \frac{m_1}{m_2}$$

$$M_c = M\eta^{3/5} \qquad \omega_{\mathrm{GW}}(t) \sim M_c^{-5/8}\left(t_0 - t\right)^{-3/8} \quad \text{"Chirping}$$

$$h(\omega_0) \propto M_c^{5/6} D^{-1} \omega_0^{-7/6} e^{i\phi(\omega_0)}$$

$$\phi(\omega_0) \propto (M_c\omega_0)^{-5/3} \qquad \omega_{\mathrm{max}} \sim 100\,\mathrm{Hz}\left(\frac{50\,M_\odot}{M}\right)$$
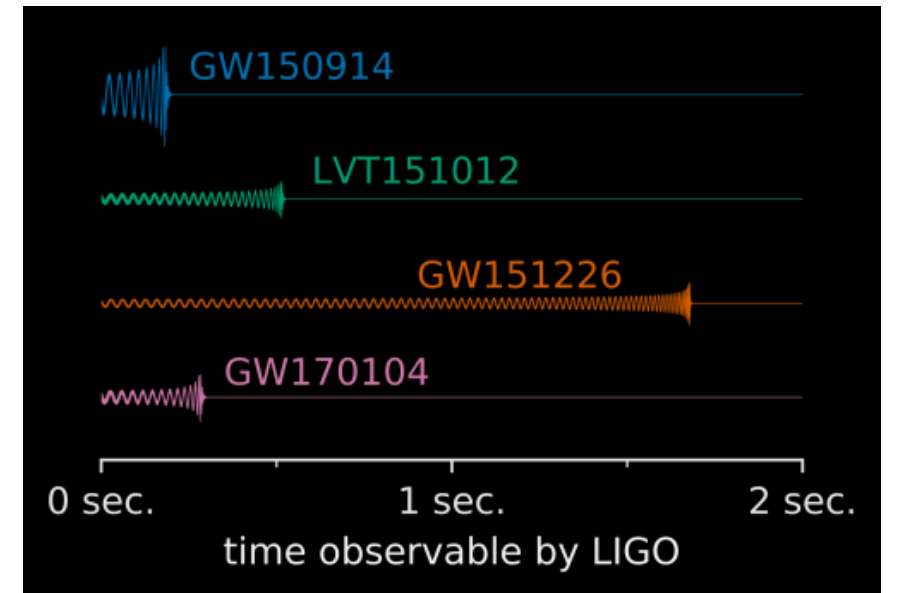
# Post Newtonian wave-forms



$$x = f/f_0$$

$$\eta = \frac{m_1 m_2}{(m_1 + m_2)^2}$$

$$\tilde{h}(f) = A(f; \theta_x) e^{i\Psi(f; \lambda_i)}$$

$$\Psi = 2\pi f_0 x t_c - \phi_c + \lambda_0 x^{-5/3} + \lambda_2 x^{-1} + \lambda_3 x^{-2/3} + \lambda_4 x^{-1/3} + \lambda_{5L} \log(x) + \lambda_6 x^{1/3} + \lambda_{6L} \log(x) x^{1/3} + \lambda_7 x^{2/3},$$

$$\lambda_0 = \frac{3}{128} (\pi \mathcal{M} f_0)^{-5/3},$$

$$\lambda_2 = \frac{5}{96\eta^{2/5}} \left( \frac{743}{336} + \frac{11}{4}\eta \right) (\pi \mathcal{M} f_0)^{-1},$$

$$\lambda_3 = -\frac{3\pi}{8\eta^{3/5}} \left( 1 - \frac{1}{4\pi}\beta \right) (\pi \mathcal{M} f_0)^{-2/3},$$

$$\lambda_4 = \frac{15}{64\eta^{4/5}} \left( \frac{3058673}{1016064} + \frac{5429}{1008}\eta + \frac{617}{144}\eta^2 - \sigma \right) (\pi \mathcal{M} f_0)^{-1/3}$$

$$\beta = \frac{1}{12} \sum_{i=1}^{2} \left[ 113 \left( \frac{m_i}{m_1 + m_2} \right)^2 + 75\eta \right] \hat{\boldsymbol{L}} \cdot \boldsymbol{\chi}_i$$

$$\sigma = \frac{\eta}{48} \left( -247 \boldsymbol{\chi}_1 \cdot \boldsymbol{\chi}_2 + 721 \hat{\boldsymbol{L}} \cdot \boldsymbol{\chi}_1 \hat{\boldsymbol{L}} \cdot \boldsymbol{\chi}_2 \right).$$
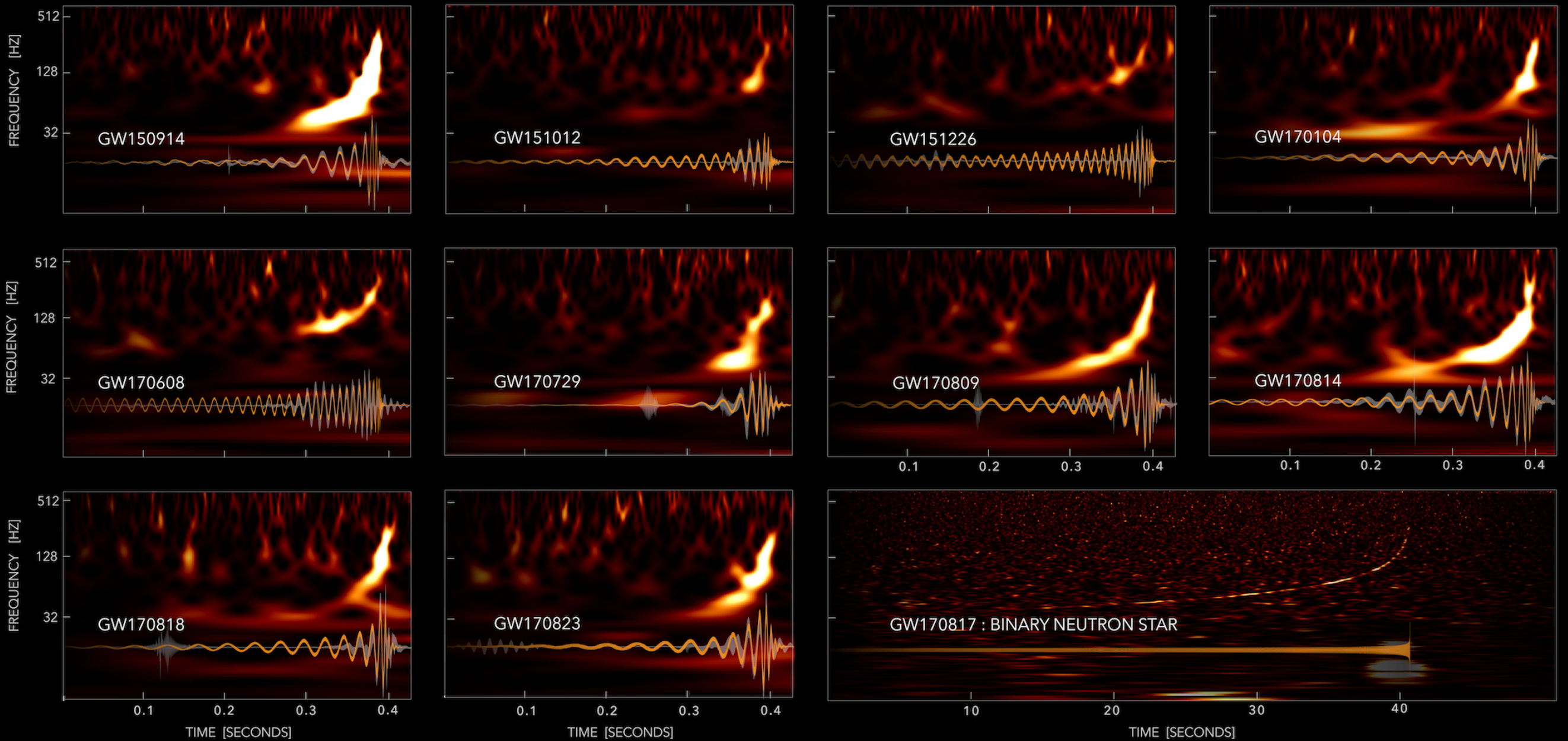
Dependence approximated by two parameter model:

$$\chi_{\text{eff}} = \frac{m_1 \chi_{1,z} + m_2 \chi_{2,z}}{m_1 + m_2} = \frac{q \chi_{1,z} + \chi_{2,z}}{q + 1},$$

$$\chi_{\text{p}} = \frac{1}{A_1 m_1^2} \max\left( A_1 S_{1,\perp}, A_2 S_{2,\perp} \right) = \max\left( \chi_{1,\perp}, \frac{A_2}{A_1 q^2} \chi_{2,\perp} \right)$$

**So far only the chirp mass, mass ratio and spin-orbit phase have been detected in an event.**

In addition there can be precession in the orbit.

# Gravitational-Wave Transient Catalog-1

LIGO · VIRGO · NSF · Georgia Tech

GW150914 · GW151012 · GW151226 · GW170104

GW170608 · GW170729 · GW170809 · GW170814

GW170818 · GW170823 · GW170817 : BINARY NEUTRON STAR

FREQUENCY [HZ]: 512, 128, 32

TIME [SECONDS]

WAVELET (UNMODELED) · EINSTEIN'S THEORY

S. GHONGE, K. JANI | GEORGIA TECH
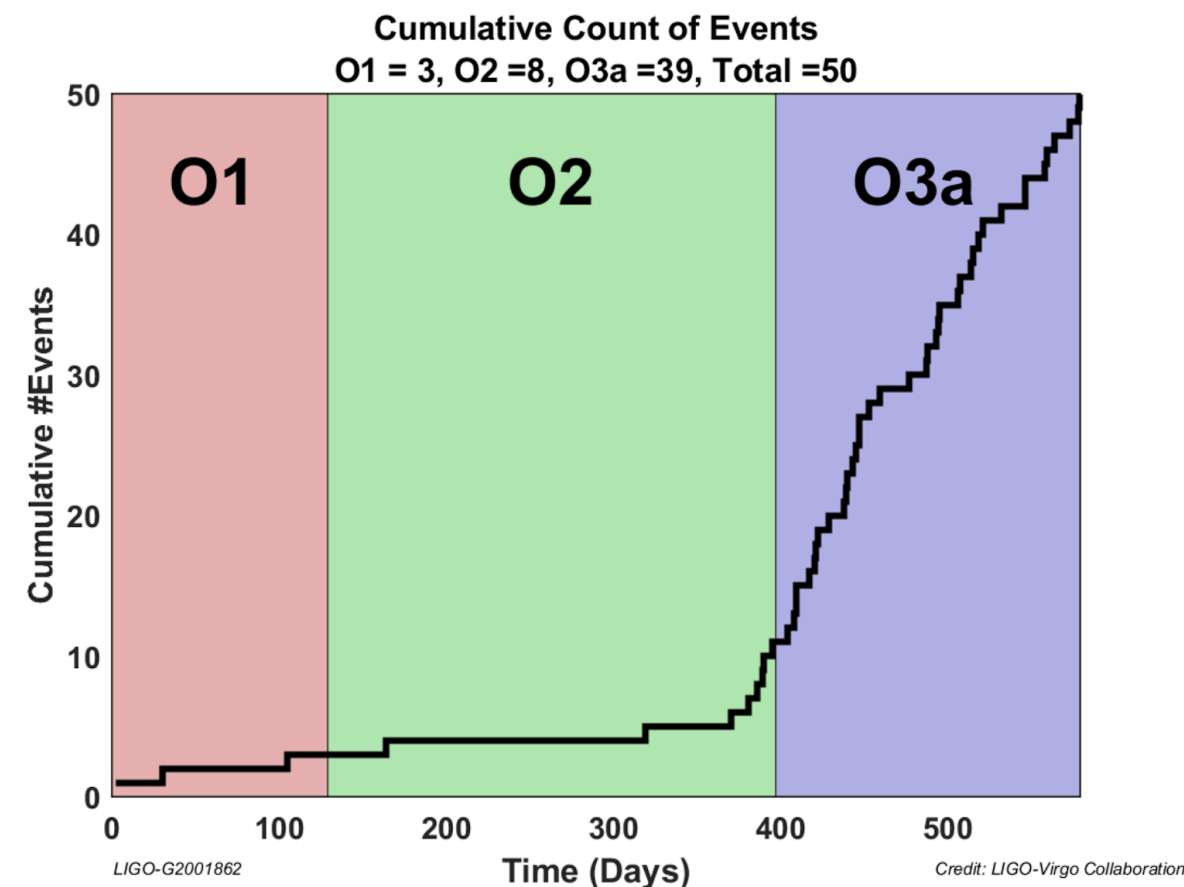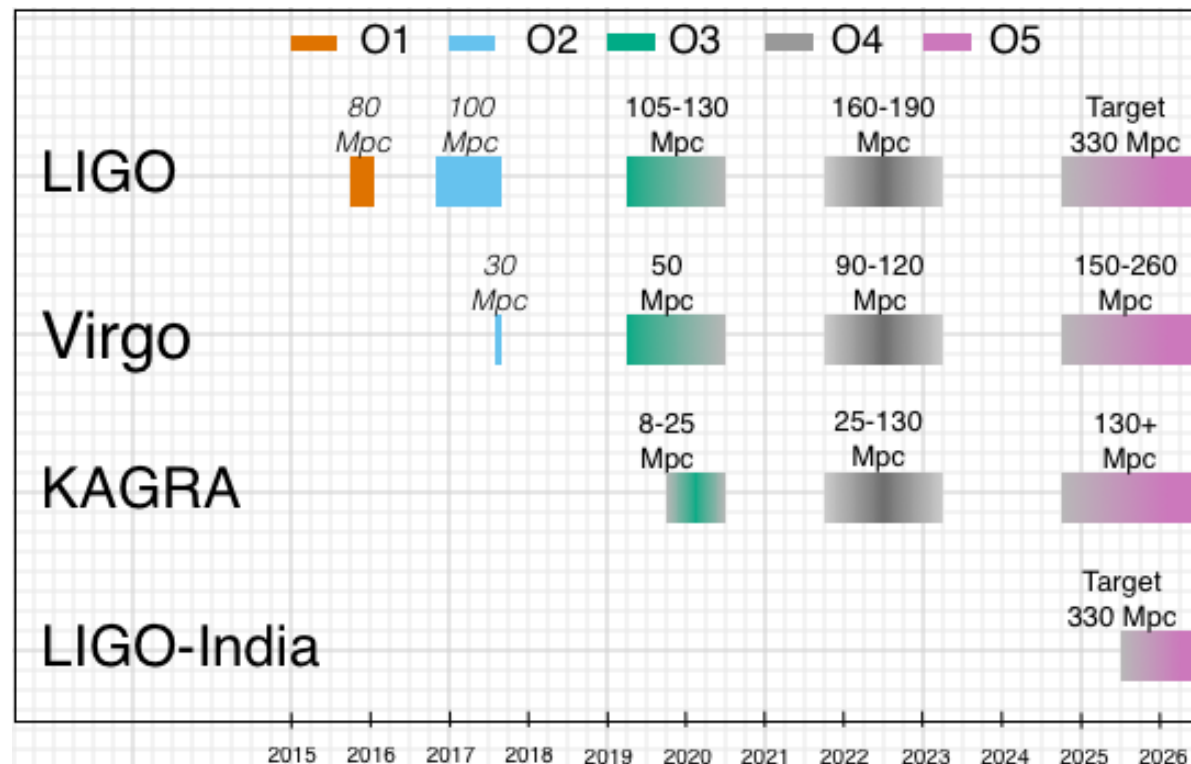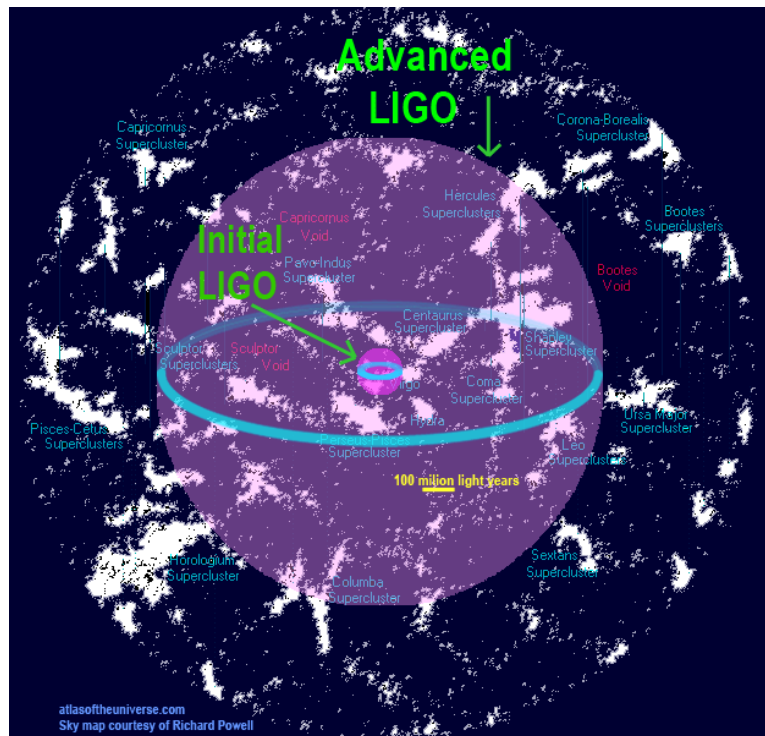
# What can we learn

- Properties of Black Holes and Neutron Stars.

- Test the laws of gravity in a regime we have never done so before.

- Processes that result in Black Hole and Black Hole binary systems.

# Status of Observations

# LIGO Observing Runs



In the volume from where binary black holes are visible by LIGO in O3 there are roughly 10 million Milky Way size galaxies.

In these volume there were forty black hole mergers in six months.





Cumulative Count of Events
O1 = 3, O2 =8, O3a =39, Total =50

LIGO-G2001862

Credit: LIGO-Virgo Collaboration

# Highlight O1

## Die Feldgleichungen der Gravitation.

### Von A. Einstein.

In zwei vor kurzem erschienenen Mitteilungen[1] habe ich gezeigt, wie man zu Feldgleichungen der Gravitation gelangen kann, die dem Postulat allgemeiner Relativität entsprechen, d. h. die in ihrer allgemeinen Fassung beliebigen Substitutionen der Raumzeitvariabeln gegenüber kovariant sind.

Der Entwicklungsgang war dabei folgender. Zunächst fand ich Gleichungen, welche die Newtonsche Theorie als Näherung enthalten und beliebigen Substitutionen von der Determinante 1 gegenüber kovariant waren. Hierauf fand ich, daß diesen Gleichungen allgemein kovariante entsprechen, falls der Skalar des Energietensors der »Materie« verschwindet. Das Koordinatensystem war dann nach der einfachen Regel zu spezialisieren, daß $\sqrt{-g}$ zu 1 gemacht wird, wodurch die Gleichungen der Theorie eine eminente Vereinfachung erfahren. Dabei mußte aber, wie erwähnt, die Hypothese eingeführt werden, daß der Skalar des Energietensors der Materie verschwinde.

Neuerdings finde ich nun, daß man ohne Hypothese über den Energietensor der Materie auskommen kann, wenn man den Energietensor der Materie in etwas anderer Weise in die Feldgleichungen einsetzt, als dies in meinen beiden früheren Mitteilungen geschehen ist. Die Feldgleichungen für das Vakuum, auf welche ich die Erklärung der Perihelbewegung des Merkur gegründet habe, bleiben von dieser Modifikation unberührt. Ich gebe hier nochmals die ganze Betrachtung, damit der Leser nicht genötigt ist, die früheren Mitteilungen unausgesetzt heranzuziehen.

Aus der bekannten Riemannschen Kovariante vierten Ranges leitet man folgende Kovariante zweiten Ranges ab:

$$G_{im} = R_{im} + S_{im} \tag{1}$$

$$R_{im} = -\sum_l \frac{\partial \begin{Bmatrix} im \\ l \end{Bmatrix}}{\partial x_l} + \sum_{l\varrho} \begin{Bmatrix} il \\ \varrho \end{Bmatrix}\begin{Bmatrix} m\varrho \\ l \end{Bmatrix} \tag{1a}$$

$$S_{im} = \sum_l \frac{\partial \begin{Bmatrix} il \\ l \end{Bmatrix}}{\partial x_m} - \sum_{l\varrho} \begin{Bmatrix} im \\ \varrho \end{Bmatrix}\begin{Bmatrix} \varrho l \\ l \end{Bmatrix} \tag{1b}$$

[1] Sitzungsber. XLIV. S. 778 und XLVI. S. 799. 1915.

---

**President Obama** ✓ @POTUS — Follow

Einstein was right! Congrats to @NSF and @LIGO on detecting gravitational waves - a huge breakthrough in how we understand the universe.

6:43 PM - 11 Feb 2016

↩ ⟲ 9,499 ♥ 21,112

---

**LIGO** @LIGO — Follow

#GravitationalWaves detected from #BinaryBlackHole 100y after Einstein's prediction. #EinsteinWasRight

Highlight O2

# Multi-messenger Observations of a Binary Neutron Star Merger

LIGO Scientific Collaboration and Virgo Collaboration, Fermi GBM, INTEGRAL, IceCube Collaboration, AstroSat Cadmium Zinc Telluride Imager Team, IPN Collaboration, The Insight-Hxmt Collaboration, ANTARES Collaboration, The Swift Collaboration, AGILE Team, The 1M2H Team, The Dark Energy Camera GW-EM Collaboration and the DES Collaboration, The DLT40 Collaboration, GRAWITA: GRAvitational Wave Inaf TeAm, The Fermi Large Area Telescope Collaboration, ATCA: Australia Telescope Compact Array, ASKAP: Australian SKA Pathfinder, Las Cumbres Observatory Group, OzGrav, DWF (Deeper, Wider, Faster Program), AST3, and CAASTRO Collaborations, The VINROUGE Collaboration, MASTER Collaboration, J-GEM, GROWTH, JAGWAR, Caltech-NRAO, TTU-NRAO, and NuSTAR Collaborations, Pan-STARRS, The MAXI Team, TZAC Consortium, KU Collaboration, Nordic Optical Telescope, ePESSTO, GROND, Texas Tech University, SALT Group, TOROS: Transient Robotic Observatory of the South Collaboration, The BOOTES Collaboration, MWA: Murchison Widefield Array, The CALET Collaboration, IKI-GW Follow-up Collaboration, H.E.S.S. Collaboration, LOFAR Collaboration, LWA: Long Wavelength Array, HAWC Collaboration, The Pierre Auger Collaboration, ALMA Collaboration, Euro VLBI Team, Pi of the Sky Collaboration, The Chandra Team at McGill University, DFN: Desert Fireball Network, ATLAS, High Time Resolution Universe Survey, RIMAS and RATIR, and SKA South Africa/MeerKAT
(See the end matter for the full list of authors.)

## Abstract

On 2017 August 17 a binary neutron star coalescence candidate (later designated GW170817) with merger time 12:41:04 UTC was observed through gravitational waves by the Advanced LIGO and Advanced Virgo detectors. The *Fermi* Gamma-ray Burst Monitor independently detected a gamma-ray burst (GRB 170817A) with a time delay of $\sim 1.7$ s with respect to the merger time. From the gravitational-wave signal, the source was initially localized to a sky region of 31 deg$^2$ at a luminosity distance of $40^{+8}_{-8}$ Mpc and with component masses consistent with neutron stars. The component masses were later measured to be in the range 0.86 to 2.26 $M_\odot$. An extensive observing campaign was launched across the electromagnetic spectrum leading to the discovery of a bright optical transient (SSS17a, now with the IAU identification of AT 2017gfo) in NGC 4993 (at $\sim$40 Mpc) less than 11 hours after the merger by the One-Meter, Two Hemisphere (1M2H) team using the 1 m Swope Telescope. The optical transient was independently detected by multiple teams within an hour. Subsequent observations targeted the object and its environment. Early ultraviolet observations revealed a blue transient that faded within 48 hours. Optical and infrared observations showed a redward evolution over $\sim$10 days. Following early non-detections, X-ray and radio emission were discovered at the transient's position $\sim$9 and $\sim$16 days, respectively, after the merger. Both the X-ray and radio emission likely arise from a physical process that is distinct from the one that generates the UV/optical/near-infrared emission. No ultra-high-energy gamma-rays and no neutrino candidates consistent with the source were found in follow-up searches. These observations support the hypothesis that GW170817 was produced by the merger of two neutron stars in NGC 4993 followed by a short gamma-ray burst (GRB 170817A) and a kilonova/macronova powered by the radioactive decay of $r$-process nuclei synthesized in the ejecta.

*Key words:* gravitational waves – stars: neutron



**Figure 1.** Localization of the gravitational-wave, gamma-ray, and optical signals. The left panel shows an orthographic projection of the 90% credible regions from LIGO (190 deg$^2$; light green), the initial LIGO-Virgo localization (31 deg$^2$; dark green), IPN triangulation from the time delay between *Fermi* and *INTEGRAL* (light blue), and *Fermi*-GBM (dark blue). The inset shows the location of the apparent host galaxy NGC 4993 in the Swope optical discovery image at 10.9 hr after the merger (top right) and the DLT40 pre-discovery image from 20.5 days prior to merger (bottom right). The reticle marks the position of the transient in both images.
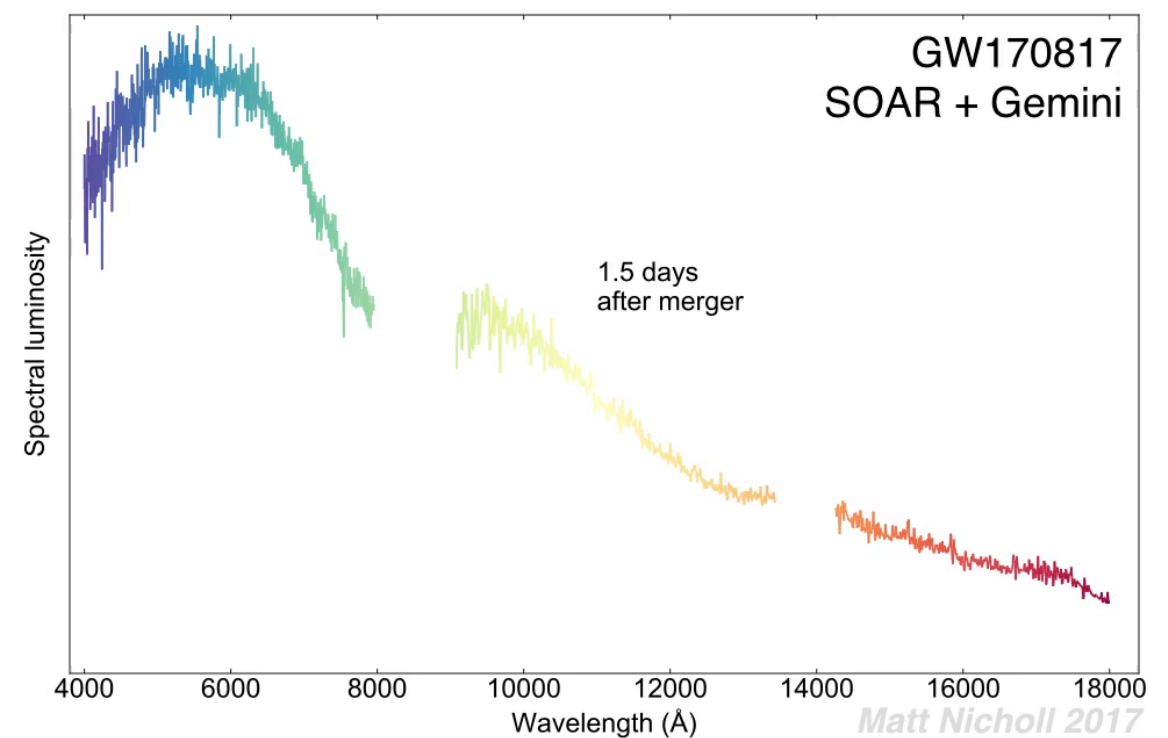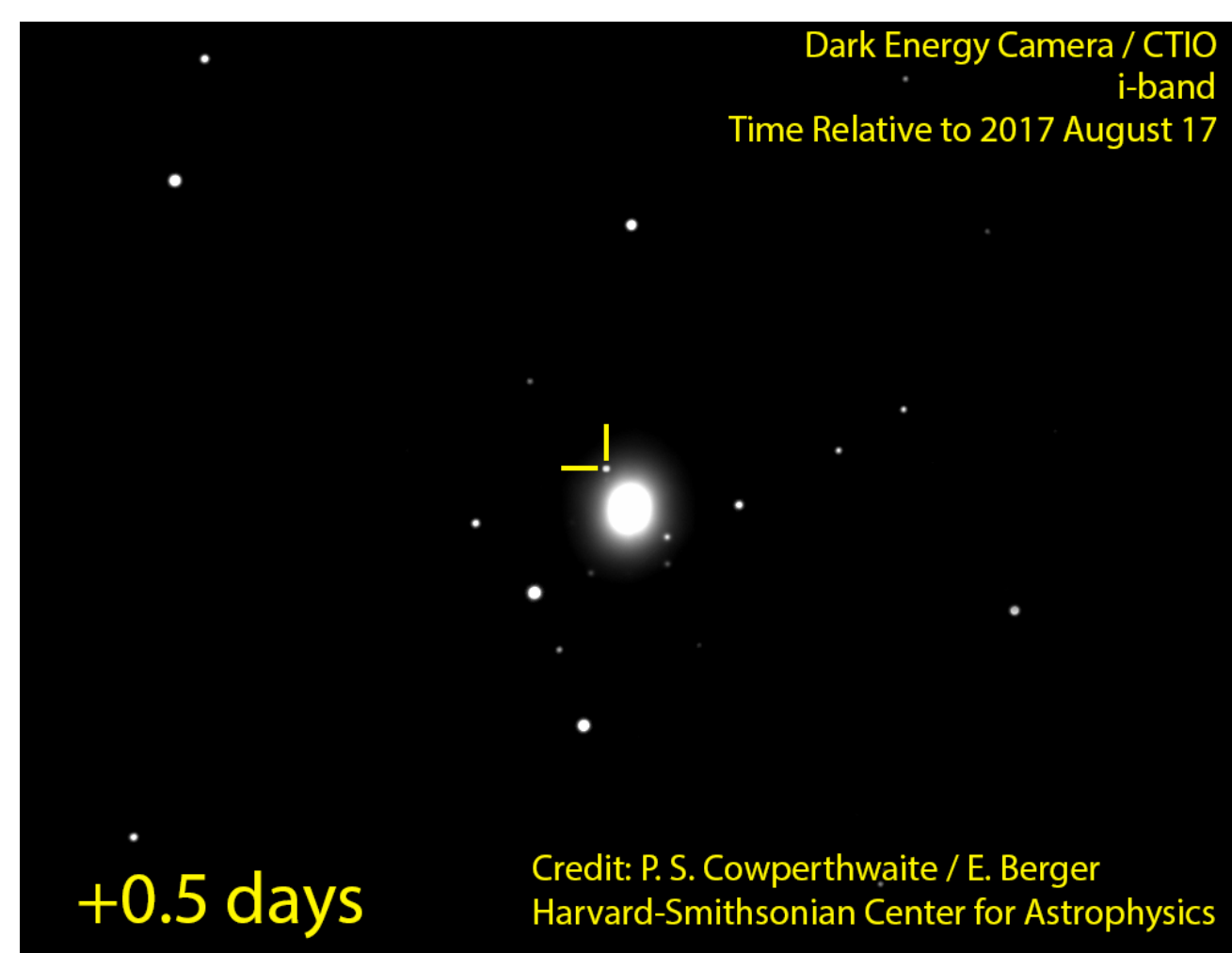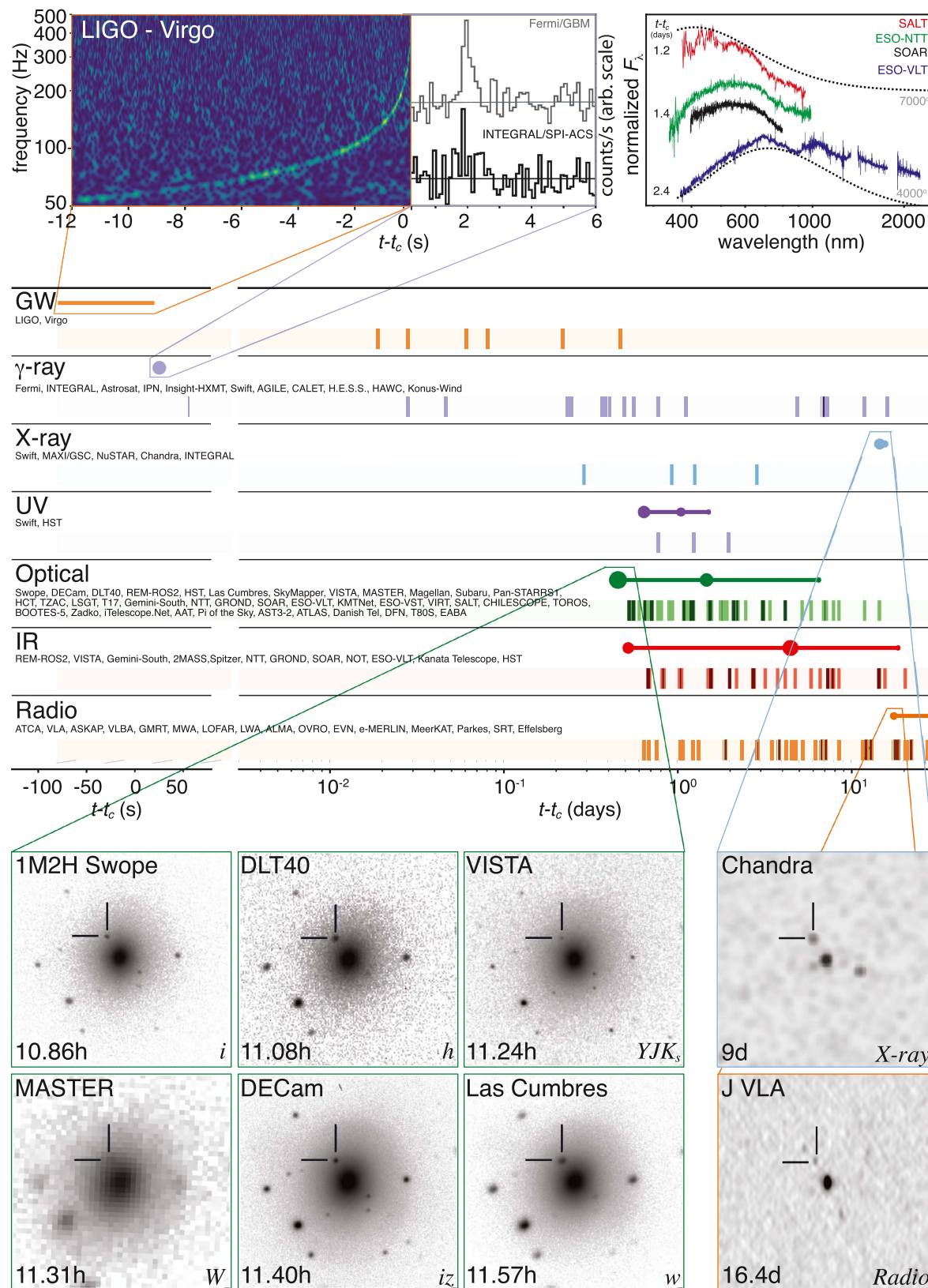
**Figure 2.** Timeline of the discovery of GW170817, GRB 170817A, SSS17a/AT 2017gfo, and the follow-up observations are shown by messenger and wavelength relative to the time $t_c$ of the gravitational-wave event. Two types of information are shown for each band/messenger. First, the shaded dashes represent the times when information was reported in a GCN Circular. The names of the relevant instruments, facilities, or observing teams are collected at the beginning of the row. Second, representative observations (see Table 1) in each band are shown as solid circles with their areas approximately scaled by brightness; the solid lines indicate when the source was detectable by at least one telescope. Magnification insets give a picture of the first detections in the gravitational-wave, gamma-ray, optical, X-ray, and radio bands. They are respectively illustrated by the combined spectrogram of the signals received by LIGO-Hanford and LIGO-Livingston (see Section 2.1), the *Fermi*-GBM and *INTEGRAL*/SPI-ACS lightcurves matched in time resolution and phase (see Section 2.2), $1'.5 \times 1'.5$ postage stamps extracted from the initial six observations of SSS17a/AT 2017gfo and four early spectra taken with the SALT (at $t_c + 1.2$ days; Buckley et al. 2017; McCully et al. 2017b), ESO-NTT (at $t_c + 1.4$ days; Smartt et al. 2017), the SOAR 4 m telescope (at $t_c + 1.4$ days; Nicholl et al. 2017d), and ESO-VLT-XShooter (at $t_c + 2.4$ days; Smartt et al. 2017) as described in Section 2.3, and the first X-ray and radio detections of the same source by *Chandra* (see Section 3.3) and JVLA (see Section 3.4). In order to show representative spectral energy distributions, each spectrum is normalized to its maximum and shifted arbitrarily along the linear y-axis (no absolute scale). The high background in the SALT spectrum below 4500 Å prevents the identification of spectral features in this band (for details McCully et al. 2017b).

# Highlight O3

With so many events we can start to ask questions about the way these binary black hole systems formed.

There are two main puzzles:

- How come many of the Black Holes are so heavy?

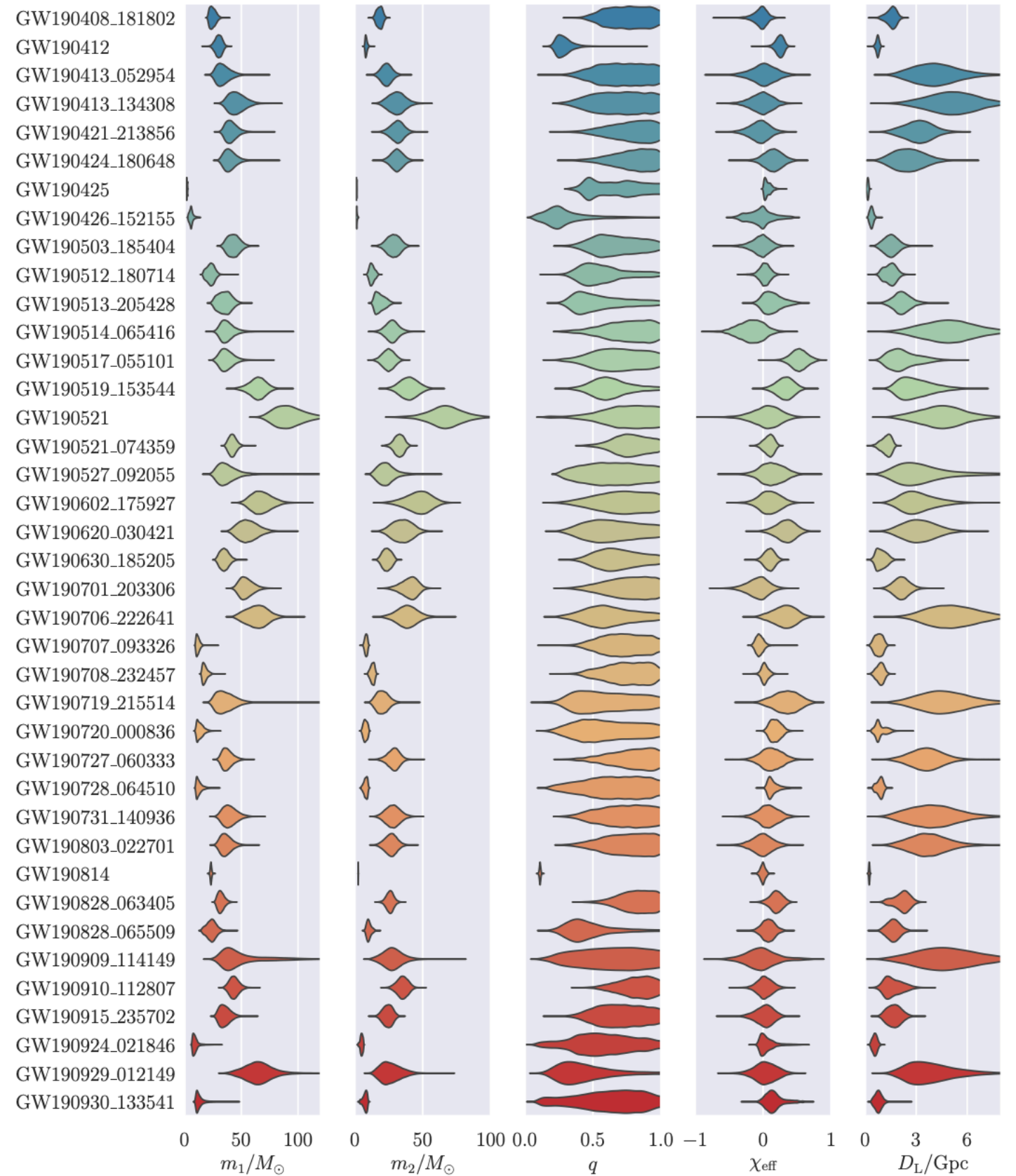- How did the pair of black holes get so close to eventually merge by emitting GW



FIG. 8. Marginal posterior distributions on primary mass $m_1$, secondary mass $m_2$, mass ratio $q$, effective spin $\chi_{eff}$, and the luminosity distance $d_L$ for all candidate events in O3a. The vertical extent of each colored region is proportional to one-dimensional marginal posterior distribution at a given parameter value for the corresponding event.

# Masses of individual Black Holes

The BHs observed by LIGO are surprisingly heavy. They are both heavier than the BH in binaries in our own galaxy and some of them seem heavier than what our theoretical calculations seem to allow.
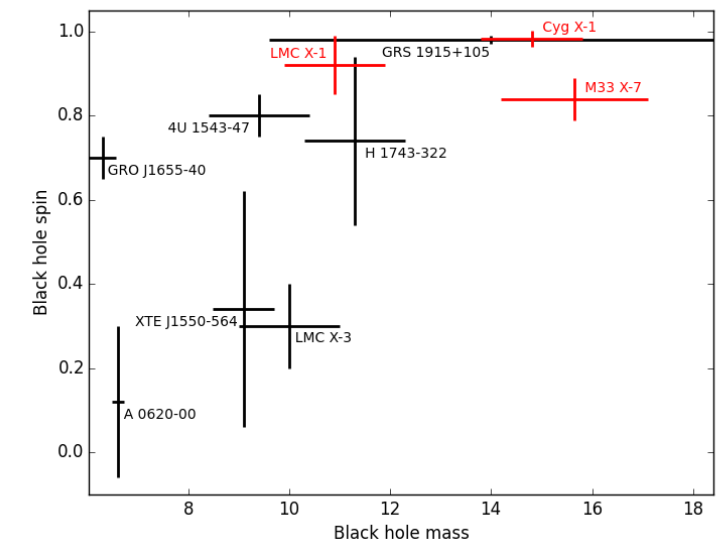




**Figure 1.** Masses and spins for 10 black holes with approximate error bars. The three high-mass-X-ray-binary systems, LMC X-1, Cygnus X-1 and M33 X-7 are indicated by names above the line and in red online.

Nielsen 1604.00778

Cygnus X-1 contains a 21-solar mass black hole – implications for massive star winds

James C.A. Miller-Jones,[1*] Arash Bahramian,[1] Jerome A. Orosz,[2] Ilya Mandel,[3,4,5] Lijun Gou,[6,7] Thomas J. Maccarone,[8] Coenraad J. Neijssel,[3,4,5] Xueshan Zhao,[6,7] Janusz Ziółkowski,[9] Mark J. Reid,[10] Phil Uttley,[11] Xueying Zheng,[6,7] Do-Young Byun,[12,13] Richard Dodson,[14] Victoria Grinberg,[15] Taehyun Jung,[12,13] Jeong-Sook Kim,[12] Benito Marcote,[16] Sera Markoff,[11,17] María J. Rioja,[14,18,19] Anthony P. Rushton,[20,21] David M. Russell,[22] Gregory R. Sivakoff,[23] Alexandra J. Tetarenko,[24] Valeriu Tudose,[25] Joern Wilms[26]
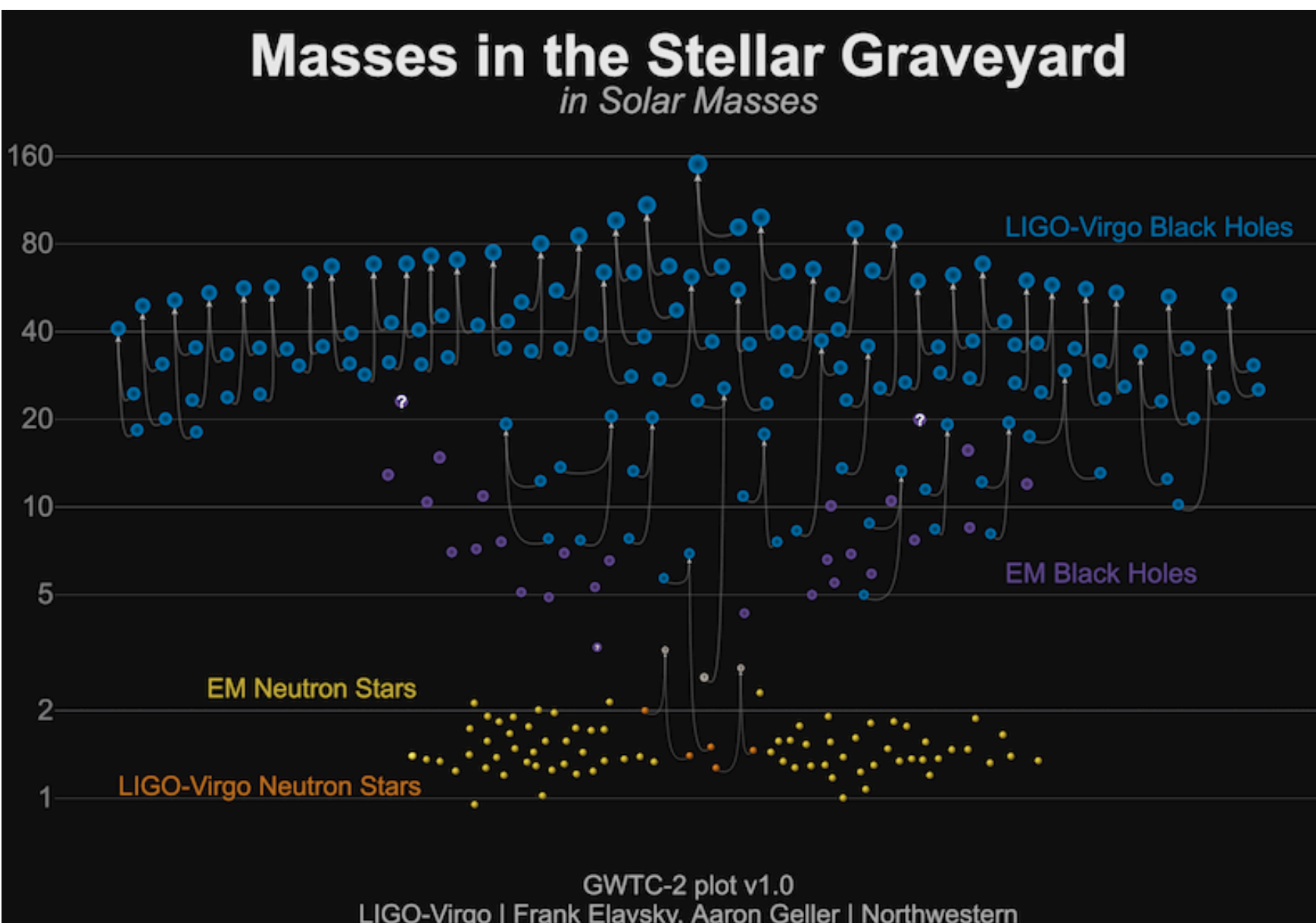
# High Mass End after O2
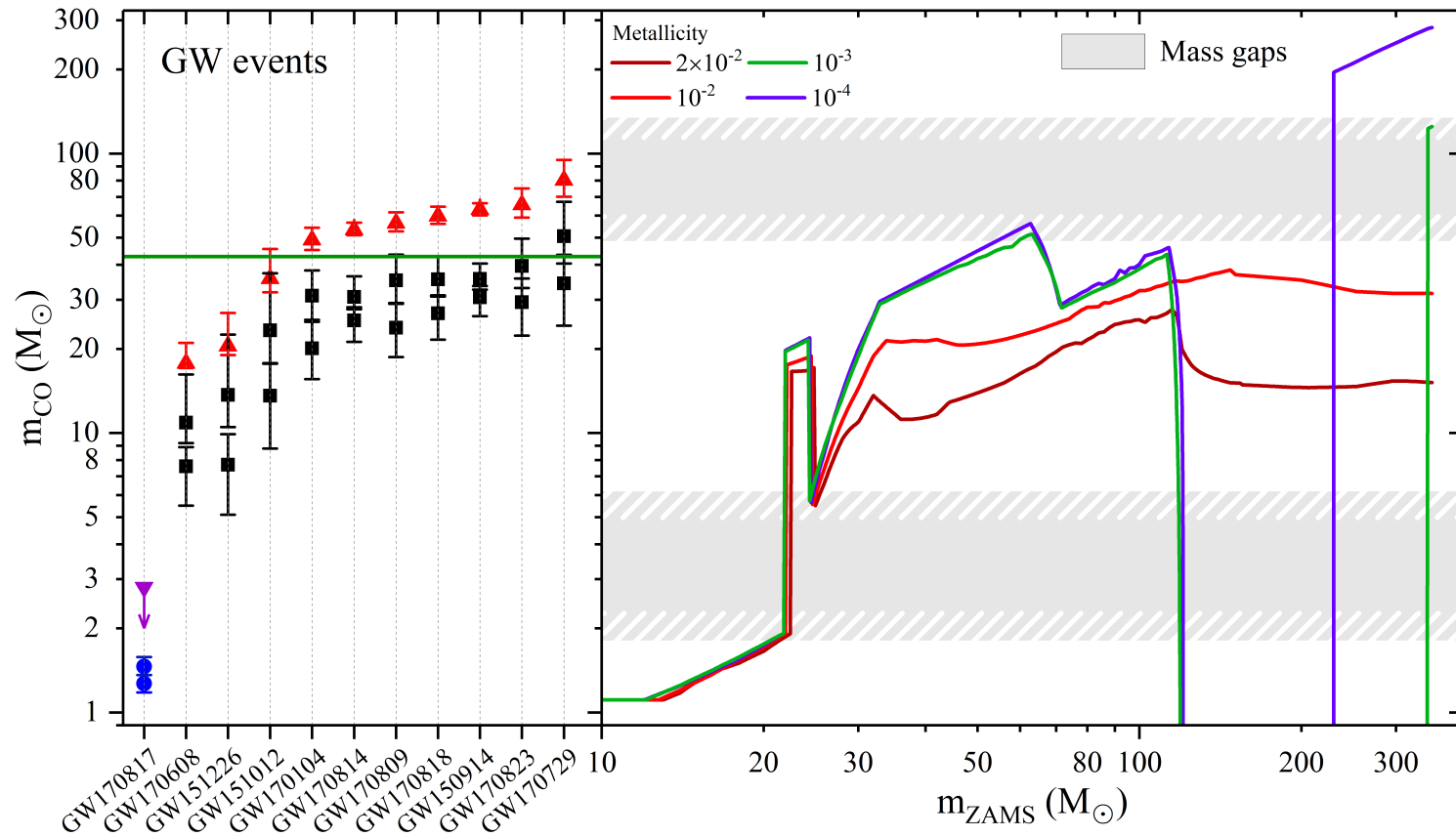
**Figure 4.** The left-hand panel shows compact object masses ($m_{CO}$) from GW detections in O1 and O2, with the black squares and error bars representing the component masses of the merging black holes and their uncertainties, and red triangles representing the mass and associated uncertainties of the merger products. The horizontal green line shows the 99th percentile of the mass distribution inferred from the Model B PPD. In the right-hand panel, the predicted compact-object mass is shown as a function of the zero-age main sequence mass of the progenitor star ($m_{ZAMS}$) and for four different metallicities of the progenitor star (ranging from $Z = 10^{-4}$ to $Z = 2 \times 10^{-2}$, Spera & Mapelli 2017). This model accounts for single stellar evolution from the PARSEC stellar-evolution code (Bressan et al. 2012), for core-collapse supernovae (Fryer et al. 2012), and for pulsational-pair instability and pair-instability supernovae (Woosley 2017). The shaded areas represent the lower and upper mass gaps. There is uncertainty as to the final product of GW170817. It is shown in the left-hand panel to emphasize that BNS mergers might fill the lower gap.
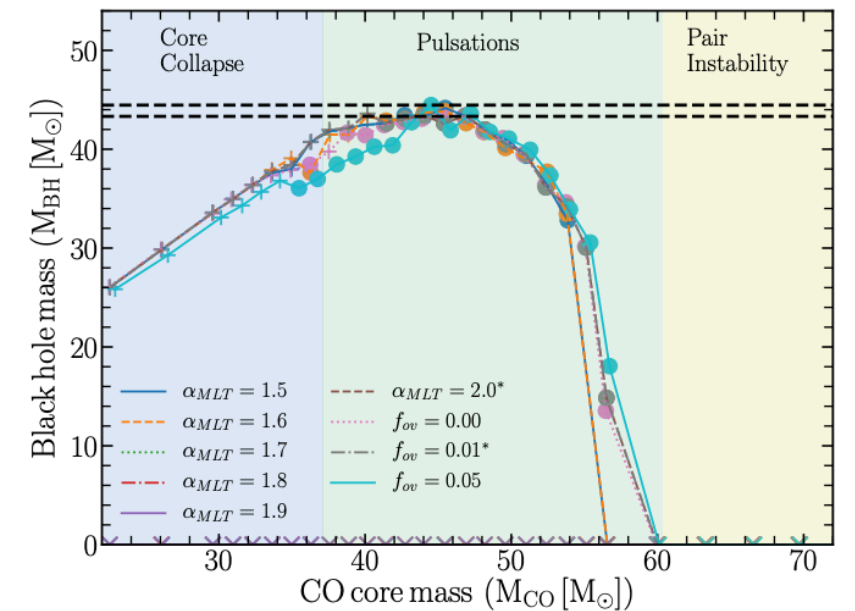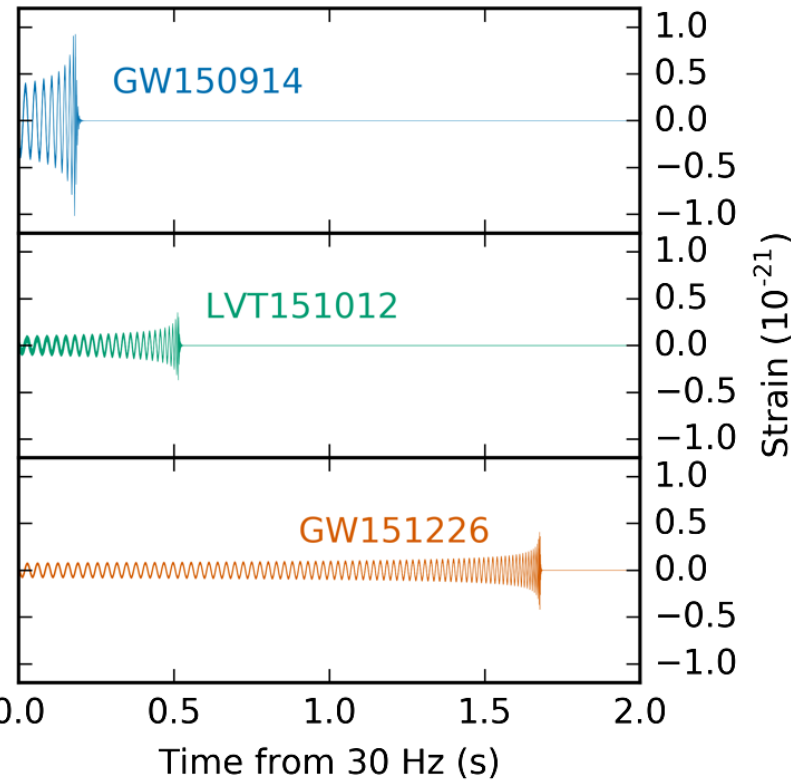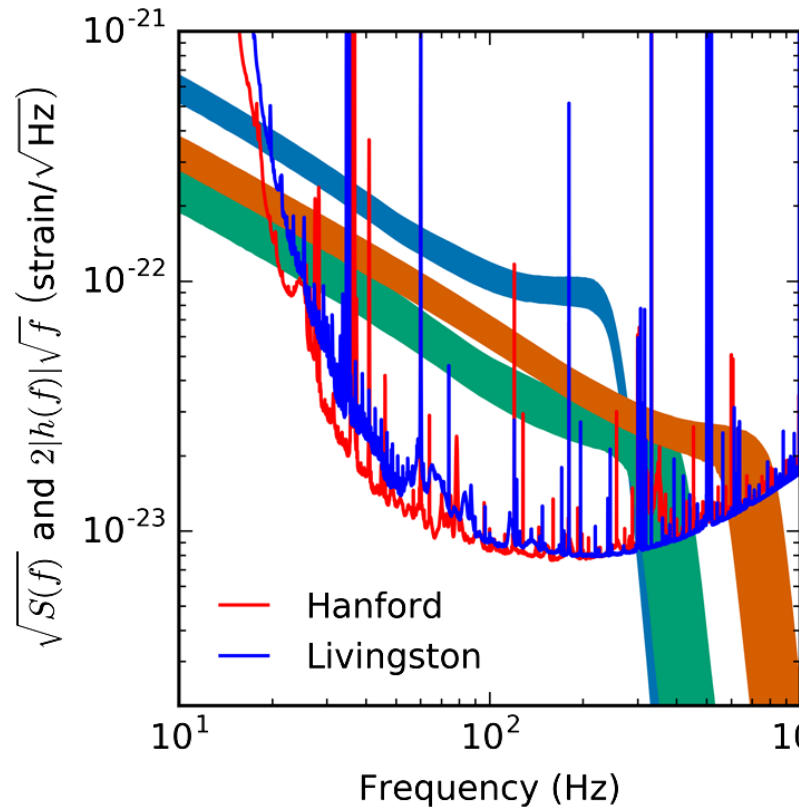
[arxiv:1910.12874]

# High Mass End
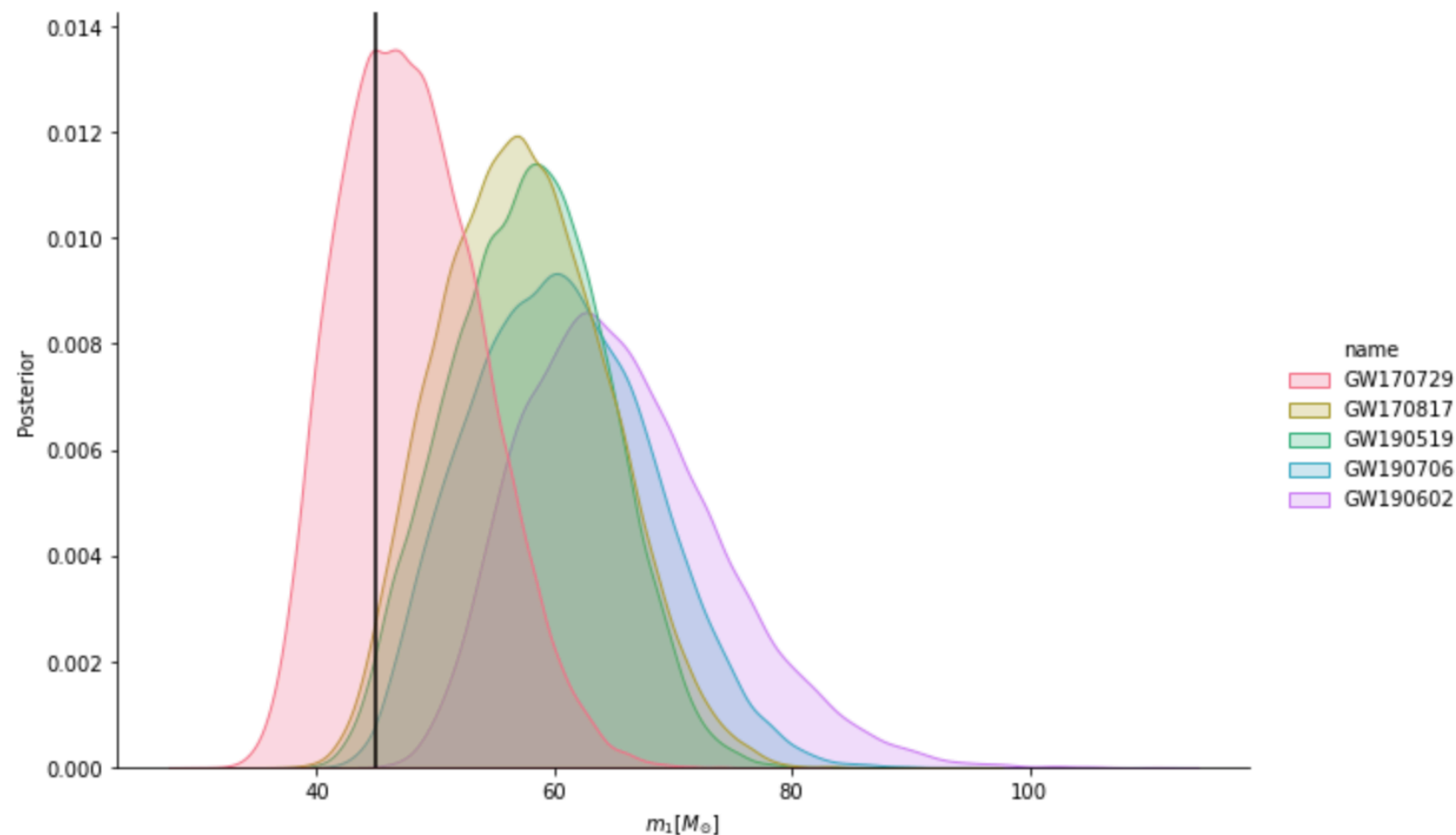


There are several examples of events with masses above the pair instability threshold.

Note that there is already one event O2 (GW170812) in the IAS sample. GW170729 was also heavy although consistent with the cut-off. It was marginal in the LIGO pipeline but was completely above the background in our search.
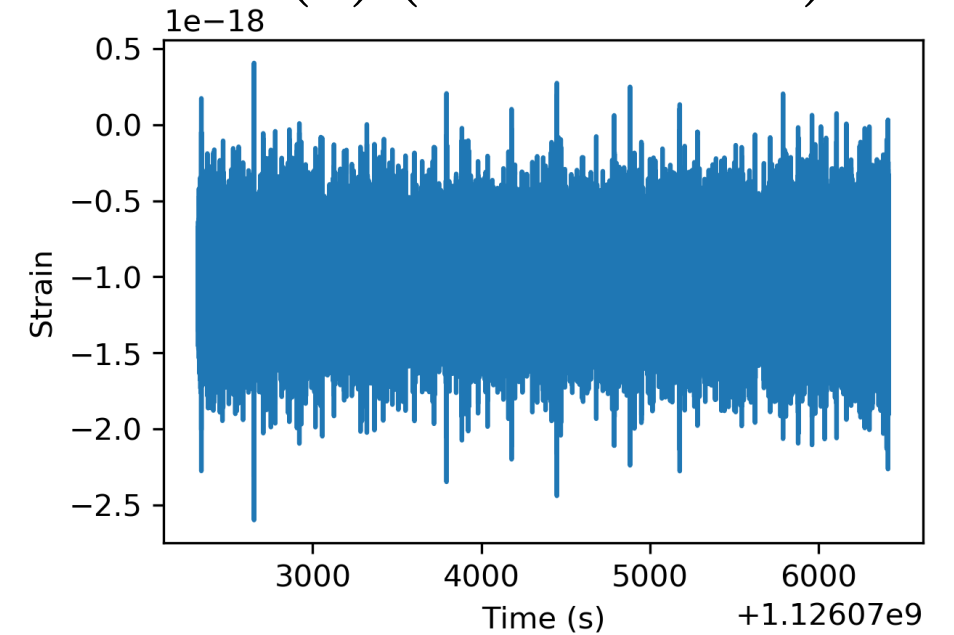
# Noise PSD

# Matched filtering



$\sqrt{S(f)}$ and $2|h(f)|\sqrt{f}$ (strain/$\sqrt{\text{Hz}}$)

Hanford
Livingston

Frequency (Hz)

GW150914
LVT151012
GW151226

Strain ($10^{-21}$)

Time from 30 Hz (s)

$h(t)$(whitened)

$d(t)$(whitened)

Strain

Time (s)    +1.12607e9

**GWTC-1: A Gravitational-Wave Transient Catalog of Compact Binary Mergers Observed by LIGO and Virgo during the First and Second Observing Runs**

FIG. 15. Normalized spectrograms of the time around common noise artifacts with a time-frequency evolution of a related trigger template overlaid. Top Left: Scattered light artifacts at Hanford with the template of trigger 170616 overlaid. Top Right: A 60-200 Hz nonstationarity at Livingston with the template of trigger 170412 overlaid. Bottom Left: A short duration transient at Livingston with the template of trigger 170630 overlaid. Bottom Right: A blip at Hanford with the template of a sub-threshold high mass trigger overlaid.

signal/noise

$$\frac{Z}{\sigma_{Z}} = \frac{\sum_{f} \frac{h^{*}(f)d(f)}{S_{n}(f)}}{\sqrt{\sum_{f} \frac{|h(f)|^{2}}{S_{n}(f)}}} \equiv \rho$$

# Effect of PSD drift and vetoes
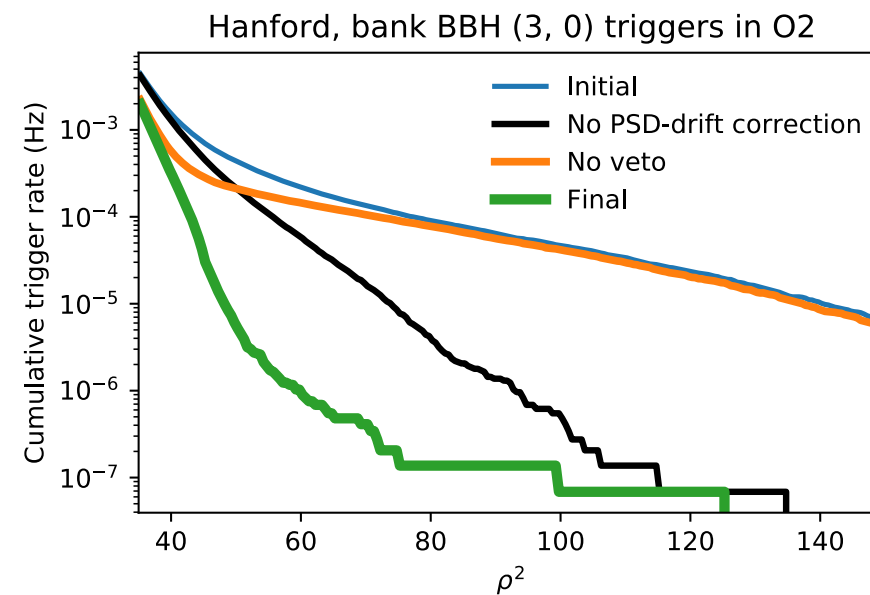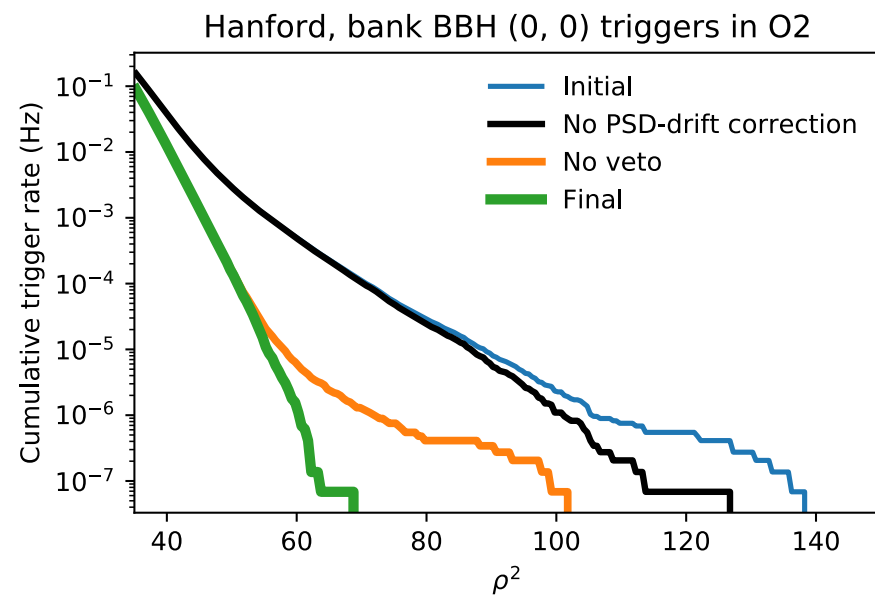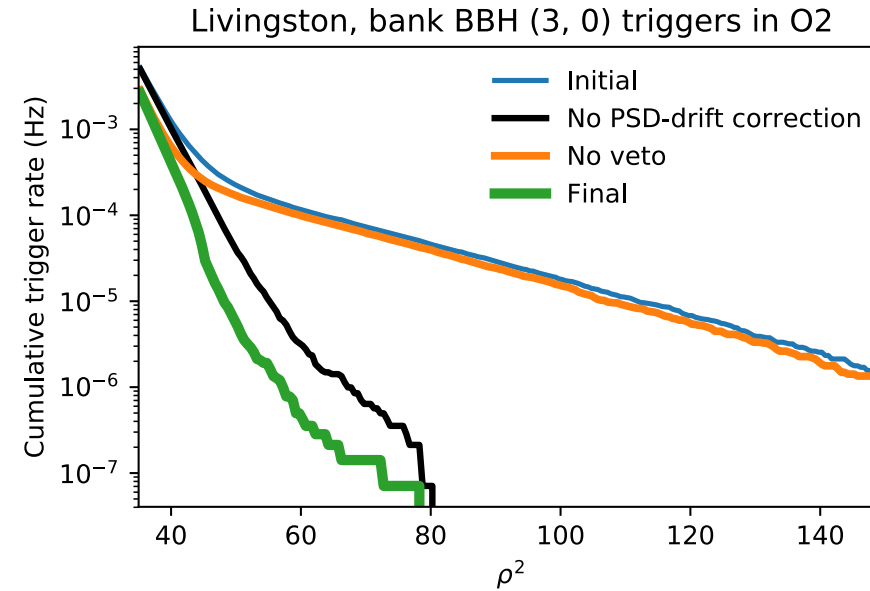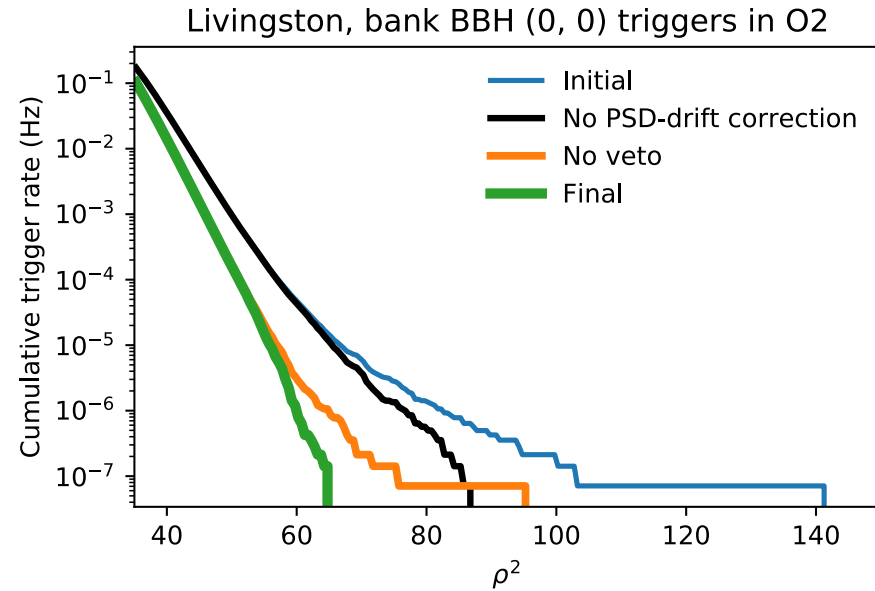


Note that these plots are produced with data after masking (holes + in-painting).
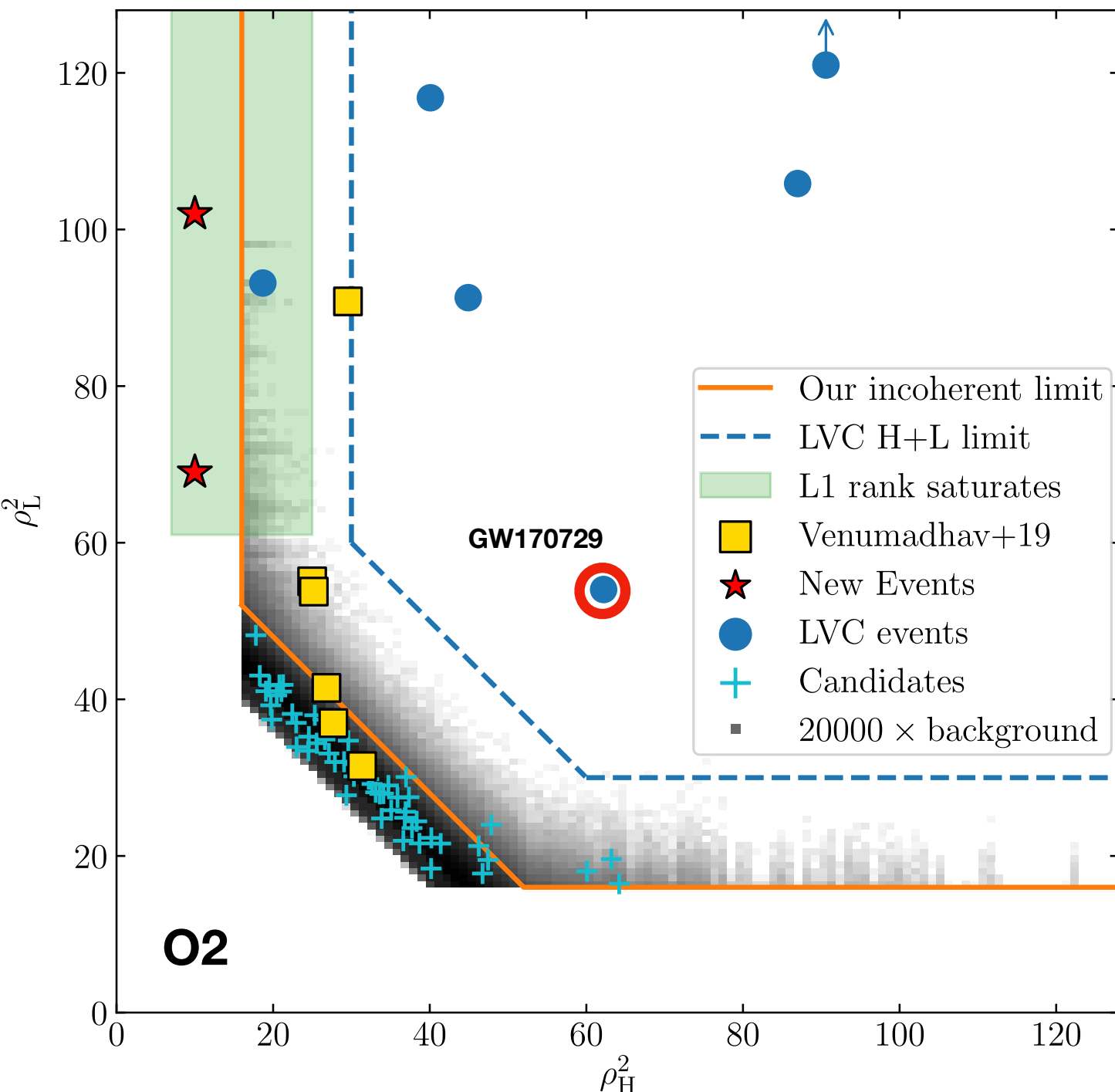
Non-G of the data results in orders of magnitude increase in the rate of triggers.

Even in this heavy BBH bank all the outliers in a single detector are real events. Light BBHs and BNS have basically no glitches after masking all the non-G is PSD drift.

Trigger rate for PyCBC above 64 approx $10^{-4}$ Hz.

# Sensitivity Comparison

**Prior to demanding consistency between detectors**



**GW170729**

LIGO FAR = 1 in 5 yrs

IAS FAR < 1 in 20000 O2 = 1 in 6500 yrs (saturated by the amount of background we collected)

Additional suppression approximately Delta snr^2=20. In trigger distributions going from 40 to 60 is approximately 3 orders of magnitude in the rate.

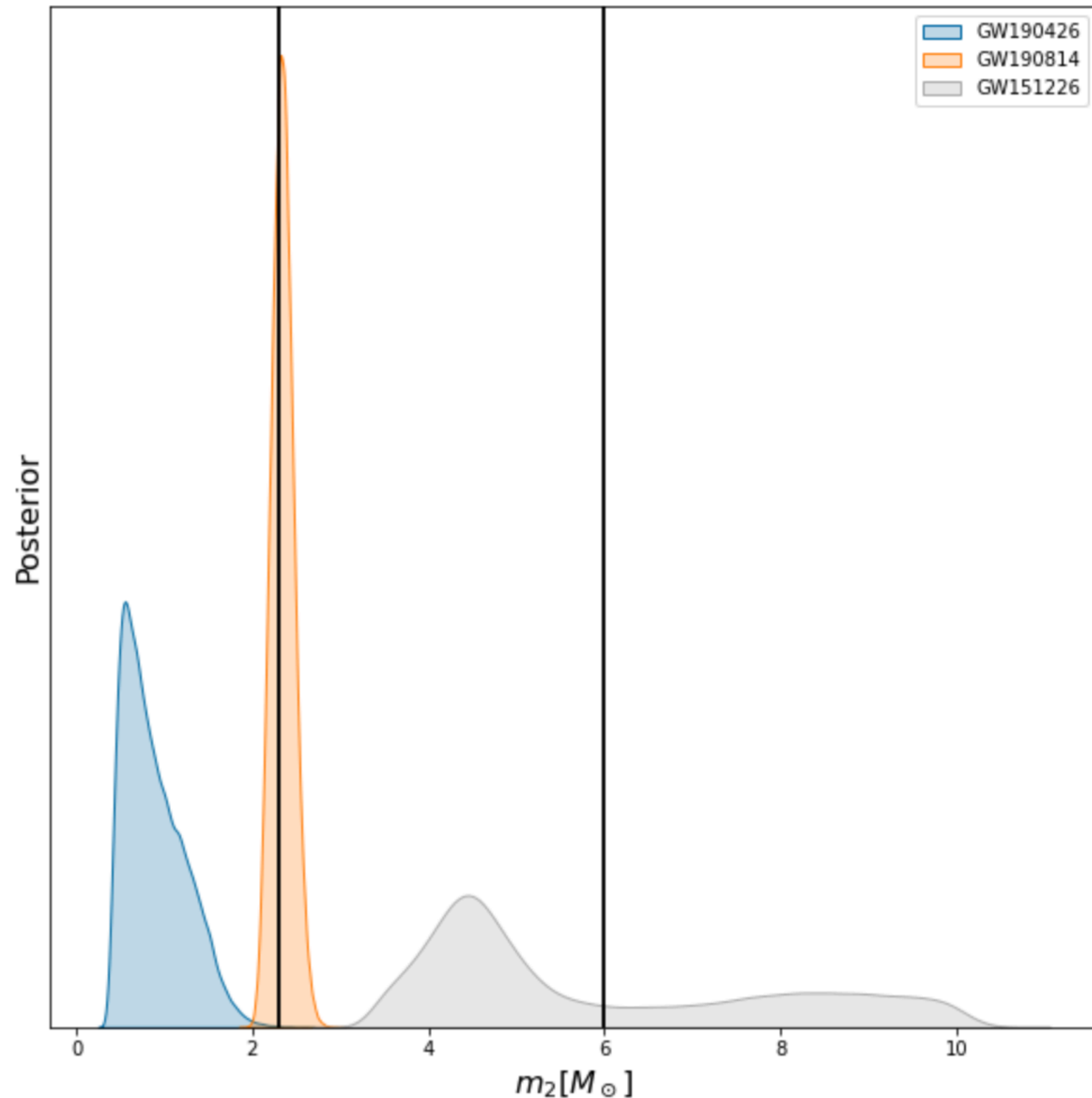$(90/64)^{1/2} = 1.2$  and $(90/64)^{3/2} = 1.7$

Equivalent to reducing the strain noise amplitude by ~ 20 %

Equivalent to increasing the volume by ~ 70 %

You can reach the same conclusion about LVT during O1. The plot looks very similar.

# Low Mass End



In O3 there are examples of low mass companions.

Note also GW151226

Non-interacting dark companions have recently been discovered. Latest example:

**A Unicorn in Monoceros: the $3M_\odot$ dark companion to the bright, nearby red giant V723 Mon is a non-interacting, mass-gap black hole candidate**

T. Jayasinghe[1,2]⋆, K. Z. Stanek[1,2], Todd A. Thompson[1,2], C. S. Kochanek[1,2], D. M. Rowan[1,2], P. J. Vallely[1,2], K. G. Strassmeier [3], M. Weber [3], J. T. Hinkle[4], F.-J. Hambsch[5,6,7], D. Martin[1,8], J. L. Prieto[9,10], T. Pessi[9], D. Huber[4], K. Auchettl[11,12,13], L. A. Lopez[1,2], I. Ilyin[3], C. Badenes[14], A. W. Howard[15], H. Isaacson[16,17], S. J. Murphy[18,19]
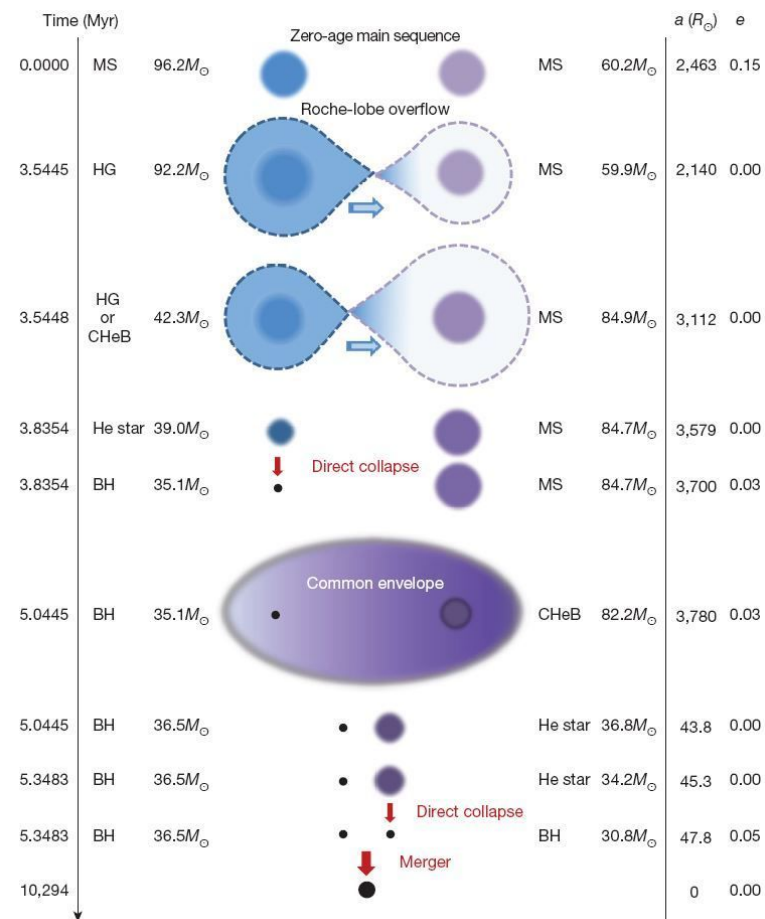
# Compact binaries

To merge due to emission of GW radiation two 20 solar mass black holes need to be closer than 30 solar radii.

The massive stars that are the progenitors of these black holes are much bigger than that during their giant phase. How did the black holes come together?
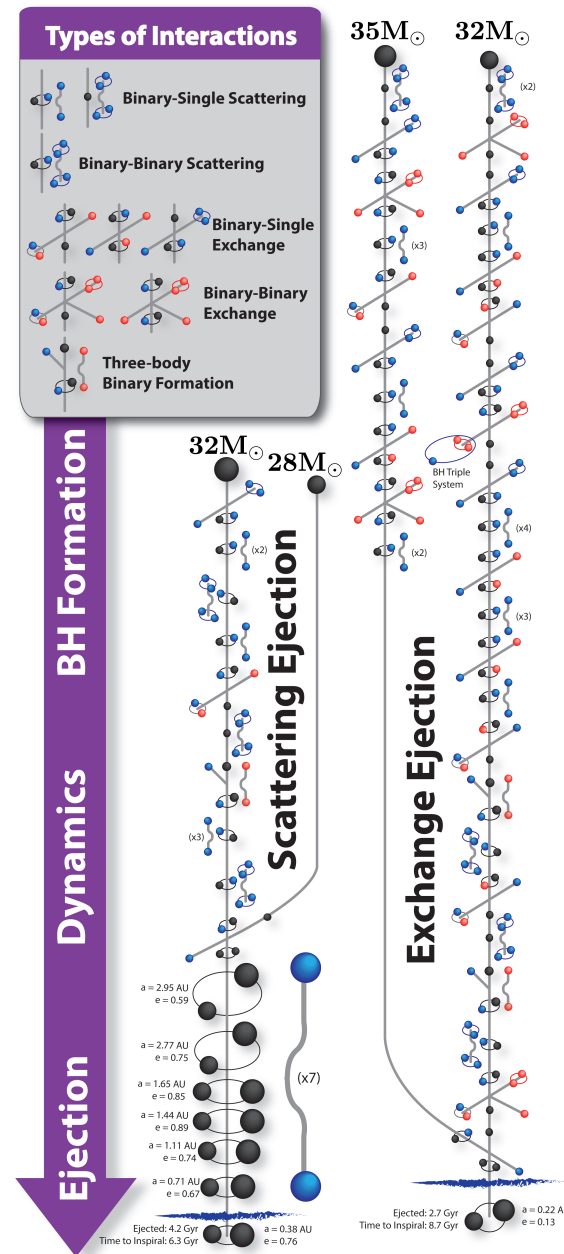
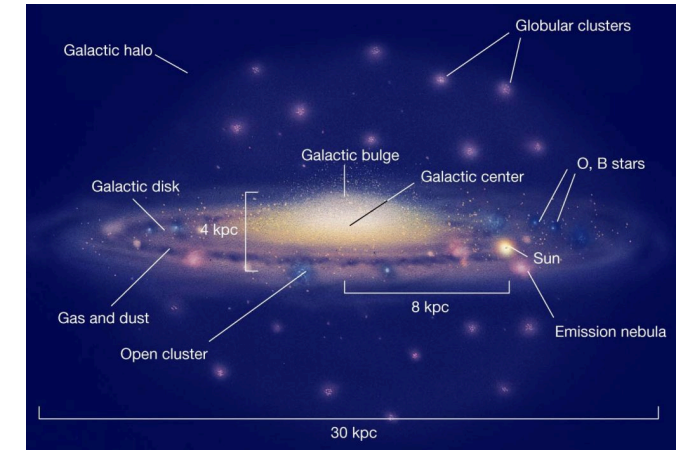Color, luminosity and sizes of stars
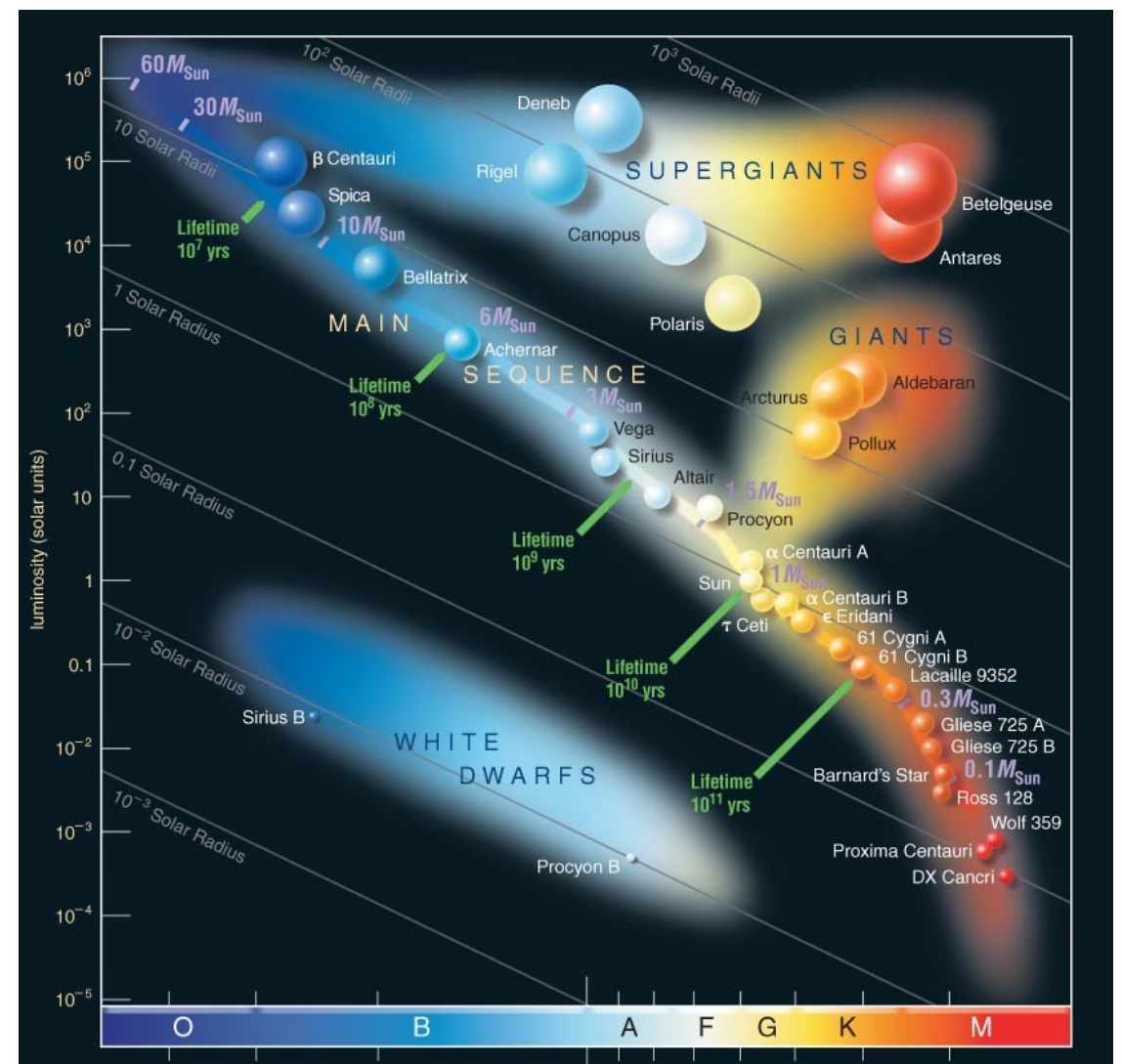
# Formation channels



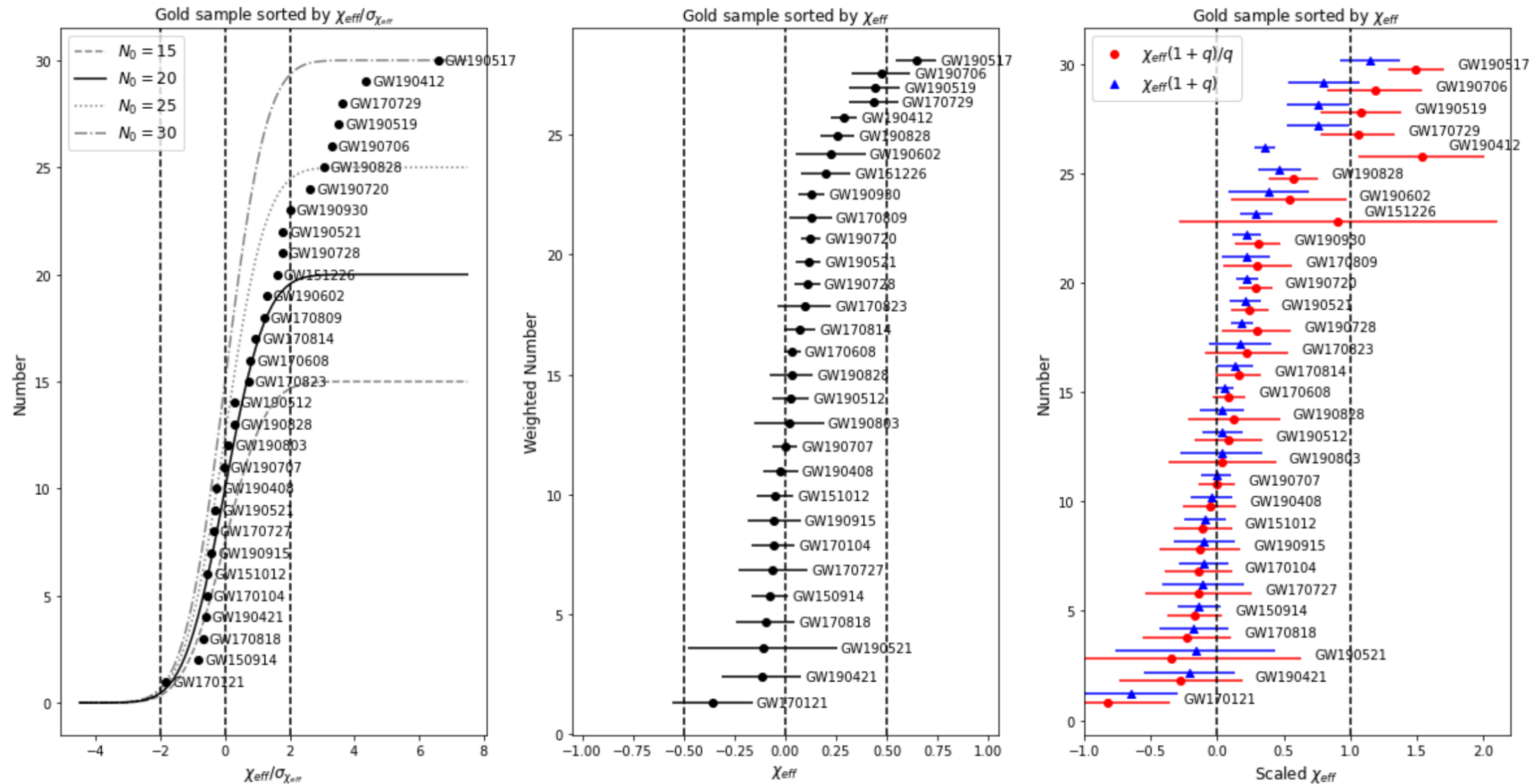Belczynski et al. 2016



Rodriguez et al. 1604.04254





- Rate
- Masses
- Spin
- Eccentricity

There already is interesting spin information

# Spin measurements

$$\chi_{\mathrm{eff}} = (m_1\,\chi_{1z} + m_2\,\chi_{2z})/M$$



Spins are small. The distribution is not consistent with no spin. All the significant detections are on the positive spin side (small caveat, positive spin events are louder). This points to a significant contribution of the binary channel.
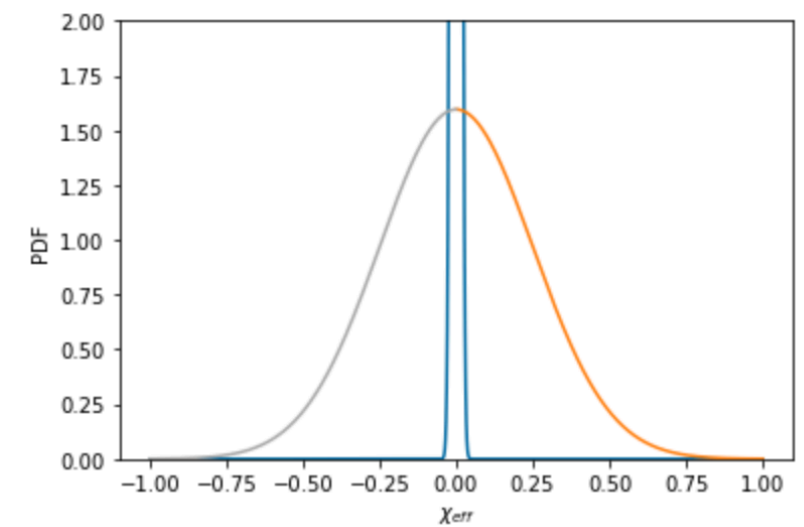
There is no evidence for negative spin.

Several of the spins that are significantly different from zero are still small. Not very consistent with the naive tide scenario.

# Spin measurements
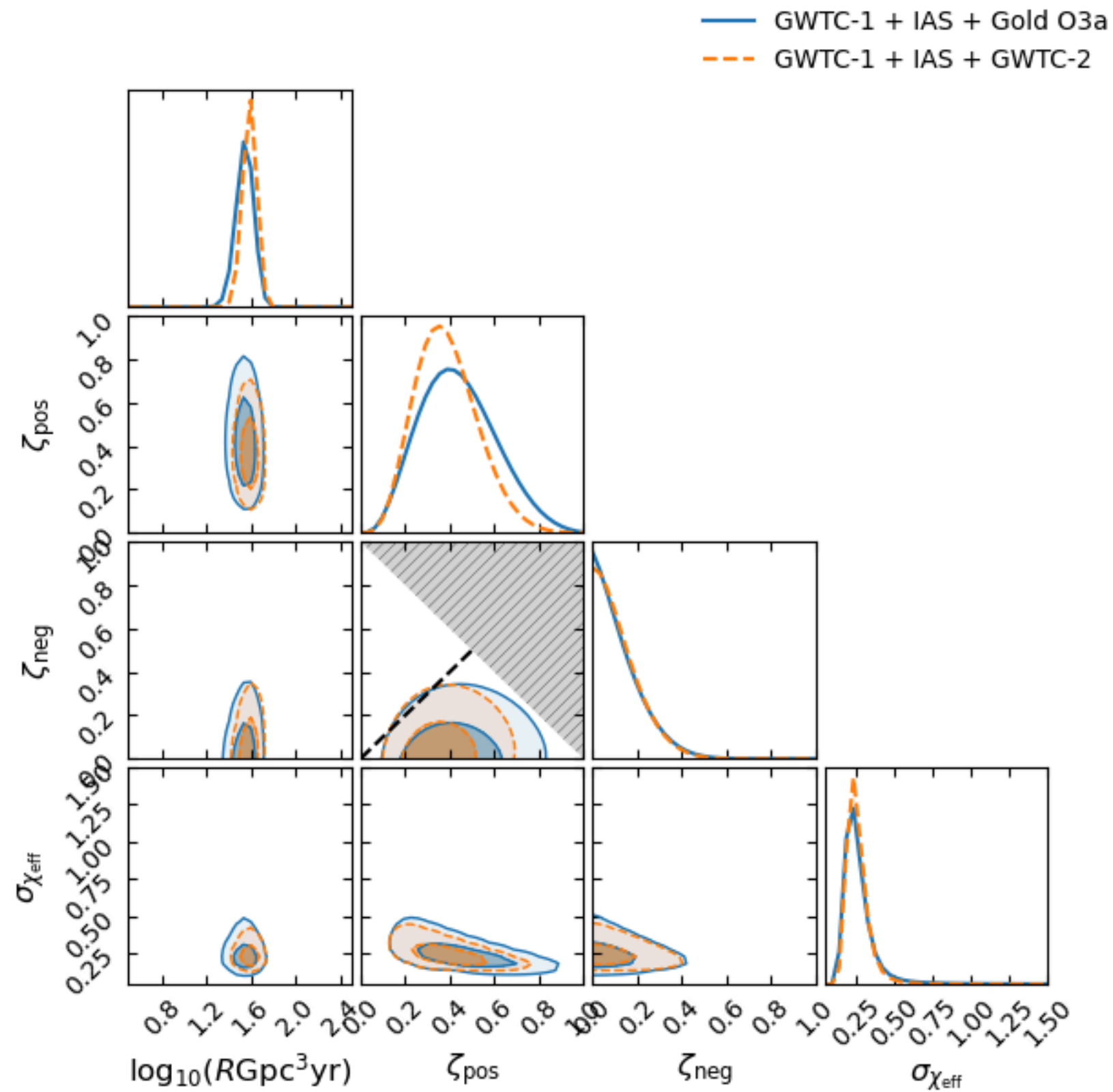


Model

# The IAS independent search for events in the LIGO data

**Barak Zackay**

**Tejaswi Venumadhav**

**Javier Roulet**

**Liang Dai**

**Matias Zaldarriaga**
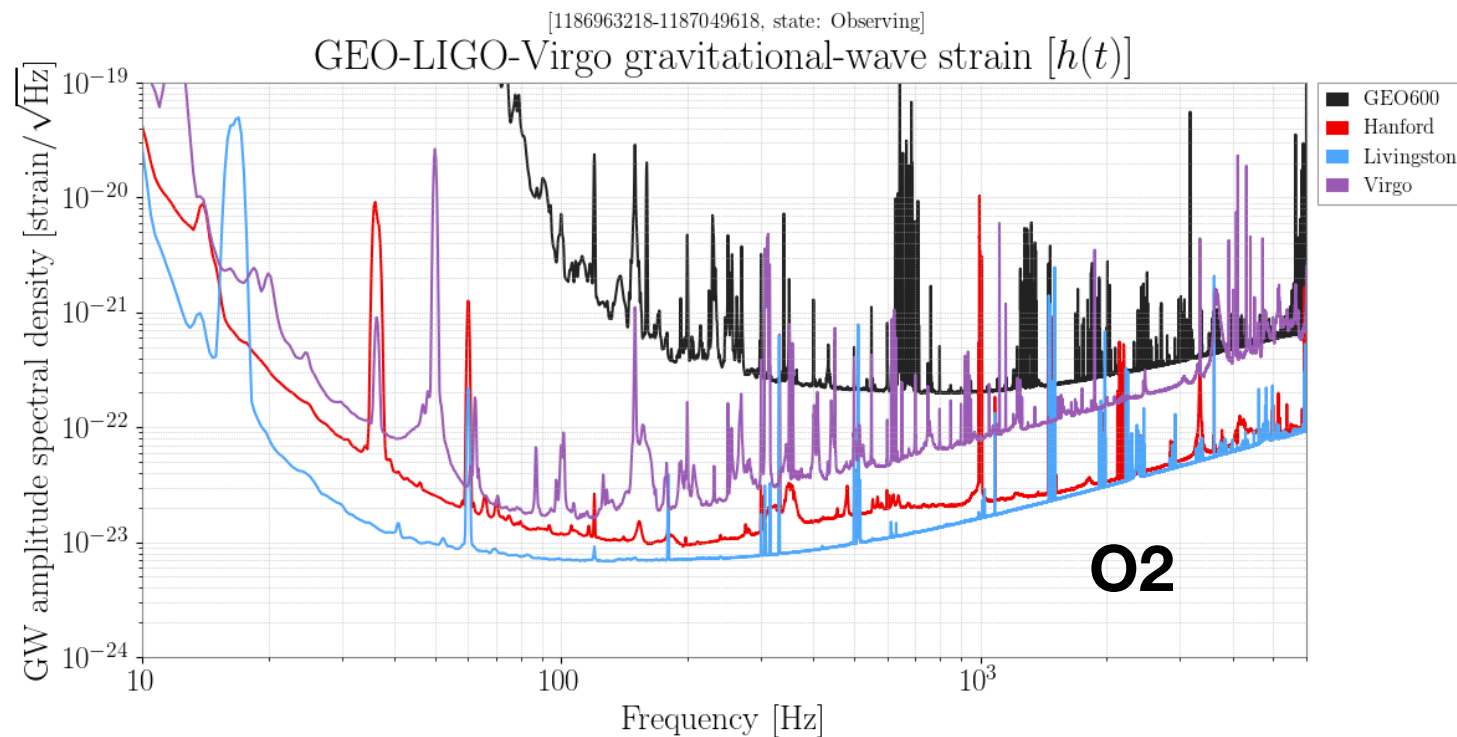
# Summary

O1: one new events (LIGO had 3)

O2: six new events  (LIGO had 7)

O2: 2 "detector and a half" events

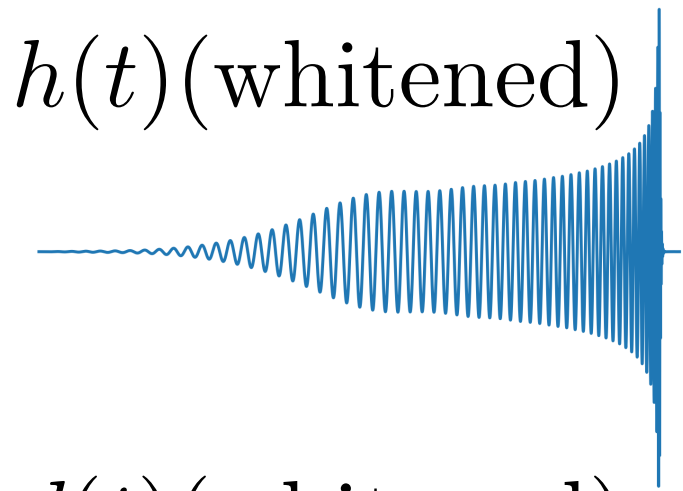O2: One intriguing triplet of events from the same location in the sky and the same parameters

Approximately double the volume where events can be found. **The criteria to declare an event is the same.**
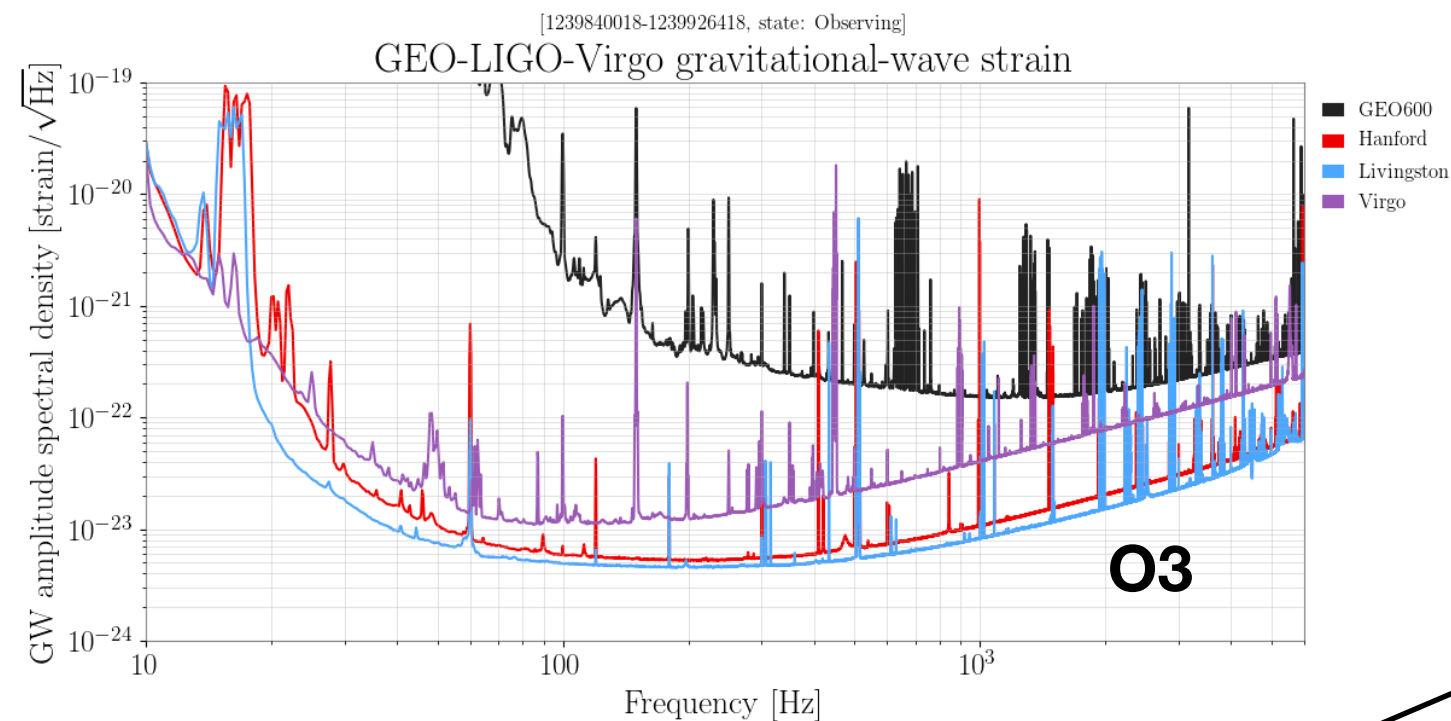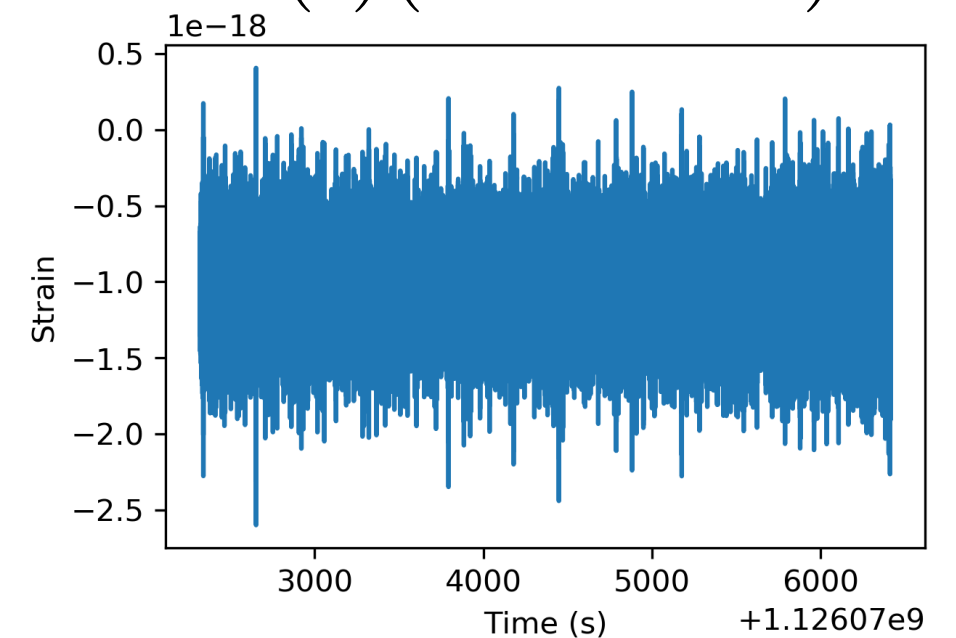
# Noise PSD



[1186963218-1187049618, state: Observing]
GEO-LIGO-Virgo gravitational-wave strain [h(t)]

**O2**

[1239840018-1239926418, state: Observing]
GEO-LIGO-Virgo gravitational-wave strain

**O3**

# Matched filtering

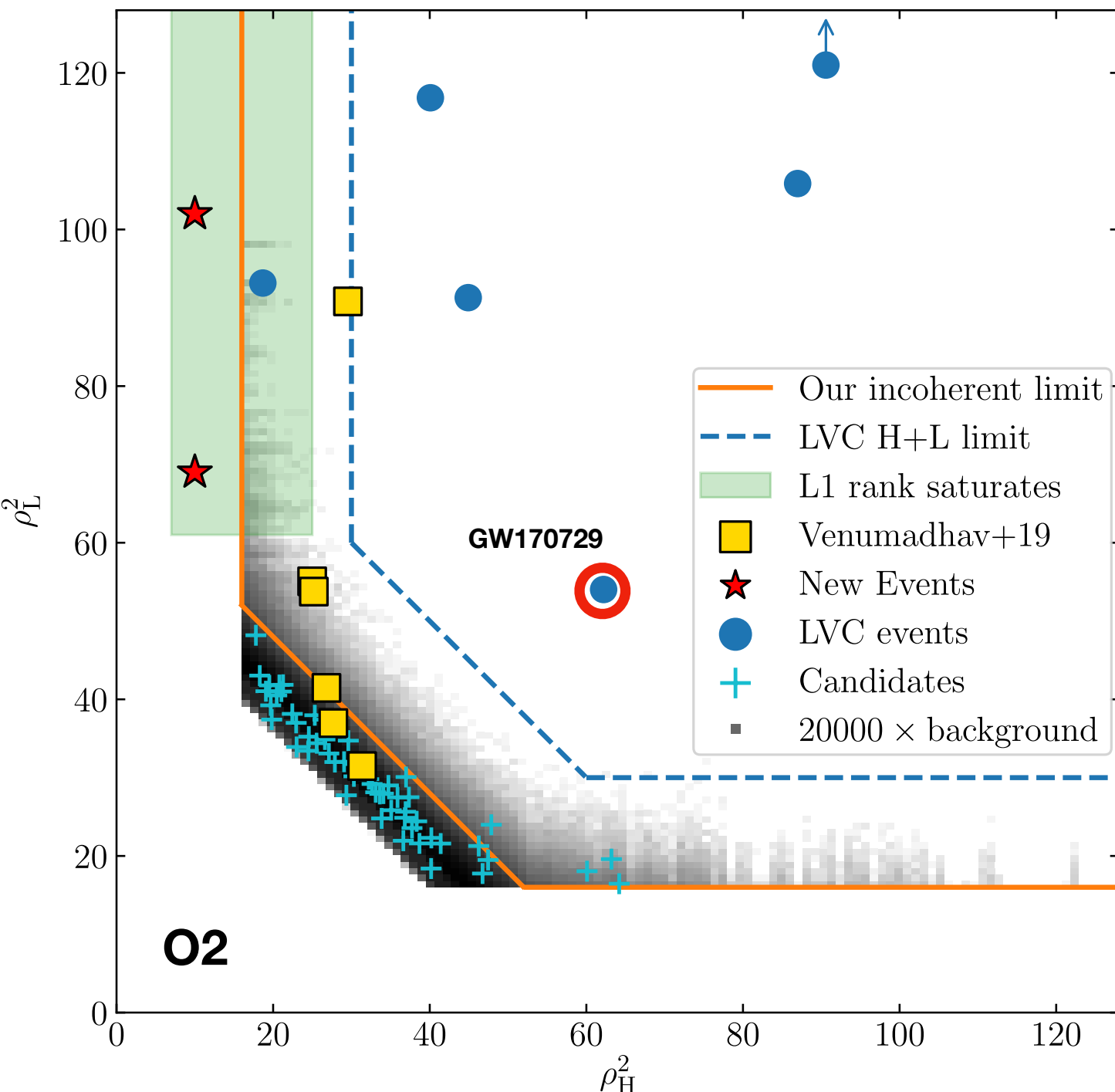$h(t)(\text{whitened})$

$d(t)(\text{whitened})$

signal/noise

$$\frac{Z}{\sigma_Z} = \frac{\sum_f \frac{h^*(f)d(f)}{S_n(f)}}{\sqrt{\sum_f \frac{|h(f)|^2}{S_n(f)}}}$$

# Sensitivity Comparison

**Prior to demanding consistency between detectors**



**GW170729**

LIGO FAR = 1 in 5 yrs

IAS FAR < 1 in 20000 O2 = 1 in 6500 yrs (saturated by the amount of background we collected)

Additional suppression approximately Delta snr^2=20. In trigger distributions going from 40 to 60 is approximately 3 orders of magnitude in the rate.

$(90/64)^{1/2} = 1.2$ and $(90/64)^{3/2} = 1.7$

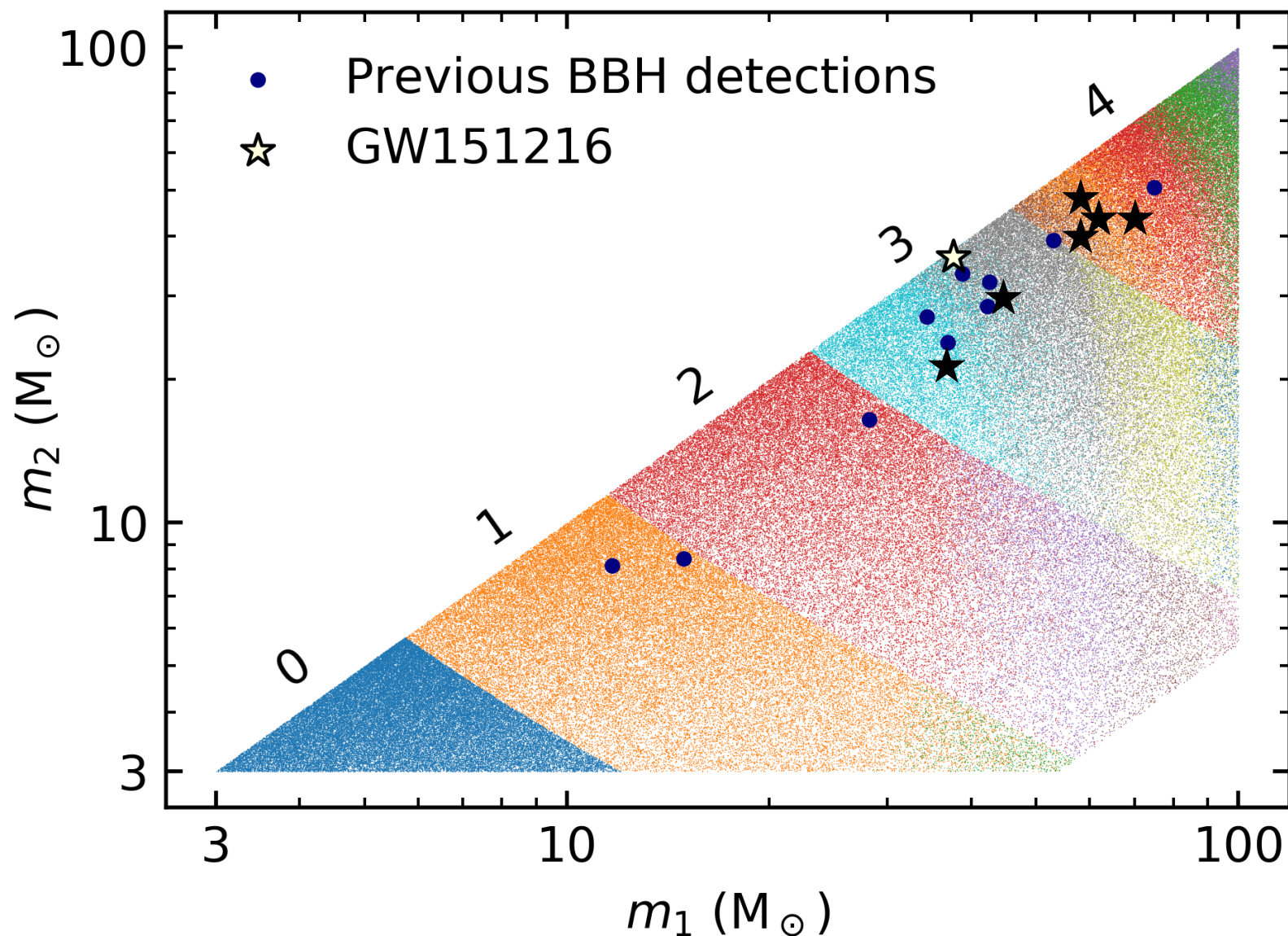Equivalent to reducing the strain noise amplitude by ~ 20 %

Equivalent to increasing the volume by ~ 70 %

You can reach the same conclusion about LVT during O1. The plot looks very similar.

# Steps in a search pipeline

- Compute waveforms.

- Define a search strategy and construct a template bank.

- Estimate detector noise and account for its non-stationary nature.

- Detect bad data segments (``glitches") and insulate good data from them.

- Compute triggers and find coincident ones.

- Asses if triggers look like GW and veto those that don't.

- Assess if triggers are consistent between detectors.

- Estimate the background.

# Splitting in Banks

O1: one new events in bank 3

O2: six new events in banks 3 and 4

BBH 3 + BBH 4 = 271 templates. The look elsewhere effect in the heavy BBH banks is down by 2 orders of magnitude relative to the BBH bank.

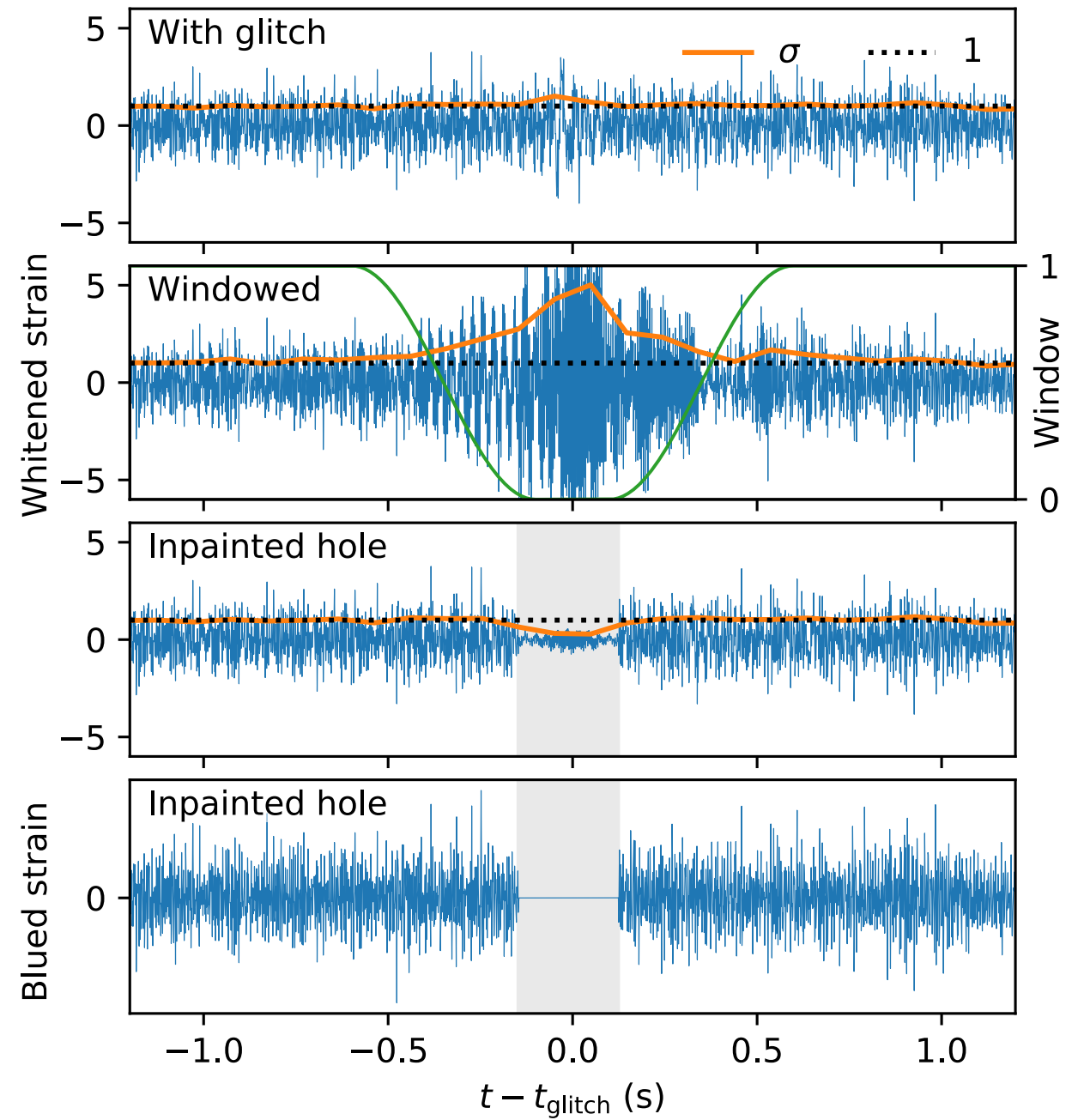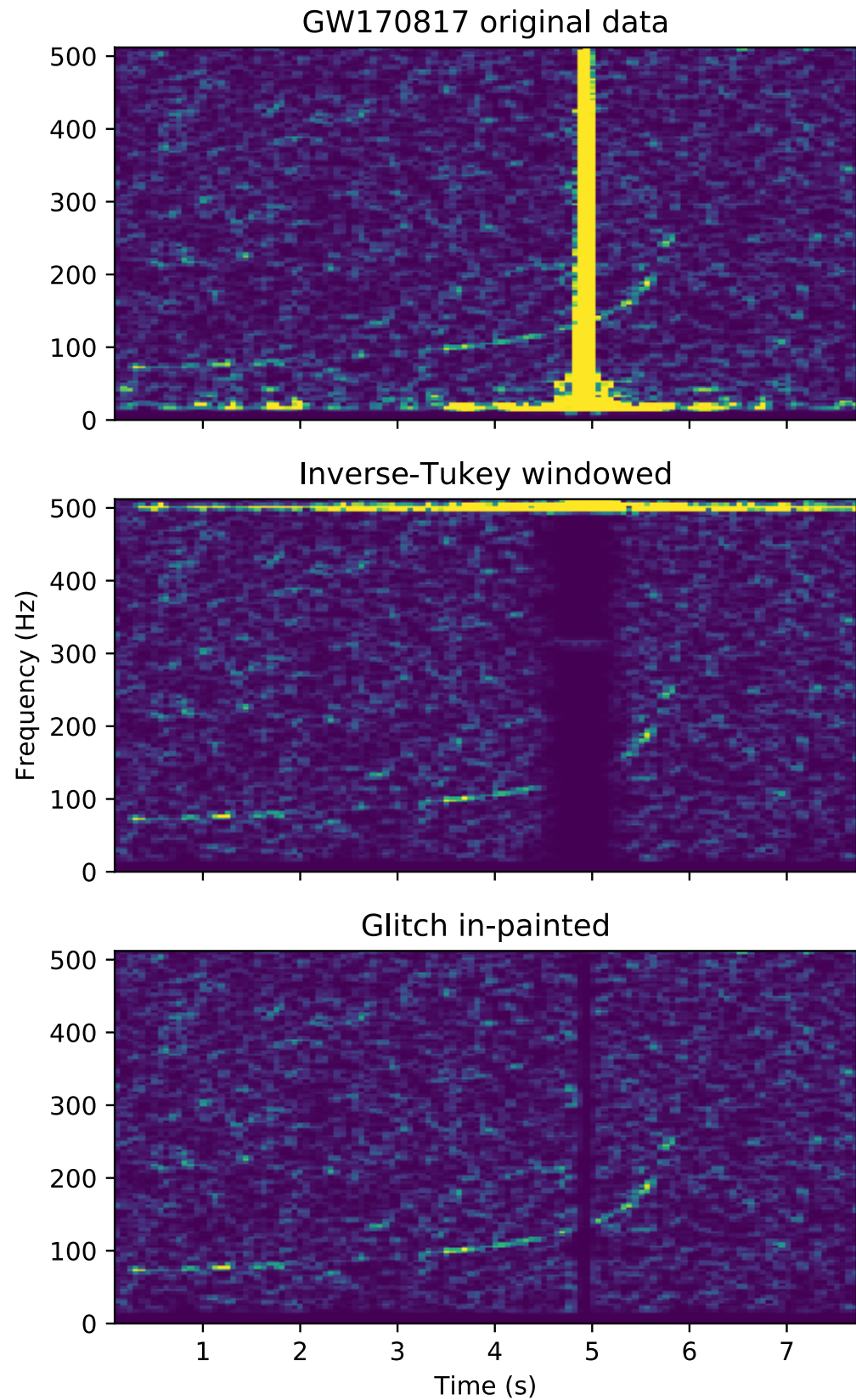| Bank | $m_1$ (M$_\odot$) | $m_2$ (M$_\odot$) | $\mathcal{M}$ (M$_\odot$) | $q_{min}$ | $|\chi_{1,2}|_{max}$ | $\zeta$ | $\Delta c_\alpha$ | $N_{subbanks}$ | $d_{subbanks}$ | $L_{max,subbanks}$ | $N_{templates}$ |
|---|---|---|---|---|---|---|---|---|---|---|---|
| BNS 0 | | | $< 1.1$ | | | | | 1 | 2 | 777.0 | 48 806 |
| BNS 1 | $(1,3)$ | $(1,3)$ | $(1.1, 1.3)$ | — | 0.99 | 0.05 | 0.55 | 1 | 2 | 434.3 | 23 856 |
| BNS 2 | | | $> 1.3$ | | | | | 1 | 2 | 824.6 | 43 781 |
| NSBH 0 | | | $< 3$ | | | | | 1 | 4 | 753.4 | 84 641 |
| NSBH 1 | $(3, 100)$ | $(1,3)$ | $(3,6)$ | 1/50 | 0.99 | 0.05 | 0.5 | 2 | 6, 6 | 259.5, 166.8 | 85 149 |
| NSBH 2 | | | $> 6$ | | | | | 3 | 5, 4, 4 | 87.5, 61.2, 9.4 | 15 628 |
| BBH 0 | | | $< 5$ | | | | 0.55 | 1 | 3 | 270.6 | 8246 |
| BBH 1 | | | $(5, 10)$ | | | | 0.55 | 2 | 4, 4 | 113.7, 50.0 | 4277 |
| BBH 2 | $(3, 100)$ | $(3, 100)$ | $(10, 20)$ | 1/18 | 0.99 | 0.05 | 0.5 | 3 | 3, 4, 3 | 41.5, 33.5, 10.3 | 1607 |
| BBH 3 | | | $(20, 40)$ | | | | 0.45 | 3 | 2, 2, 2 | 11.7, 10.8, 4.9 | 225 |
| BBH 4 | | | $> 40$ | | | | 0.35 | 5 | 2, 2, 2, 1, 1 | 2.9, 2.0, 1.1, 0.7, 0.5 | 46 |
| Total | | | | | | | | | | | 316 262 |

# Philosophy

If a piece of data cannot be explained by either Gaussian noise or a gravitational wave signal of the type we are looking at it is discarded.

The residuals in the remaining should follow Gaussian statistics

# Holes



GW170817 original data

Inverse-Tukey windowed

Glitch in-painted

With glitch

Windowed

Inpainted hole

Inpainted hole

$$z_w = \sum_f \frac{h^*(f)\, d(f)}{S_w(f)}.$$

$$z_w = C_{ij}^{-1}\, h_i^*\, d_j = h^\dagger\, C^{-1}\, d,$$

$$\tilde{z}_w = h^\dagger\, C^{-1}\, F\, d.$$

GWTC-1: A Gravitational-Wave Transient Catalog of Compact Binary Mergers Observed by LIGO and Virgo during the First and Second Observing Runs

FIG. 15. Normalized spectrograms of the time around common noise artifacts with a time-frequency evolution of a related trigger template overlaid. Top Left: Scattered light artifacts at Hanford with the template of trigger 170616 overlaid. Top Right: A 60-200 Hz nonstationarity at Livingston with the template of trigger 170412 overlaid. Bottom Left: A short duration transient at Livingston with the template of trigger 170630 overlaid. Bottom Right: A blip at Hanford with the template of a sub-threshold high mass trigger overlaid.

**Masking + Vetoing**

$$\frac{Z}{\sigma_Z} = \frac{\sum_f \frac{h^*(f)d(f)}{S_n(f)}}{\sqrt{\sum_f \frac{|h(f)|^2}{S_n(f)}}}$$

Replace: Use inverse covariance with infinite noise inside mask.
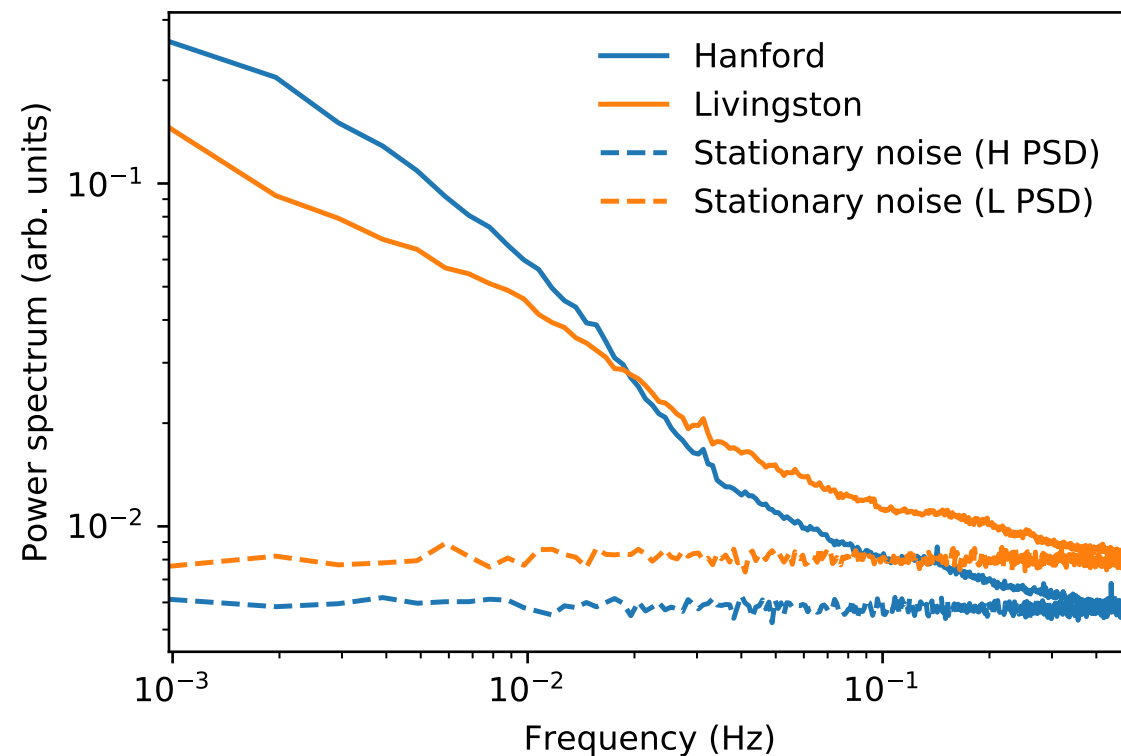
# PSD drift

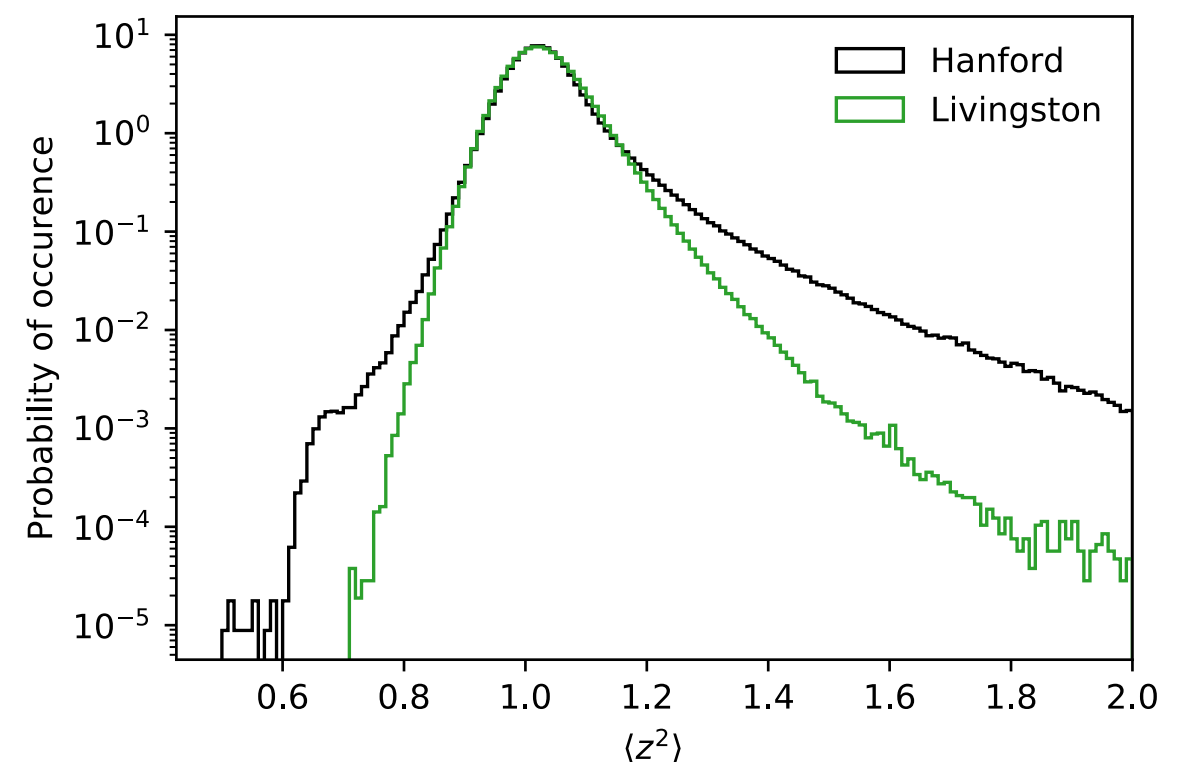## $\tau_{NL}$ non-Gaussianity

## Waveform

[1186963218-1187049618, state: Observing]
### GEO-LIGO-Virgo gravitational-wave strain $[h(t)]$
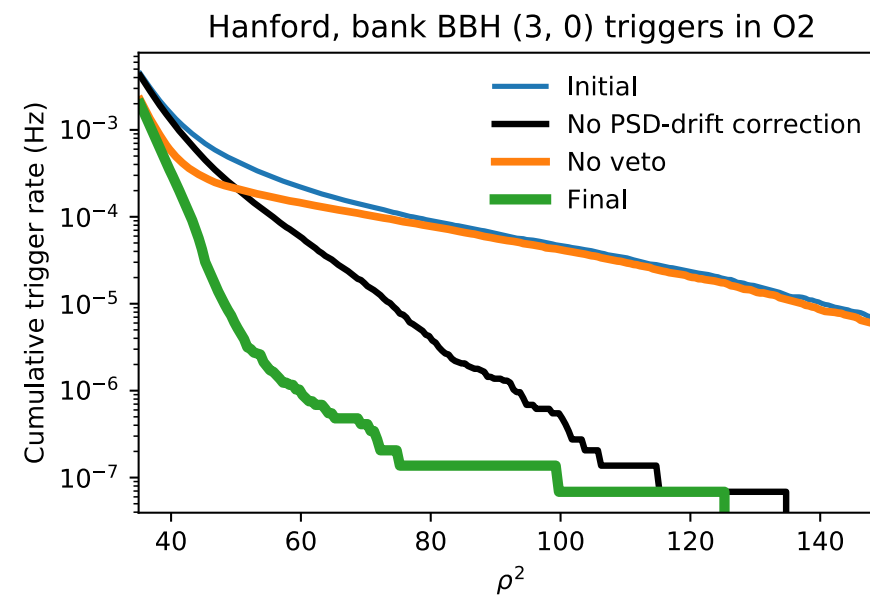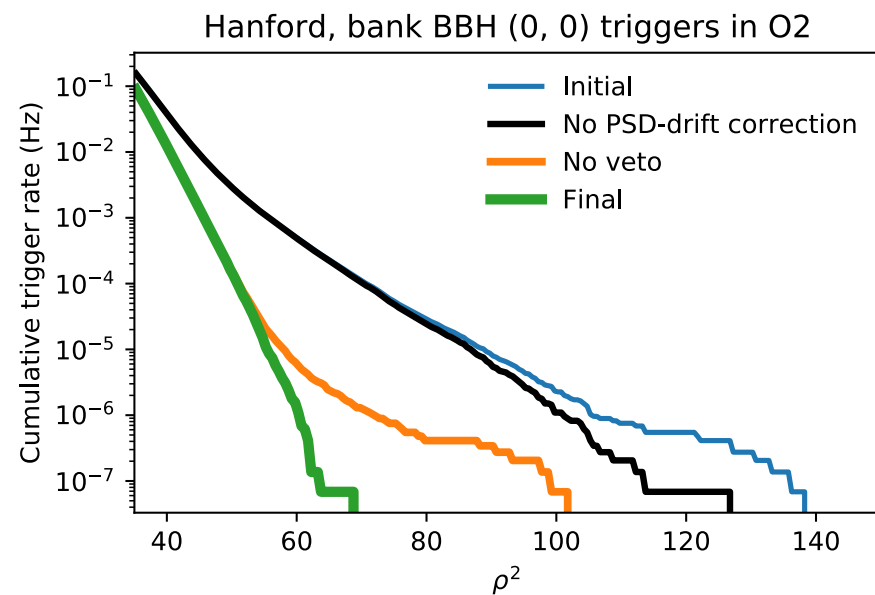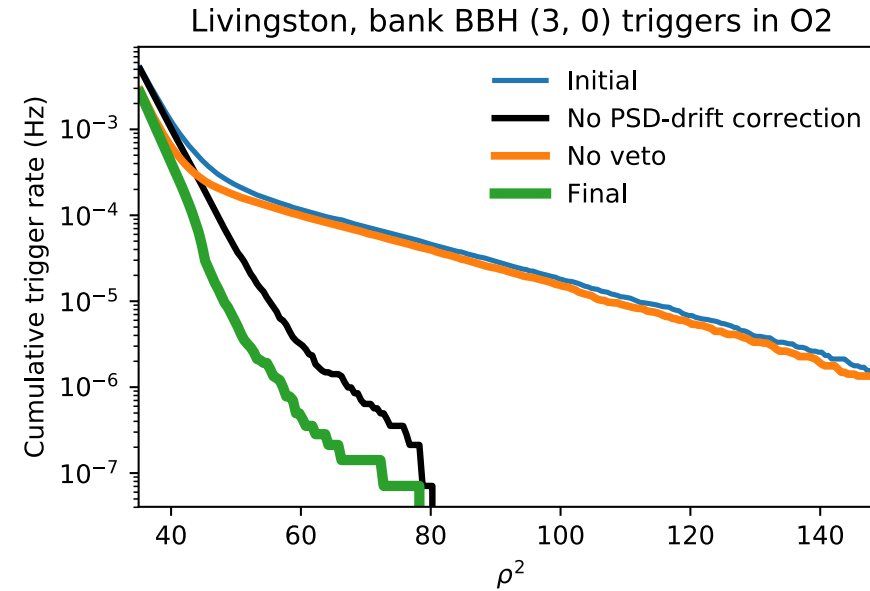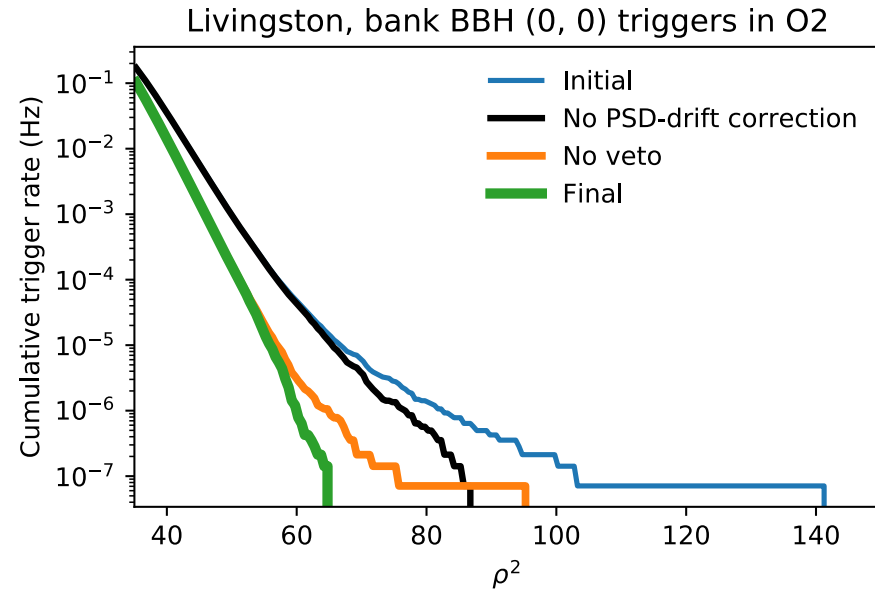
O2
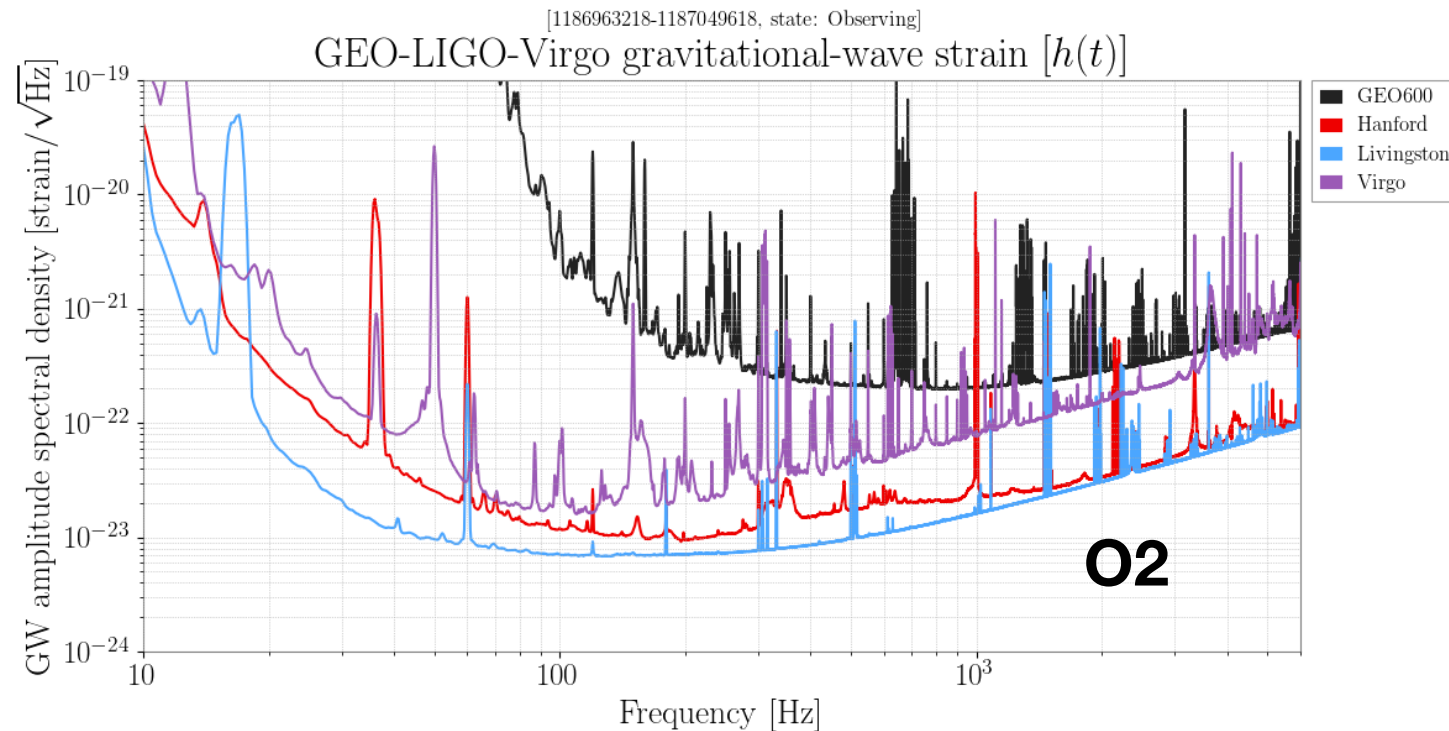
## Whitened strain
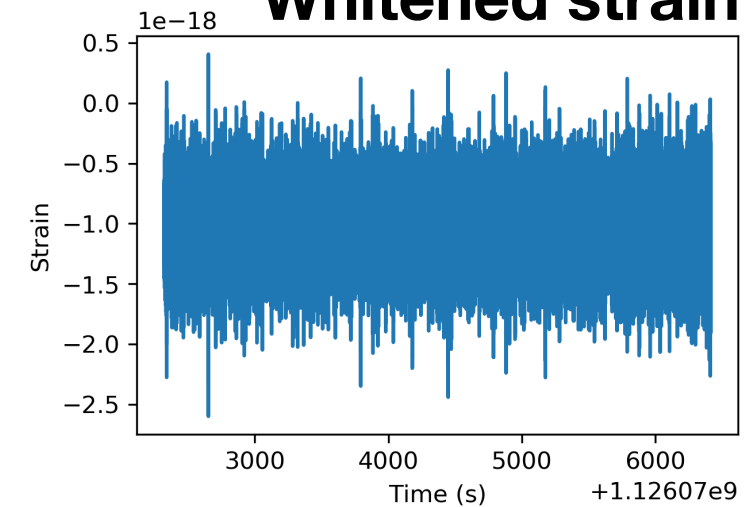
## Power spectrum of the variance of the overlaps

O3

## Distribution of the variance of the overlaps

# Effect of PSD drift and vetoes



Note that these plots are produced with data after masking (holes + in-painting).

Non-G of the data results in orders of magnitude increase in the rate of triggers.

Even in this heavy BBH bank all the outliers in a single detector are real events. Light BBHs and BNS have basically no glitches after masking all the non-G is PSD drift.

Trigger rate for PyCBC above 64 approx $10^{-4}$ Hz.

# Summary

- The origin of BH binaries is an astrophysical puzzle. We might be able to solve it in the near future by studying the properties of individual systems.

- Puzzling results in the heavy and light ends of the BH mass function.  Spin distribution begins to be informative.

- The availability of the LIGO data gives the community an opportunity to try new ideas and propose new methods. We are very grateful to the LVC.

- We have developed a new pipeline and tried to incorporate several new elements, a new geometric template bank algorithm, PSD drift correction, aggressive data masking and hole filling, objective vetoing of triggers, coherent combination of detectors, etc.

- We estimate that our pipeline is sensitive to twice the volume.We have found one new event in O1 and six new events in O2 and produced a new list of sub-threshold candidates. The properties of some of these new events are quite interesting.

- We think that our improvements carry over to the O3 data. Unfortunately that data is not public but will be soon.

# Extra:

# Advanced Ligo Observing Runs
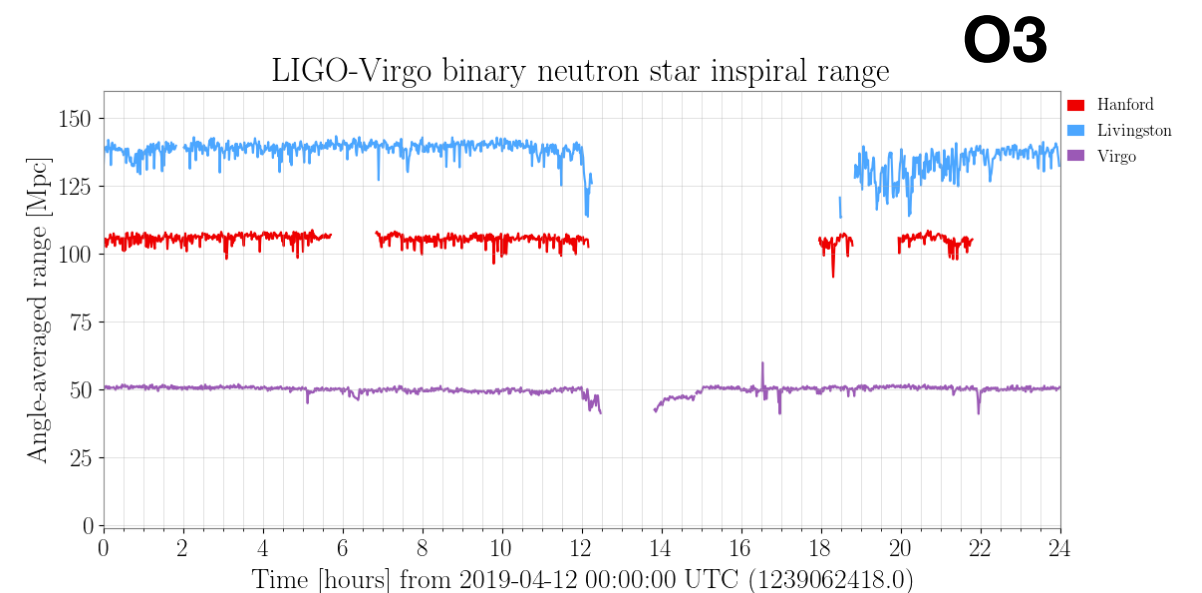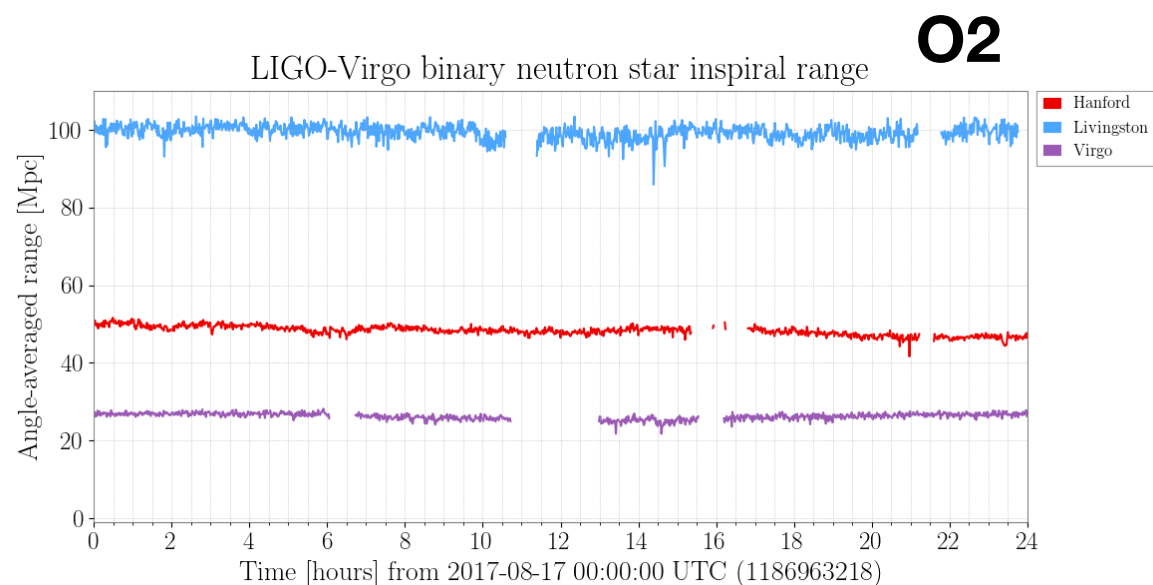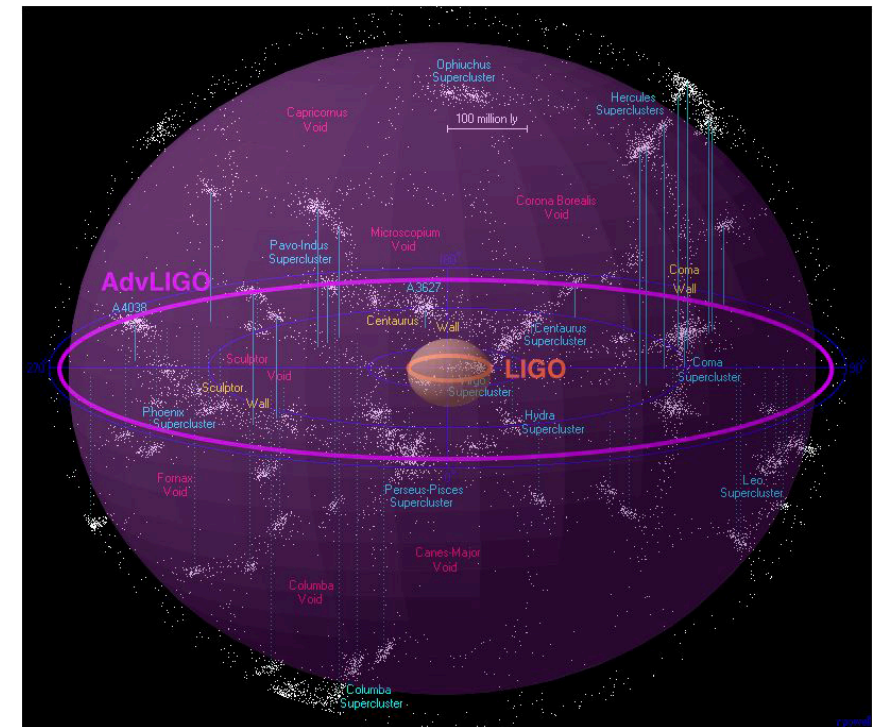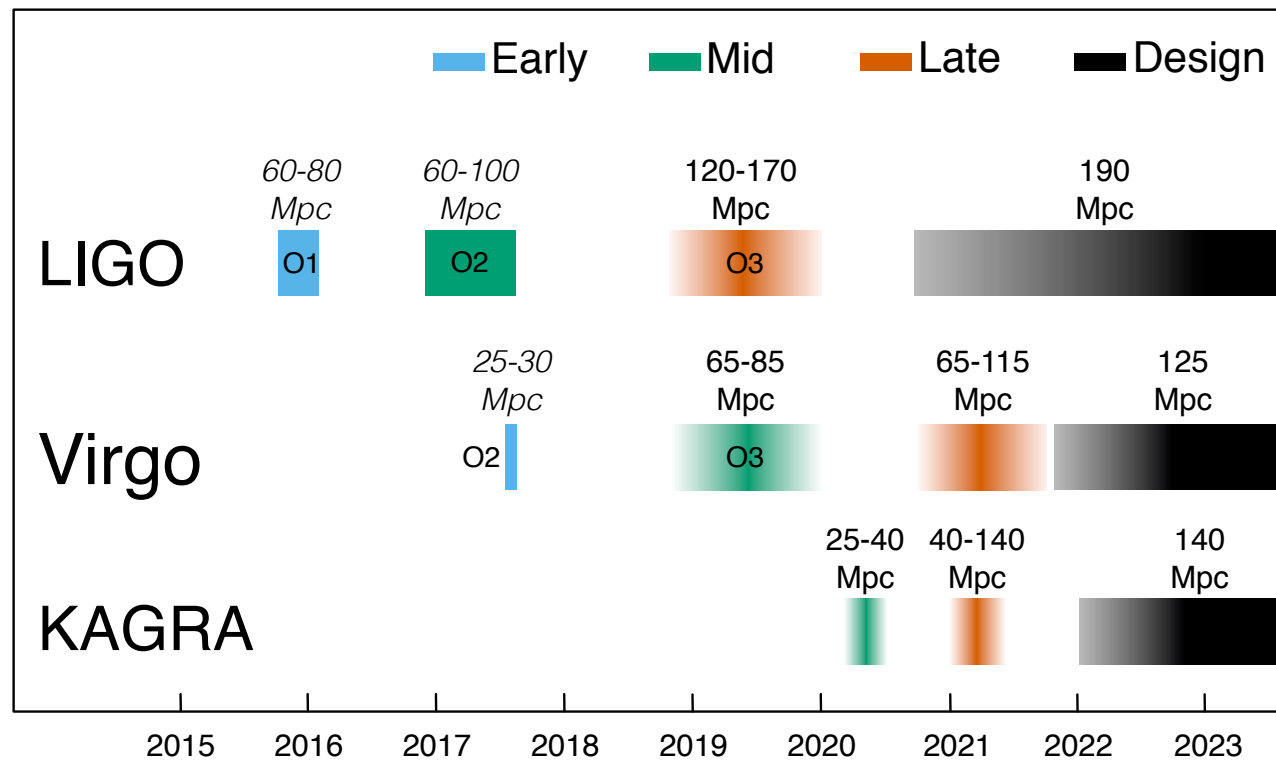
# Neutron star mergers

- What happens when two neutron stars merge? What should one see at different wavelengths and in different directions?

- Sizes of neutron stars (high frequencies in the GW signal)

- What is left after the merger?

- Origin of heavy elements (r-process elements)

- Speed of propagation of gravitational waves (part in $10^{15}$)

- Distance scale (Hubble constant; error 10 km/s/Mpc per event)
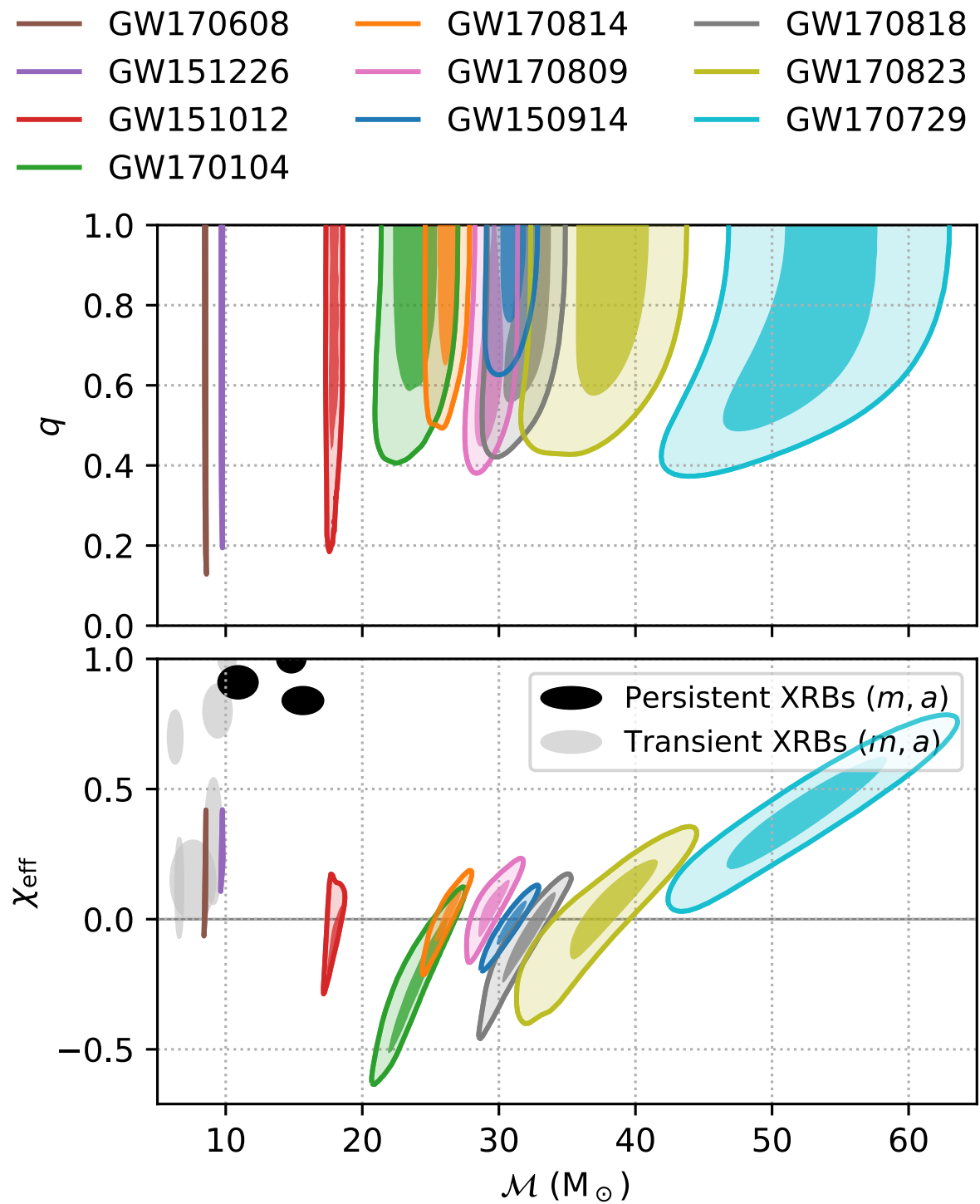
# Binary Black Holes (stellar)

- Do BH behave as GR predicts?

- Distance scale (Hubble constant; no counter-part so only statistical through clustering)

- Properties of the evolution of massive stars (BH mass vs initial mass)

- What is the origin of the black hole binaries?
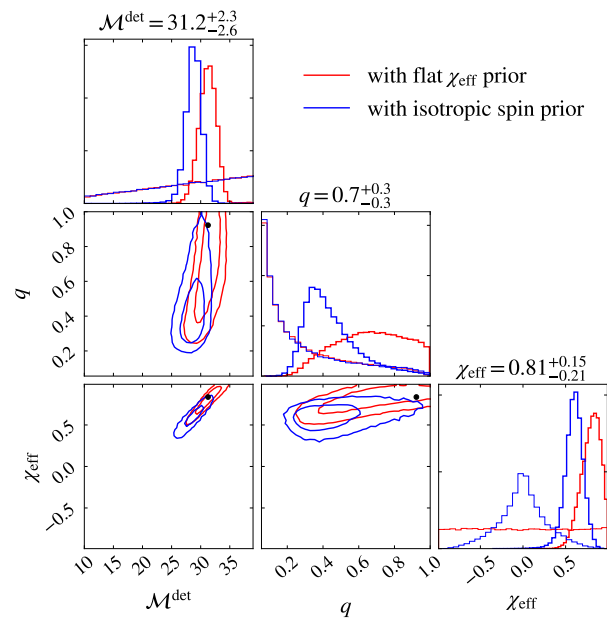
# LIGO Events O1 + O2



Mass ratio

**Combined spin in the direction of the angular momentum**

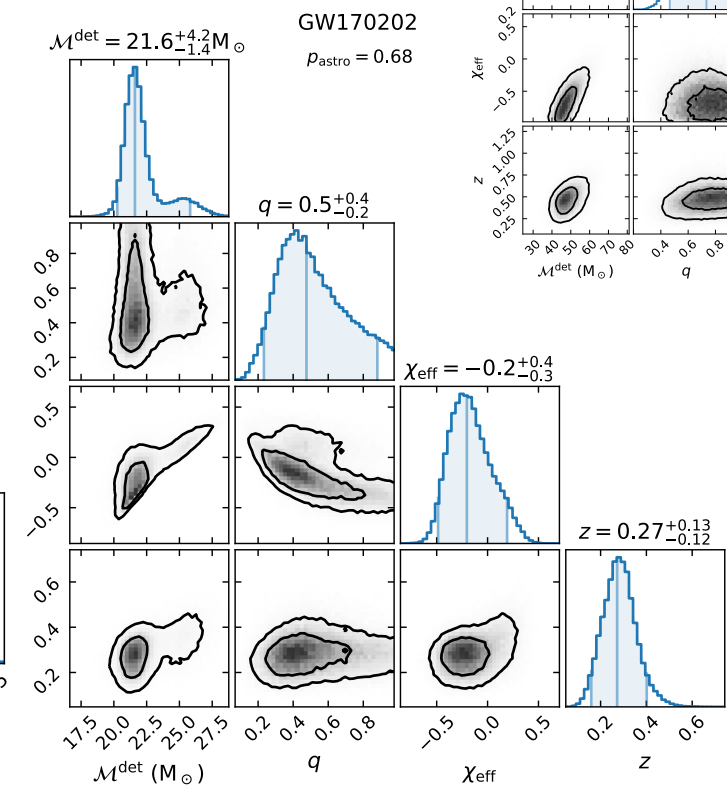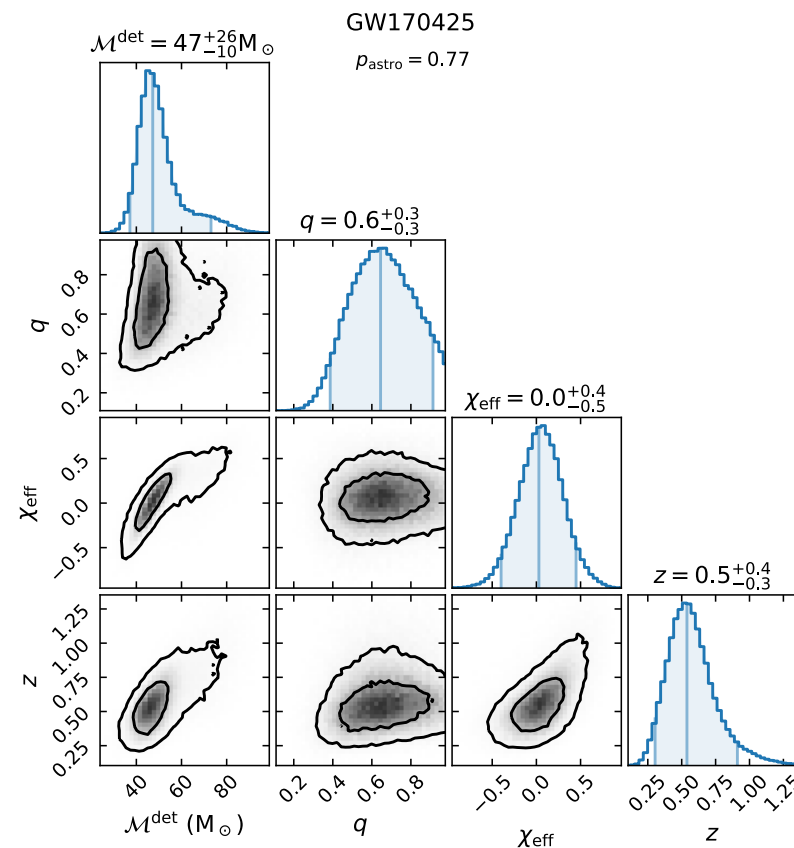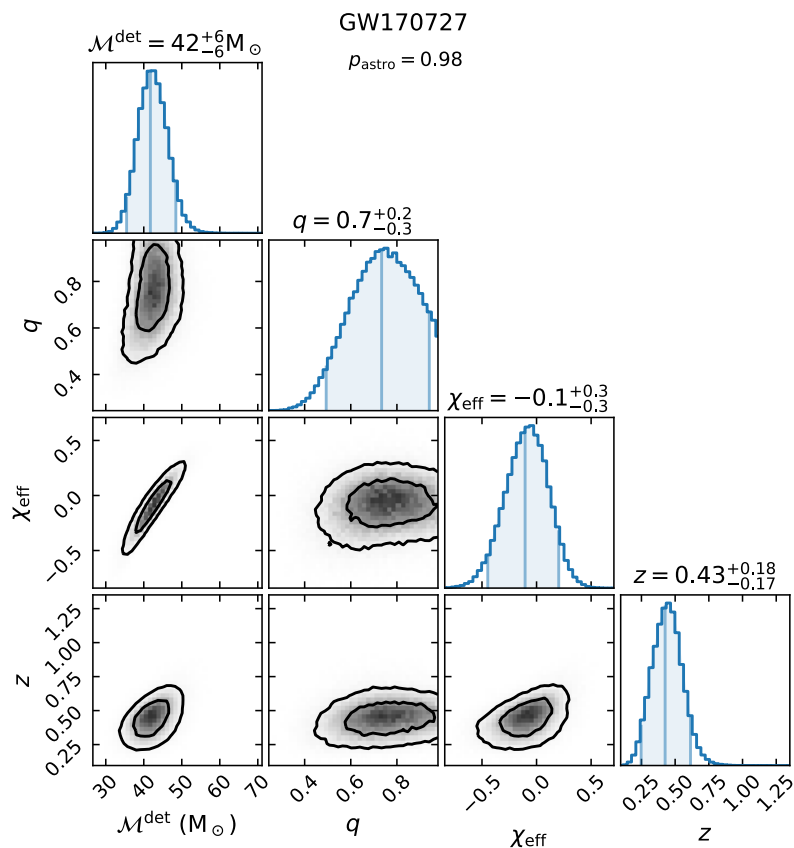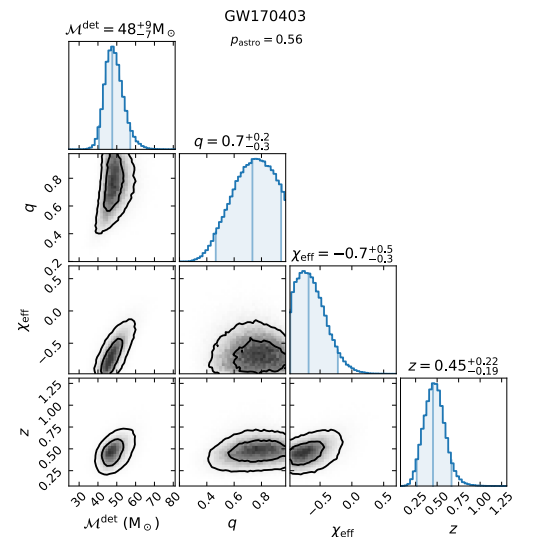$$\chi_{\text{eff}} = (m_1\,\chi_{1z} + m_2\,\chi_{2z})/M$$

Chirp mass

# Parameters of new detections



GW151216

GW170121

$\mathcal{M}^{\rm det} = 29^{+4}_{-3}{\rm M}_\odot$    $p_{\rm astro} > 0.99$

$q = 0.76^{+0.19}_{-0.26}$

$\chi_{\rm eff} = -0.3^{+0.3}_{-0.3}$

$z = 0.24^{+0.14}_{-0.13}$

GW170304

$\mathcal{M}^{\rm det} = 47^{+8}_{-9}{\rm M}_\odot$    $p_{\rm astro} = 0.985$

$q = 0.75^{+0.19}_{-0.25}$

$\chi_{\rm eff} = 0.2^{+0.3}_{-0.3}$

$z = 0.5^{+0.2}_{-0.2}$

GW170403

$\mathcal{M}^{\rm det} = 48^{+9}_{-7}{\rm M}_\odot$    $p_{\rm astro} = 0.56$

$q = 0.7^{+0.2}_{-0.3}$

$\chi_{\rm eff} = -0.7^{+0.5}_{-0.3}$

$z = 0.45^{+0.22}_{-0.19}$

GW170727

$\mathcal{M}^{\rm det} = 42^{+6}_{-6}{\rm M}_\odot$    $p_{\rm astro} = 0.98$

$q = 0.7^{+0.2}_{-0.3}$

$\chi_{\rm eff} = -0.1^{+0.3}_{-0.3}$

$z = 0.43^{+0.18}_{-0.17}$

GW170425

$\mathcal{M}^{\rm det} = 47^{+26}_{-10}{\rm M}_\odot$    $p_{\rm astro} = 0.77$

$q = 0.6^{+0.3}_{-0.3}$

$\chi_{\rm eff} = 0.0^{+0.4}_{-0.5}$

$z = 0.5^{+0.4}_{-0.3}$

GW170202

$\mathcal{M}^{\rm det} = 21.6^{+4.2}_{-1.4}{\rm M}_\odot$    $p_{\rm astro} = 0.68$

$q = 0.5^{+0.4}_{-0.2}$

$\chi_{\rm eff} = -0.2^{+0.4}_{-0.3}$

$z = 0.27^{+0.13}_{-0.12}$

$\mathcal{M}^{\rm det} = 31.2^{+2.3}_{-2.6}$

$q = 0.7^{+0.3}_{-0.3}$

$\chi_{\rm eff} = 0.81^{+0.15}_{-0.21}$

with flat $\chi_{\rm eff}$ prior
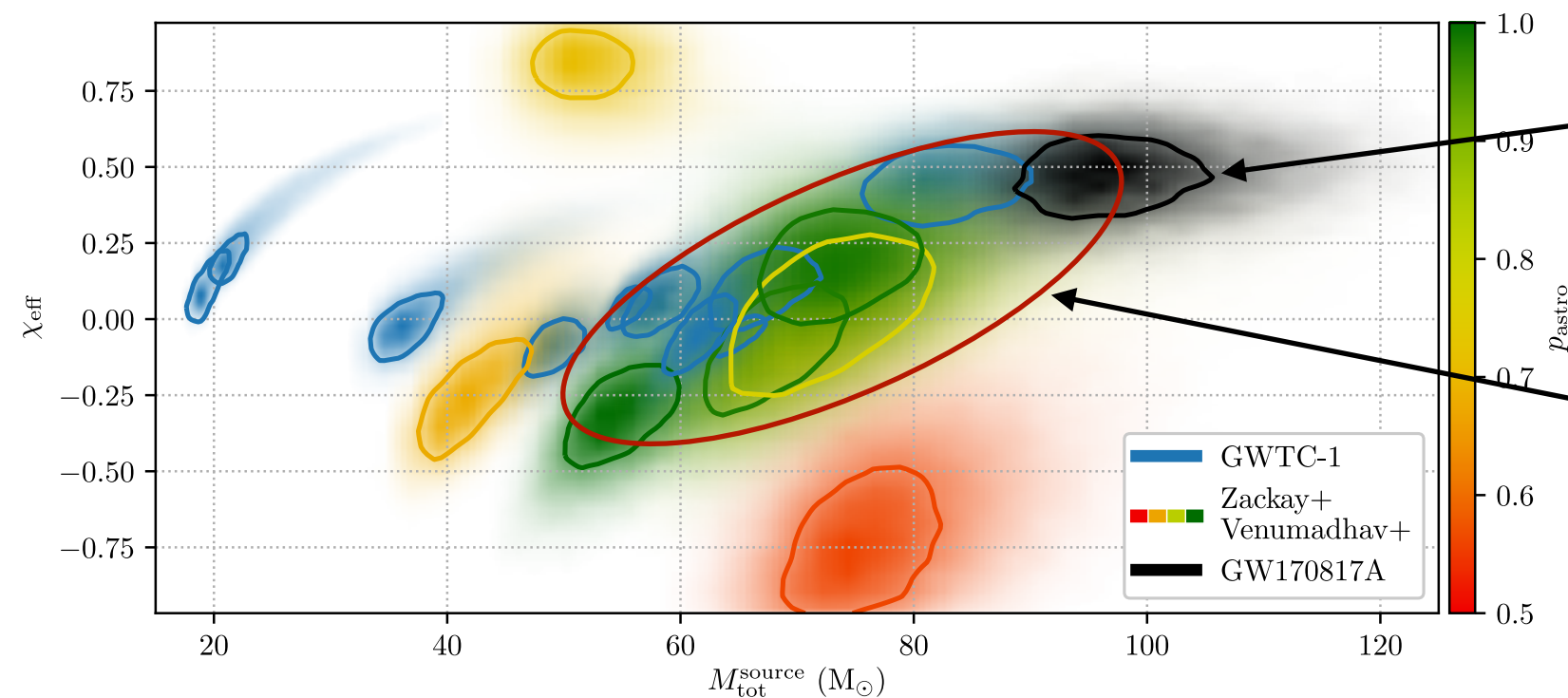with isotropic spin prior

High spin points to this system being formed through binary evolution. Inconsistent with the isotropic prior, meaning it is inconsistent with scenarios that produce this prior. Obviously outlier with respect to spin. Similar mass and both spinning or differ by factor of 2 in mass and heavy is highly spinning.
High redshift, suggestive?

Heaviest so far. Implications for mass gap? Note this is a detector and a half event.

Suggestive trend?

FIG. 7: Binary black holes events reported from O1 and O2, in the plane of source-frame total mass vs. effective spin. In blue are shown the 10 BBH events reported in GWTC-1 [1], all of them are certainly astrophysical in origin ($p_{astro} = 1$). Color coded by $p_{astro}$ are shown 7 additional events with $p_{astro} > 0.5$ that our previous searches found [2, 4]. In black we show GW170817A. Displayed are $1\sigma$ probability contours, i.e. enclosing $1 - e^{-1/2} \approx 0.39$ of the probability distribution.

# Single detector search
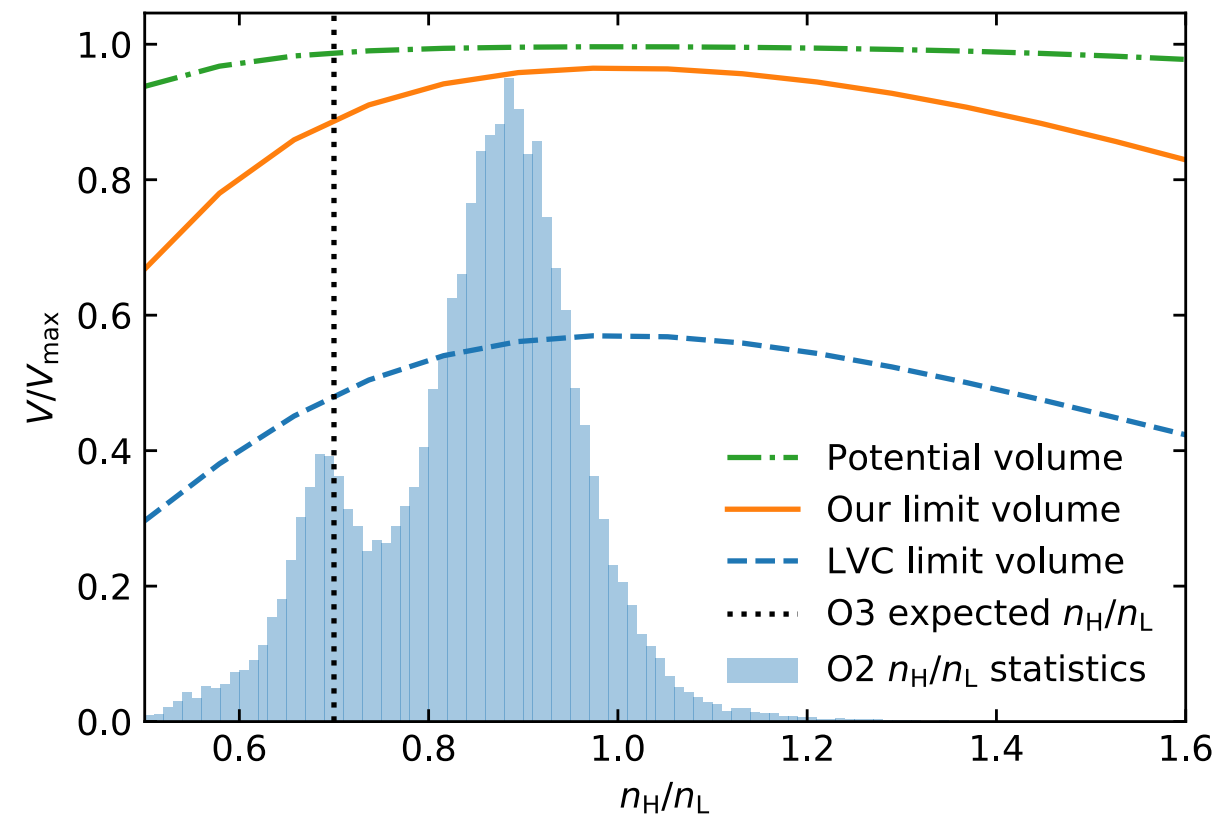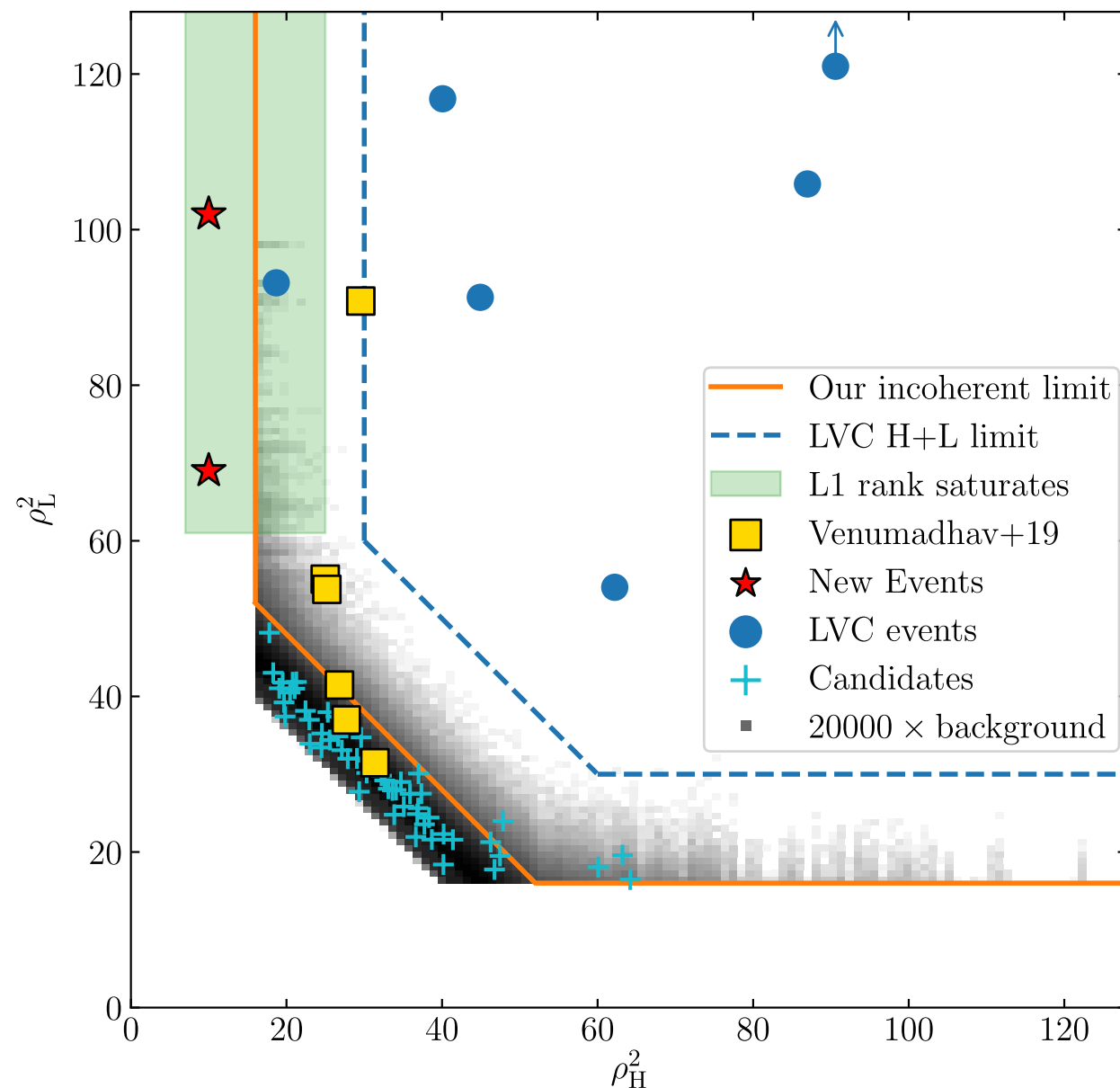


Asymmetric detectors is difficult:
1. Empirical probability in L difficult to measure
2. Signal in H can be below collection limit

# Single detector search

| Bank ID | # $\rho_L^2 > 45$ | # $\rho_L^2 > 55$ | # $\rho_L^2 > 65$ |
|---|---|---|---|
| (2,0) | 10178 | 172 | 1 |
| (2,1) | 1558 | 50 | 7 |
| (2,2) | 734 | 226 | 102 |
| (3,0) | 337 | 18 | 7[a] |
| (3,1) | 157 | 11 | 3 |
| (3,2) | 41 | 8 | 4 |
| (4,0) | 37 | 3 | 1[b] |
| (4,1) | 14 | 1 | 0 |
| (4,2) | 9 | 3 | 2 |
| (4,3) | 32 | 11 | 4 |
| (4,4) | 215 | 77 | 31 |

[a] Six of the seven triggers in bank (3,0) are previously declared gravitational wave signals. The seventh is declared in this paper
[b] This trigger is GW170823


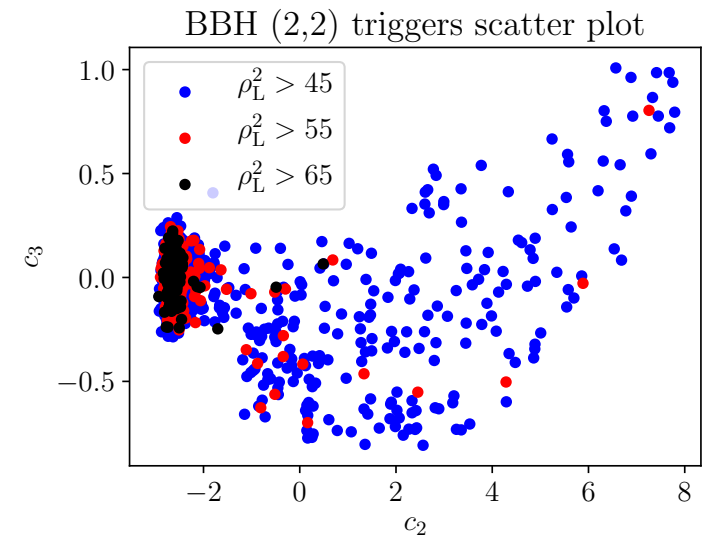
BBH (2,2) triggers scatter plot

FIG. 8: The table in the left-hand panel shows the number of veto-passing L1 triggers in each sub-bank above a few threshold values of the SNR. The non-uniform numbers of triggers with $\rho_L^2 > 65$ shows that glitches are localized within certain sub-banks. The plot in the right-hand panel shows the coefficients labeling the templates for triggers above the thresholds for bank BBH (2, 2). Note that glitches are localized within a small region of parameter space.
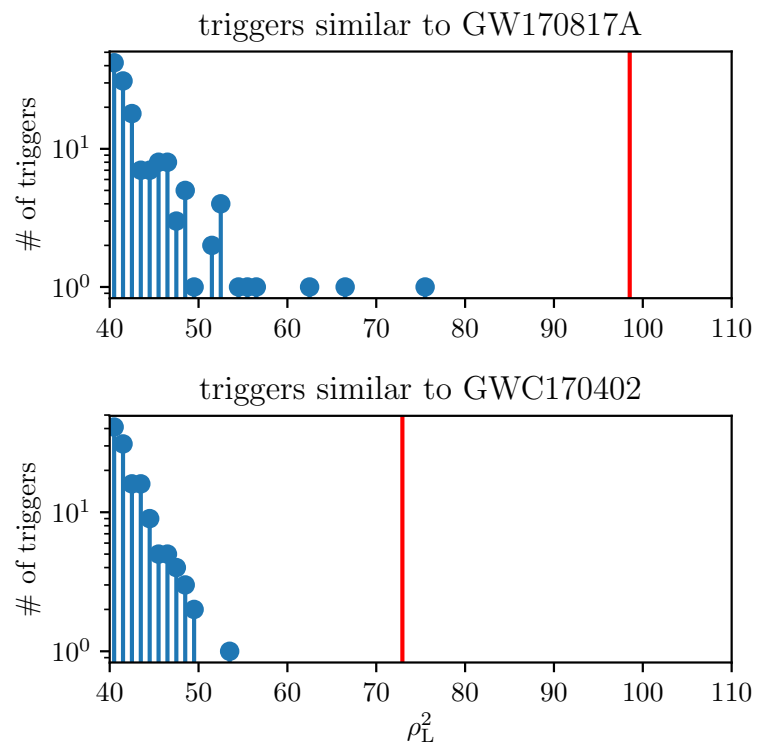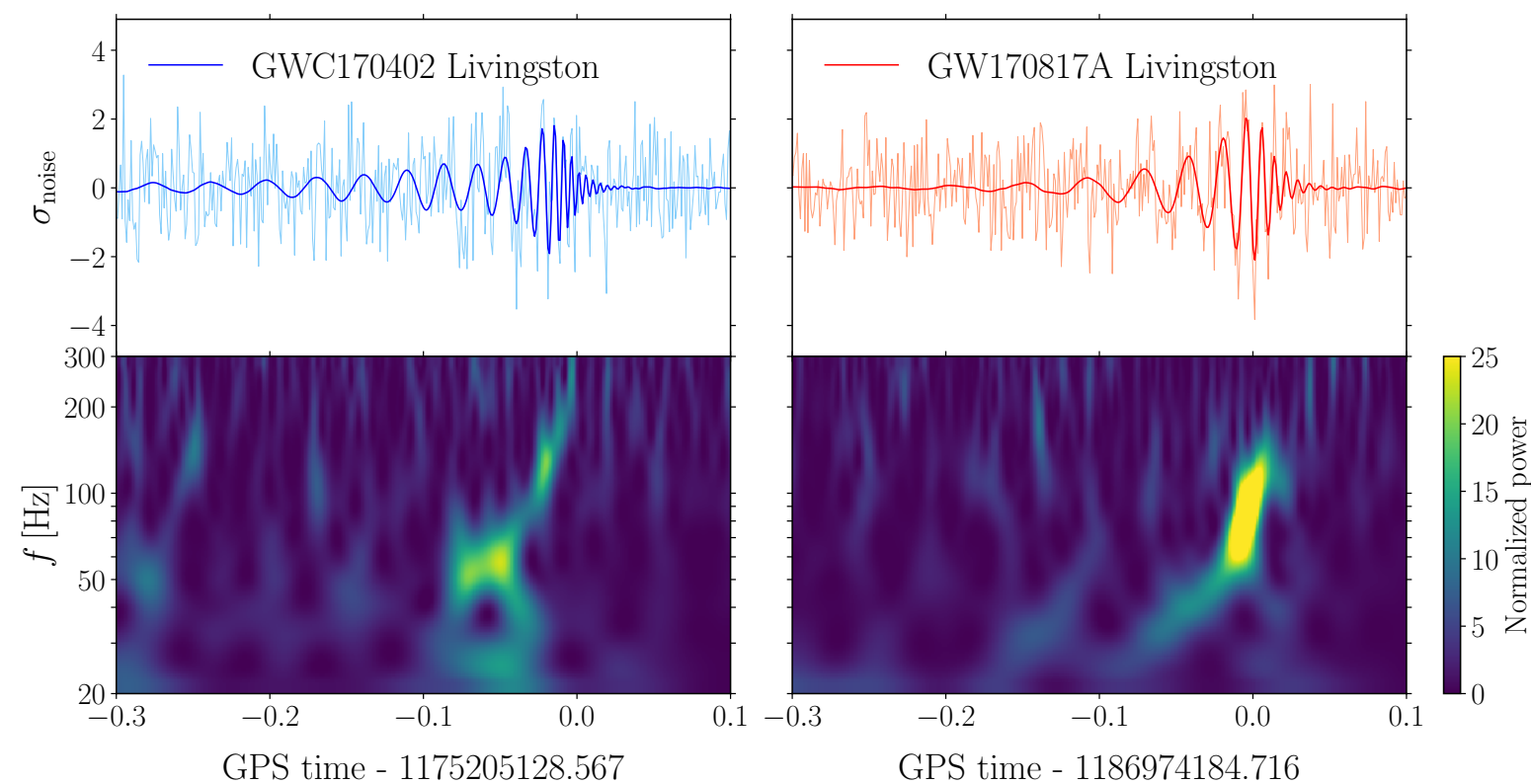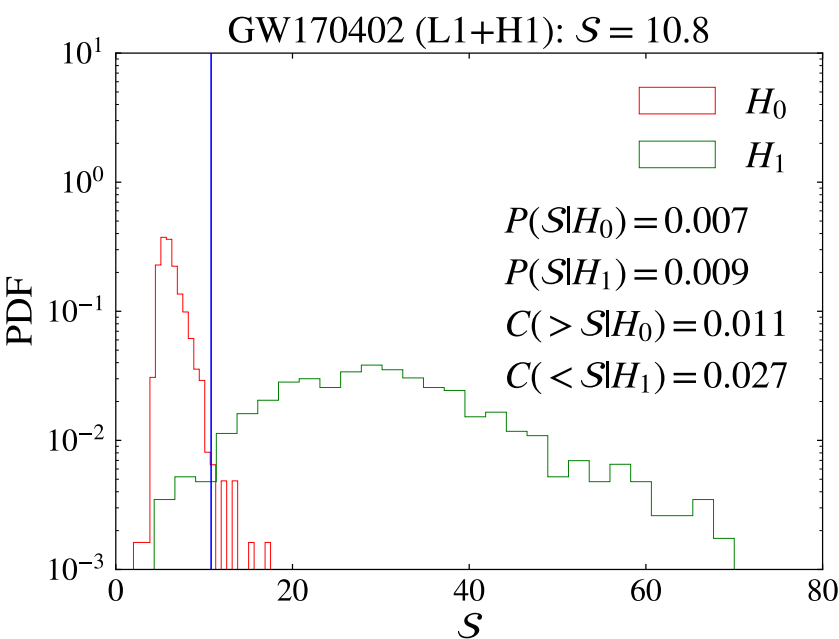


FIG. 3: Distributions of L1 SNR$^2$ for triggers for templates that are similar (match > 0.9) to the best-fit templates for the two newly found events, that occur at times when the H1 detector is operative. Vertical red lines mark the values of $\rho_L^2$ for the two events. To give context to the amount of phase space that is included in this plot, the upper (lower) panel includes triggers from 28% (0%) of bank BBH 4, and 1.8% (3.6%) of bank BBH 3.
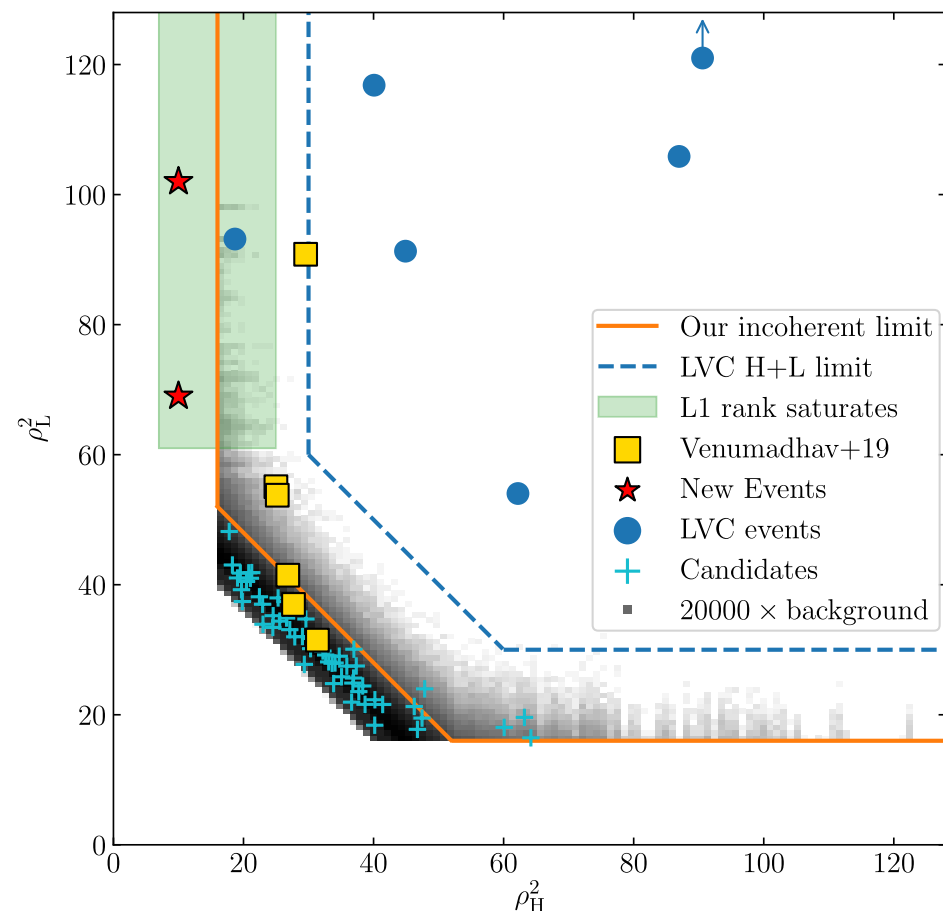
# Single detector search



$$e^{\mathcal{S}} := \int \mathcal{D}\boldsymbol{\Theta}_{\text{ext}}\, \Pi(\boldsymbol{\Theta}_{\text{ext}})\, \mathcal{L}(\boldsymbol{d}|\boldsymbol{\Theta}_{\text{intr}}, \boldsymbol{\Theta}_{\text{ext}}).$$

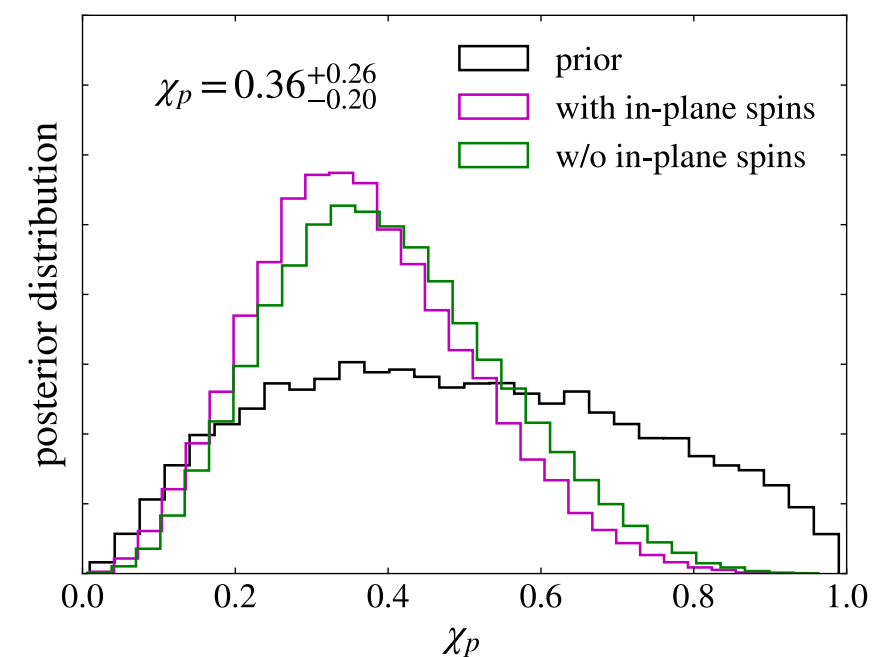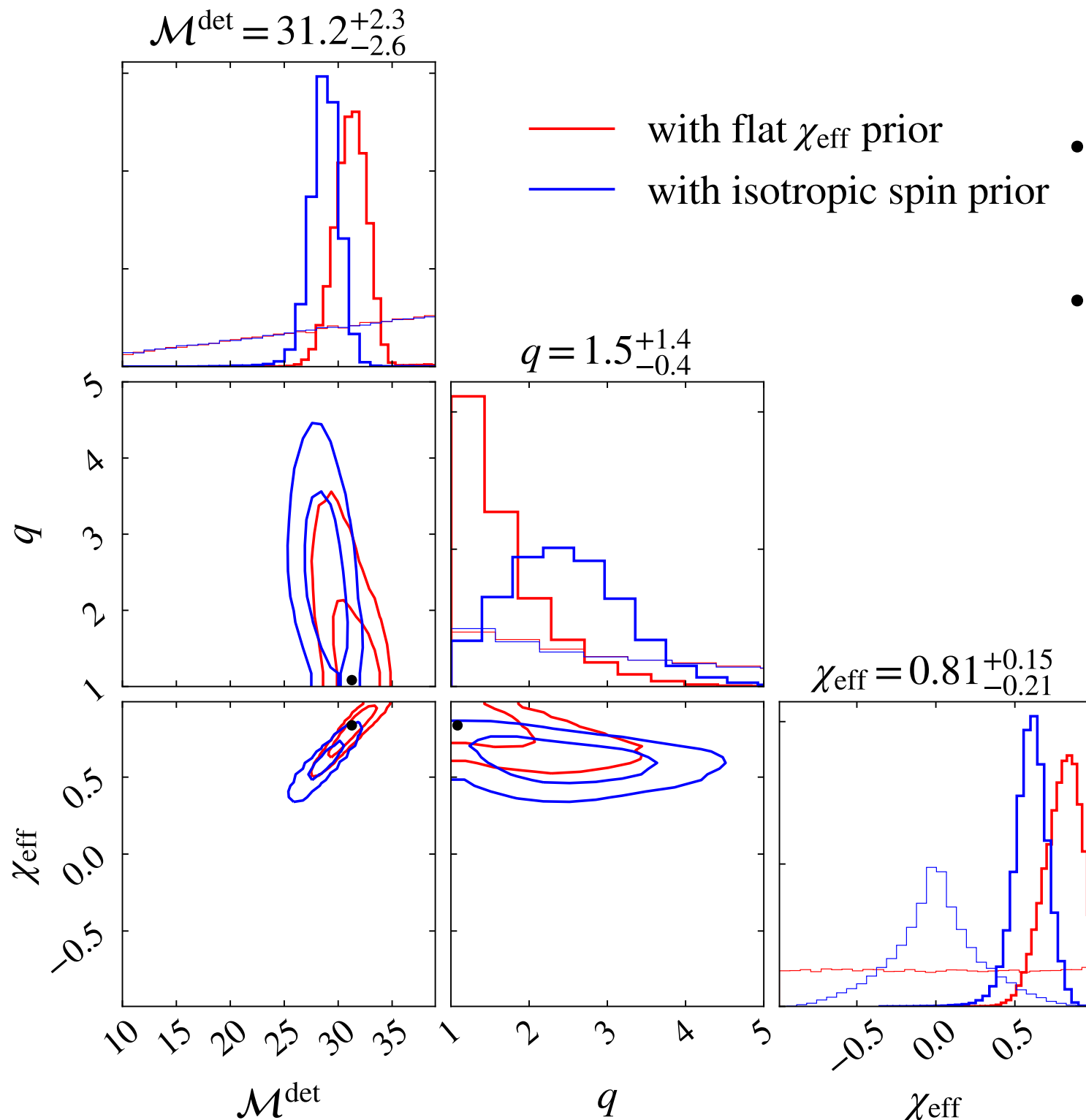| L1 rank | GPS time | $\rho_{\text{L}}^2$ | # similar triggers | $C(\mathcal{S}|H_0)$ | $C(\mathcal{S}|H_1)$ | $\frac{P(\mathcal{S}|H_1)}{P(\mathcal{S}|H_0)}$ | Comment |
|---|---|---|---|---|---|---|---|
| 1 | 1187058327.068 | 93.1 | 0 | $< 10^{-3}$ | 0.16 | 37 | GW170818[a] |
| 2 | 1187529256.504 | 92.1 | 0 | - | - | - | GW170823 |
| 3 | 1169069154.564 | 90.8 | 0 | - | - | - | GW170121 |
| **4** | **1175205128.565** | **72.9** | **0** | **0.015** | **0.022** | **0.547** | **GWC170402** |
| 5 | 1186741861.51 | 174.6 | 1 | - | - | - | GW170814 |
| 6 | 1167559936.584 | 107.3 | 1 | - | - | - | GW170104 |
| 7 | 1186302519.731 | 118.6 | 2 | - | - | - | GW170809 |
| **8** | **1186974184.716** | **98.5** | **5** | **0.028** | **0.055** | **0.98** | **GW170817A** |
| 9 | 1174043898.842 | 75.7 | 9 | 0.36 | 0.001 | 0.008 | Background |
| 10 | 1170885005.109 | 66.4 | 16 | 0.49 | 0.003 | 0.013 | Background |
| 11 | 1178083239.592 | 74.4 | 22 | 0.34 | 0.003 | 0.016 | Background |
| Removed[b] | 1173477193.704 | 69.2 | 1 | 0.38 | 0.014 | 0.011 | Artifacts present |
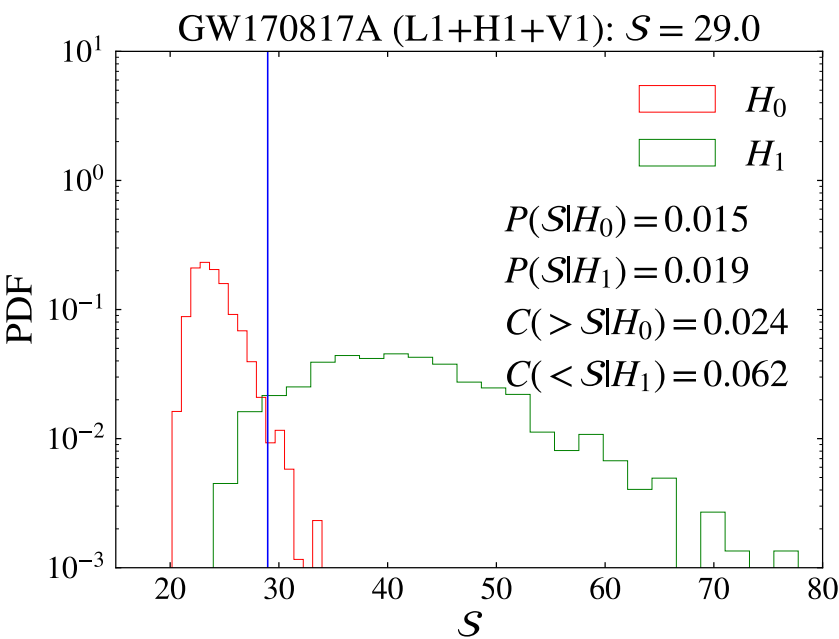
# Potential Lensing Event



TABLE I: Summary of derived significance and inferred physical parameters. Time delays, Morse phase differences, and magnification ratios are quoted for the three events GW170104, GWC170620 and GW170814 ordered according to the event date.

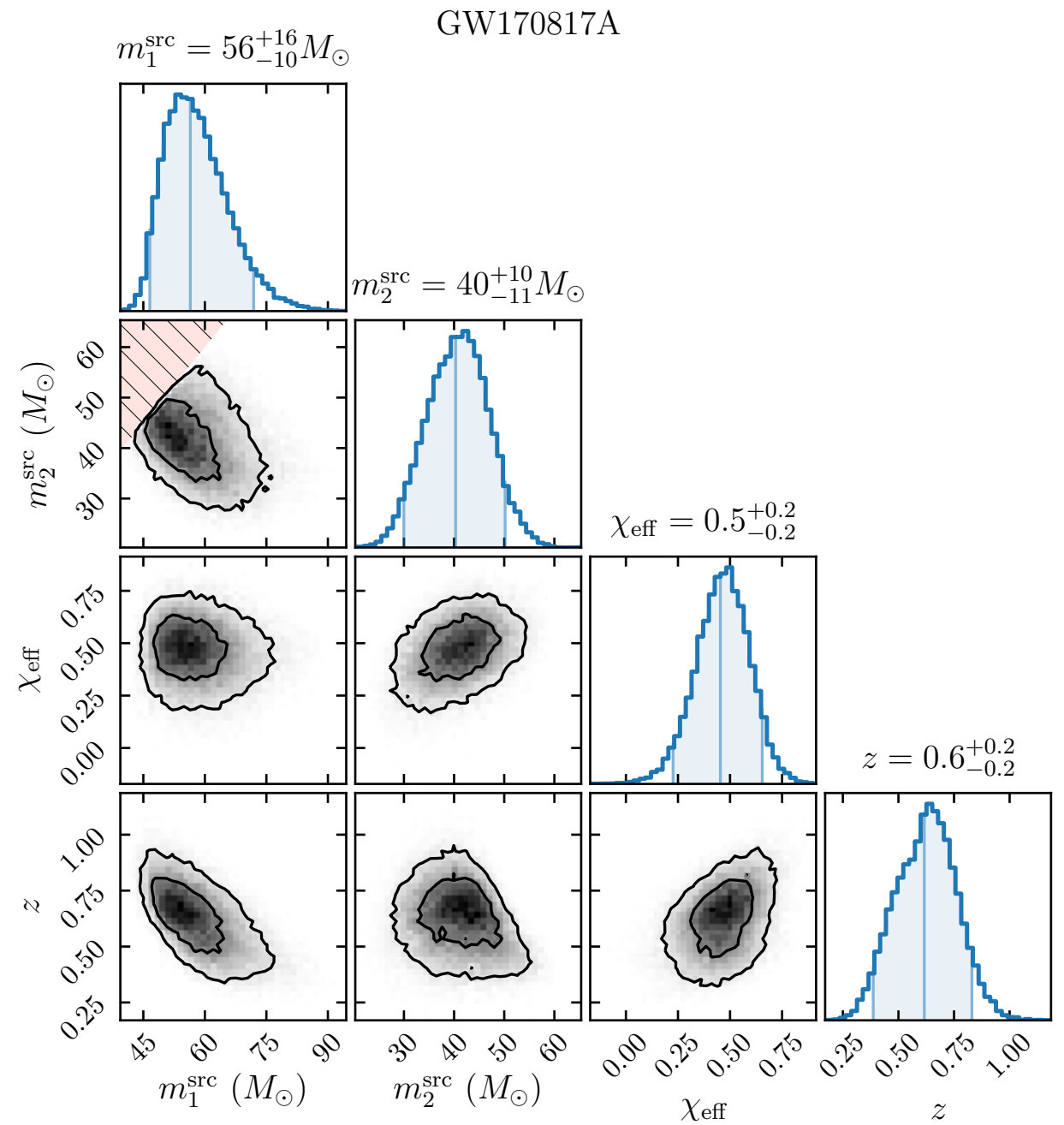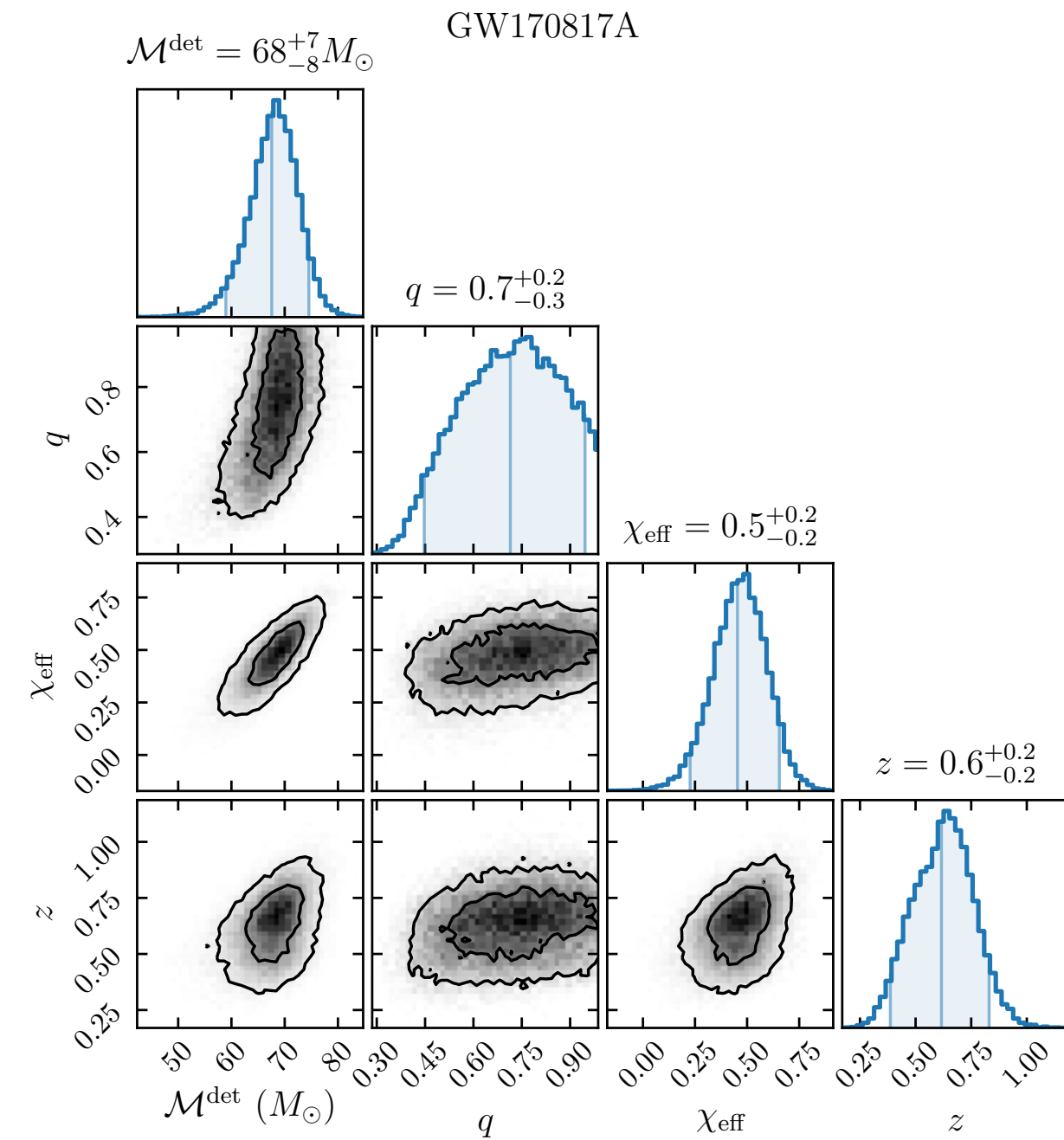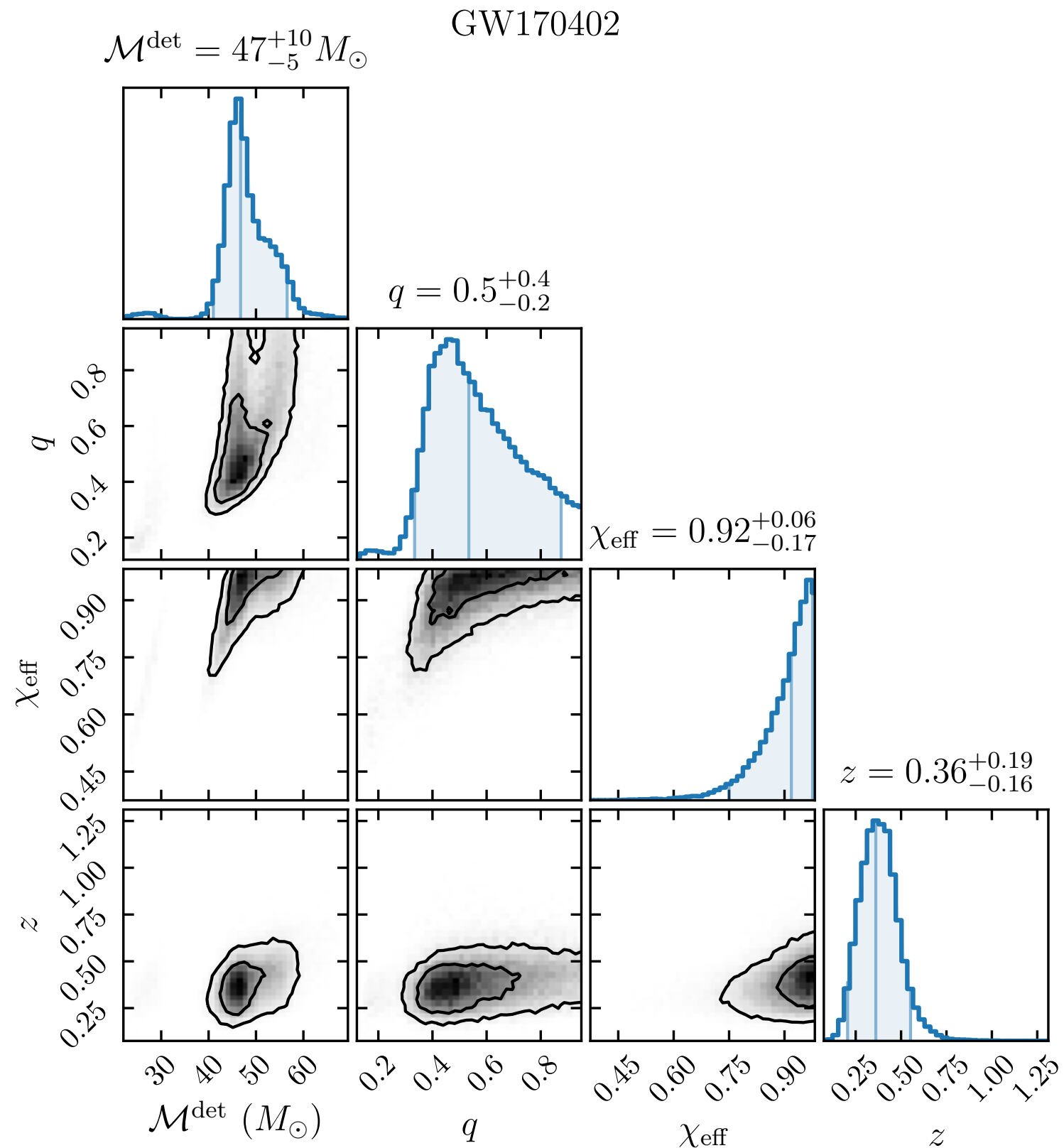| Item | Value | Reference |
|---|---|---|
| Catalog FAP (GW170104, GW170814) | $1.2 \times 10^{-2}$ | Section II |
| Existence of GWC170620 (GPS time: 1181956460) | $8.5 \times 10^{-3}$ | Section II |
| Time delays (relative to GW170104) | 0, 166.63 days, 222.01 days | Section IV |
| Morse phase differences (relative to GW170104) | $0, \pi, \pi$ | Section III |
| Magnification ratios (relative to GW170814) | $0.401 \pm 0.08$, $0.0719 \pm 0.0024$, 1 | Section III |
| Apparent luminosity distance of GW170814 | $D_L^{\mathrm{GW170814}}/\sqrt{\mu_{\mathrm{GW170814}}} = 577^{+159}_{-216}$ Mpc | Section III |
| Expected number of lensed events in O2 | $10^{-2}$–$10^{-3}$ | [5–9, 20][a] |
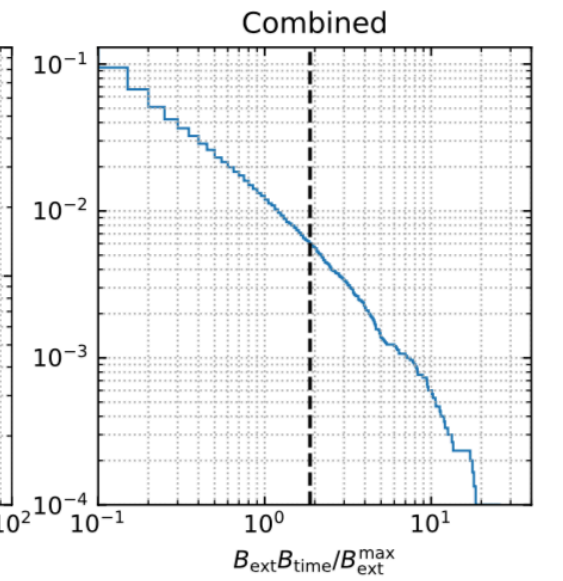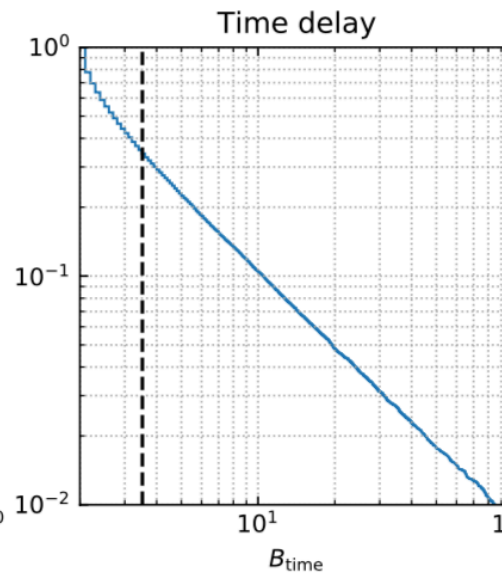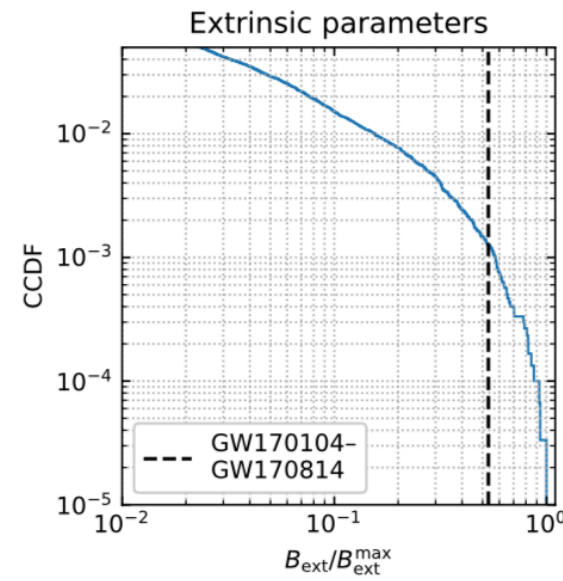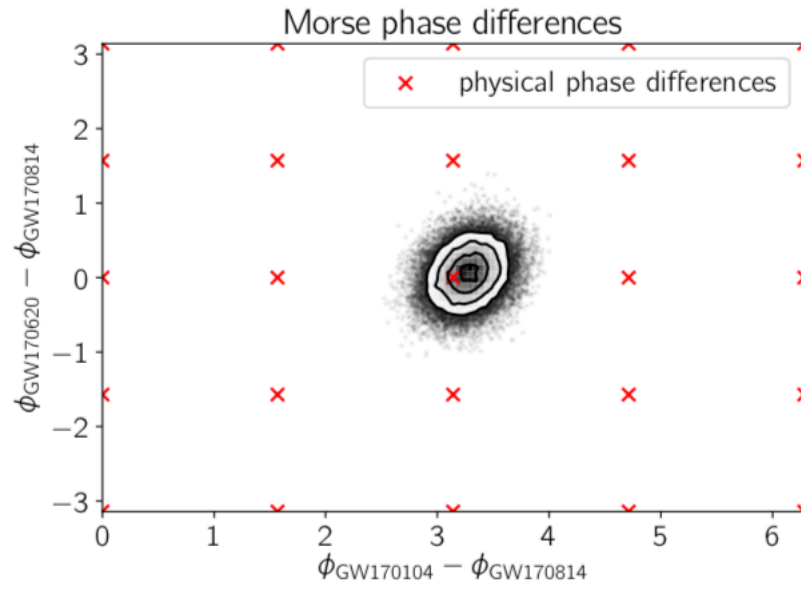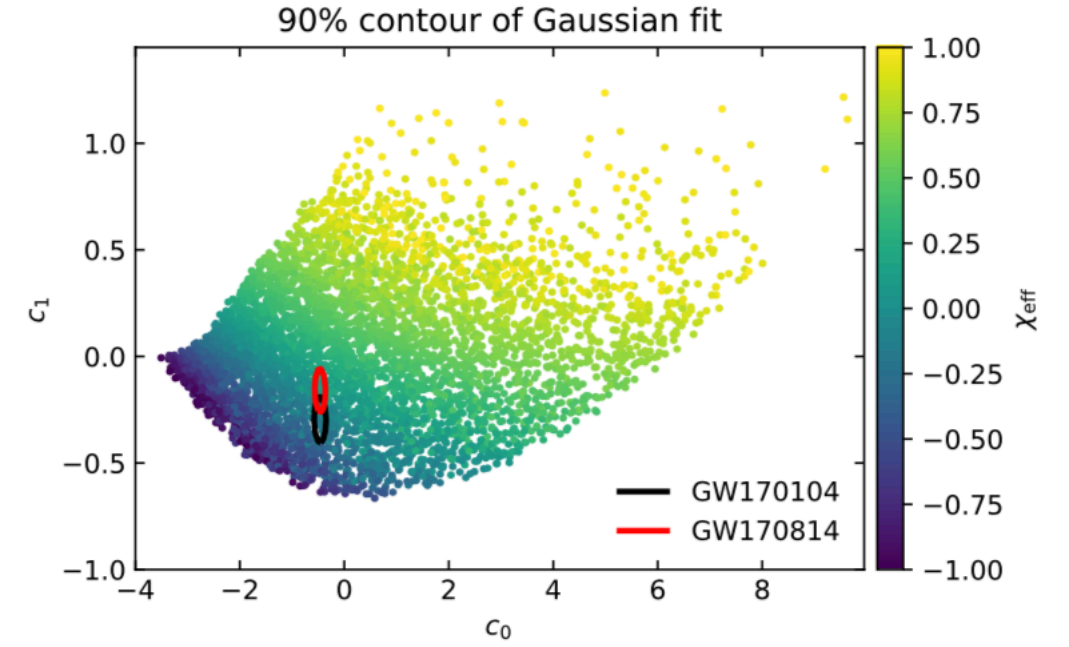
# Posteriors



- The isotropic spin prior penalizes high aligned spins. The maximum likelihood point is penalized severely.

- Adopting a flat prior in $\chi_{\rm eff}$ leads to significant shifts in parameters

- The data has no information about the perpendicular spin component.

$\mathcal{M}^{\rm det} = 31.2^{+2.3}_{-2.6}$

with flat $\chi_{\rm eff}$ prior

with isotropic spin prior

$q = 1.5^{+1.4}_{-0.4}$

$\chi_{\rm eff} = 0.81^{+0.15}_{-0.21}$

$\chi_p = 0.36^{+0.26}_{-0.20}$

prior

with in-plane spins

w/o in-plane spins

posterior distribution

$\chi_p$

# "Very massive single detector event"



GW170817A

$\mathcal{M}^{\mathrm{det}} = 68^{+7}_{-8} M_\odot$

$q = 0.7^{+0.2}_{-0.3}$

$\chi_{\mathrm{eff}} = 0.5^{+0.2}_{-0.2}$

$z = 0.6^{+0.2}_{-0.2}$

GW170817A

$m_1^{\mathrm{src}} = 56^{+16}_{-10} M_\odot$

$m_2^{\mathrm{src}} = 40^{+10}_{-11} M_\odot$

$\chi_{\mathrm{eff}} = 0.5^{+0.2}_{-0.2}$

$z = 0.6^{+0.2}_{-0.2}$

# "Highly spinning single detector event"



GW170402

$\mathcal{M}^{\rm det} = 47^{+10}_{-5} M_\odot$

$q = 0.5^{+0.4}_{-0.2}$

$\chi_{\rm eff} = 0.92^{+0.06}_{-0.17}$

$z = 0.36^{+0.19}_{-0.16}$

# New template bank construction

$$\tilde{h}(f; \boldsymbol{p}) = A(f; \boldsymbol{p})e^{i\psi(f; \boldsymbol{p})}$$
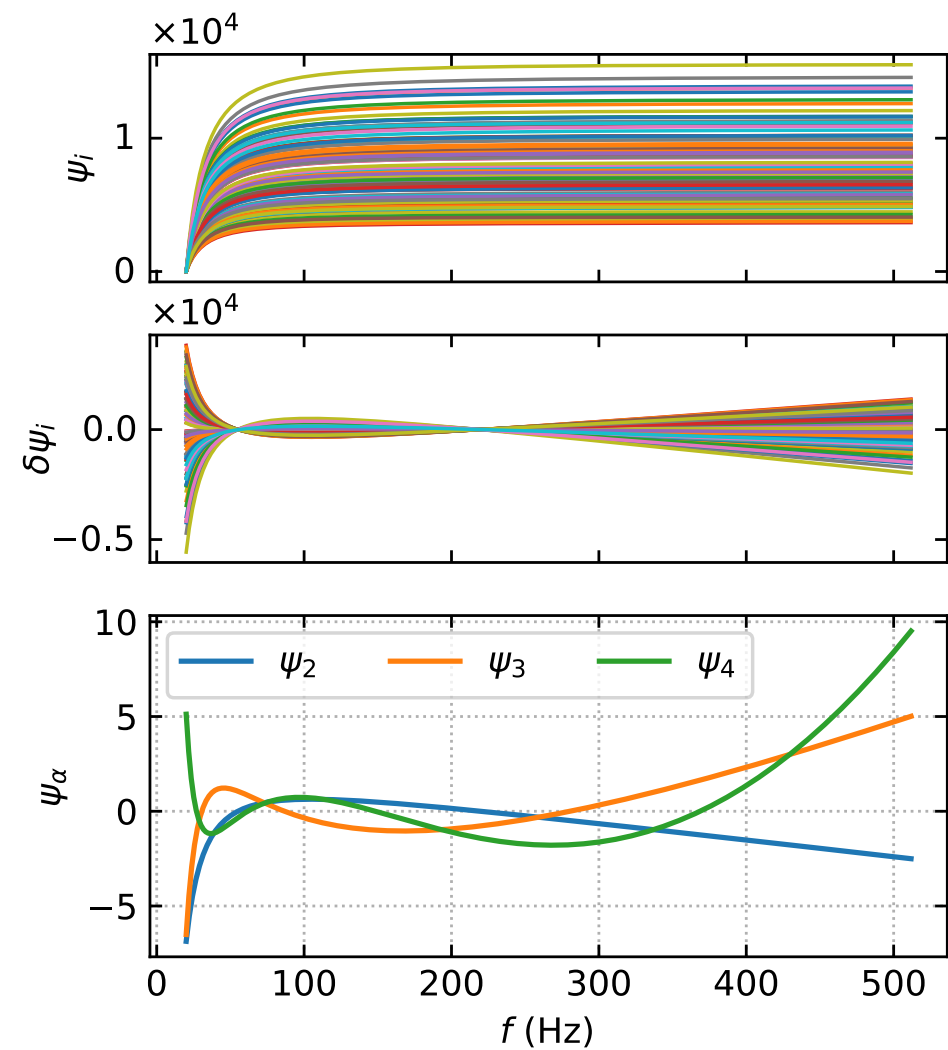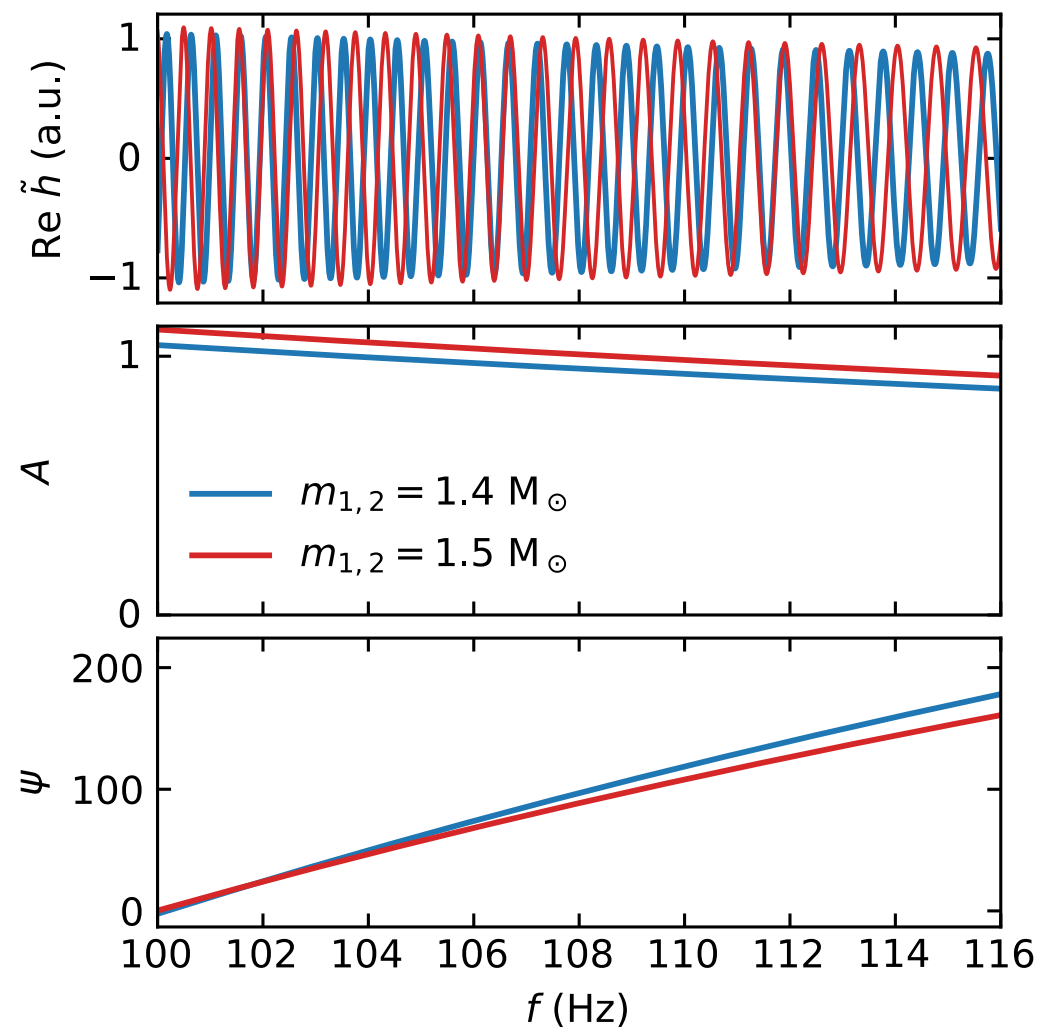


$$h(f; \boldsymbol{c}) = \overline{A}(f) \exp\left[i\left(\overline{\psi}(f) + \sum_\alpha c_\alpha \psi_\alpha(f)\right)\right]$$

# New template bank construction
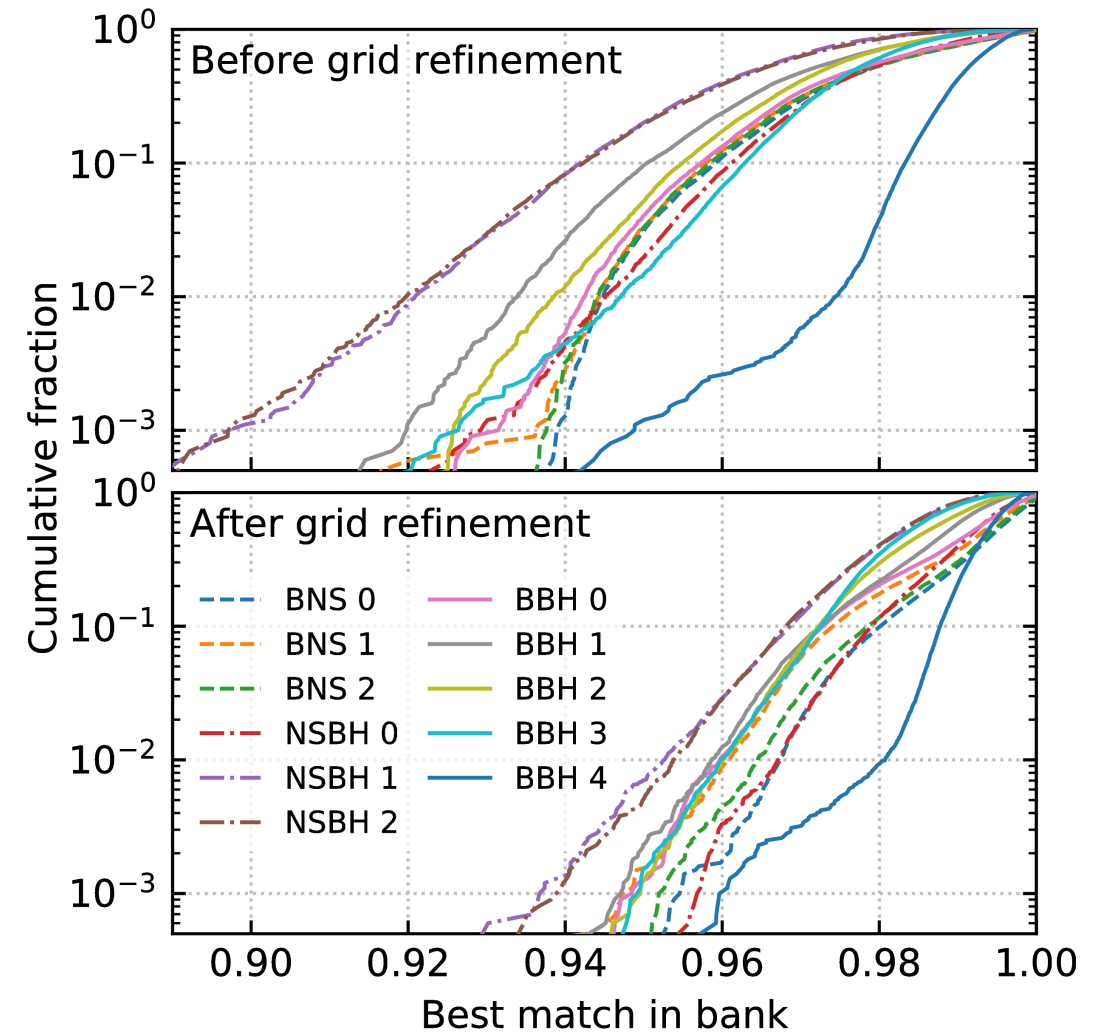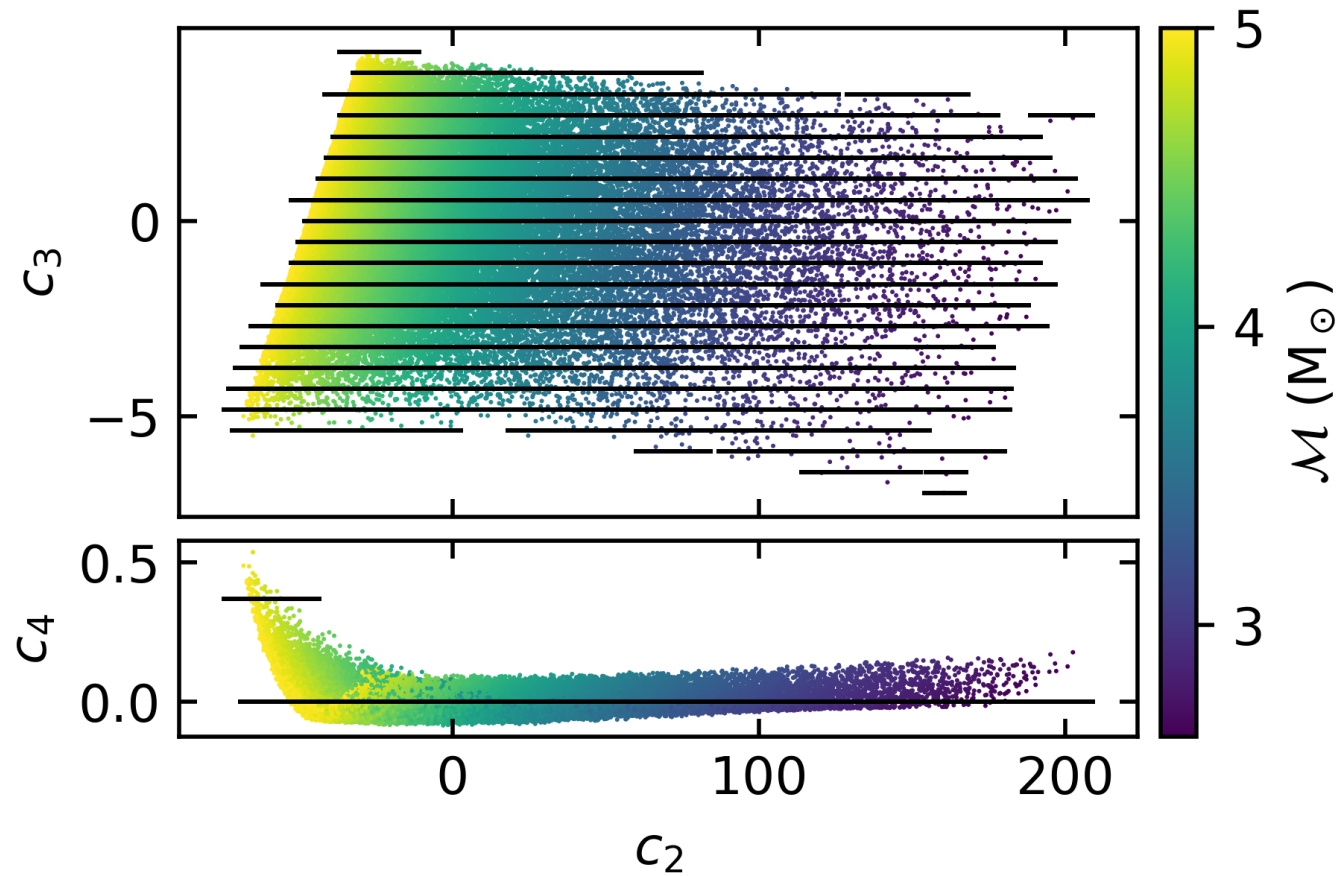


$$(h_i \mid h_j) := 4 \int_0^\infty \mathrm{d}f \, \frac{\tilde{h}_i(f)\tilde{h}_j^*(f)}{S_n(f)}, \qquad m_{ij} = \max_\tau \left| (h_i \mid h_j e^{i2\pi f \tau}) \right|;$$

$$d^2_{\boldsymbol{c},\boldsymbol{c}+\boldsymbol{\delta c}} := 1 - m(h(\boldsymbol{c}), h(\boldsymbol{c} + \boldsymbol{\delta c}))$$

$$= \frac{1}{2} \sum_\alpha \delta c_\alpha^2 + \mathcal{O}(\delta c^3).$$

# Basic estimate of the efficiency
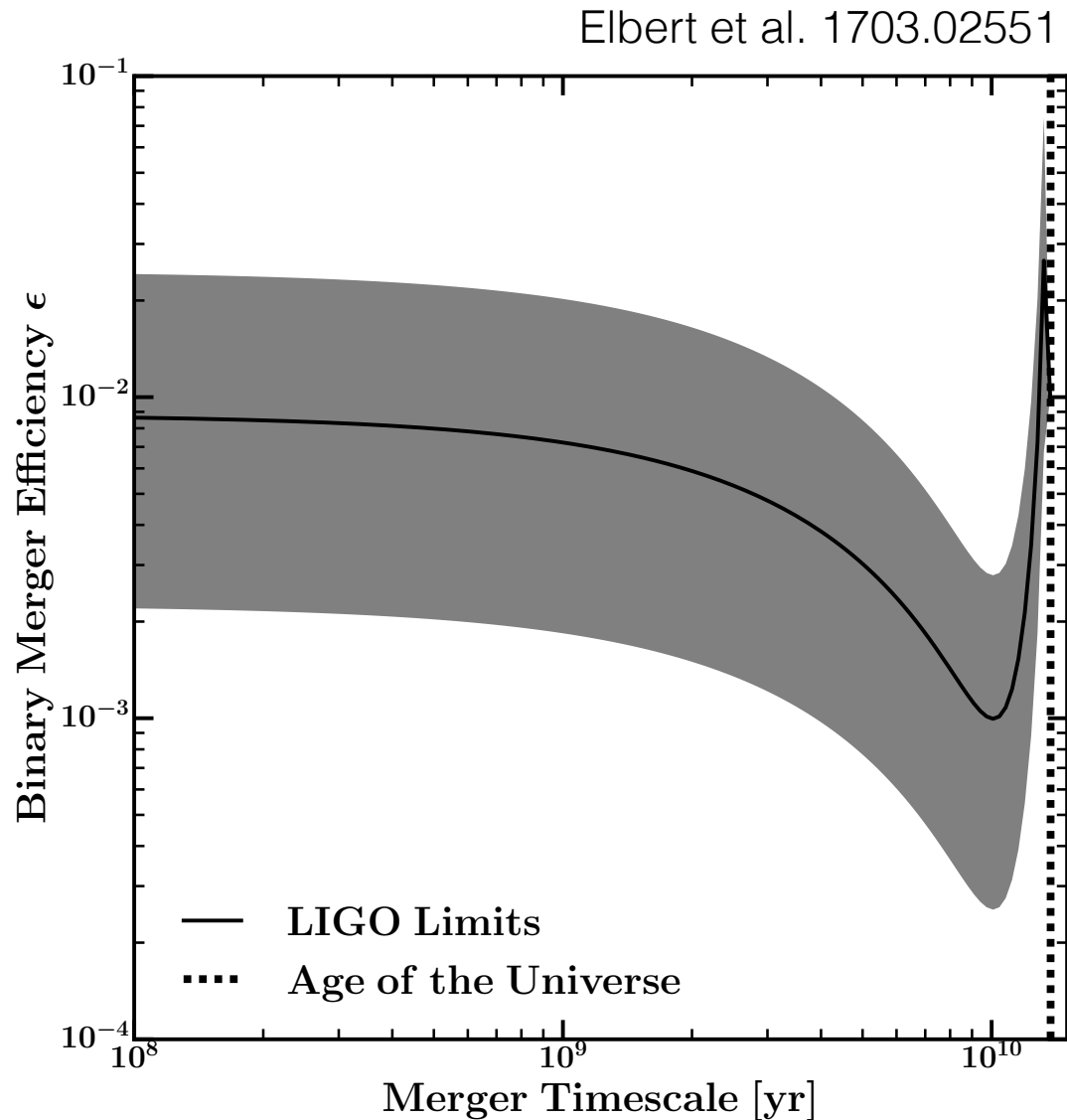


Elbert et al. 1703.02551

**Figure 6.** The shaded band shows the joint region of parameter space in binary efficiency $\epsilon$ and merger timescale $\tau$ that reproduces the merger rate density of black holes reported by Abbott et al. (2016b) for all black hole pairs more massive than $5M_\odot$.
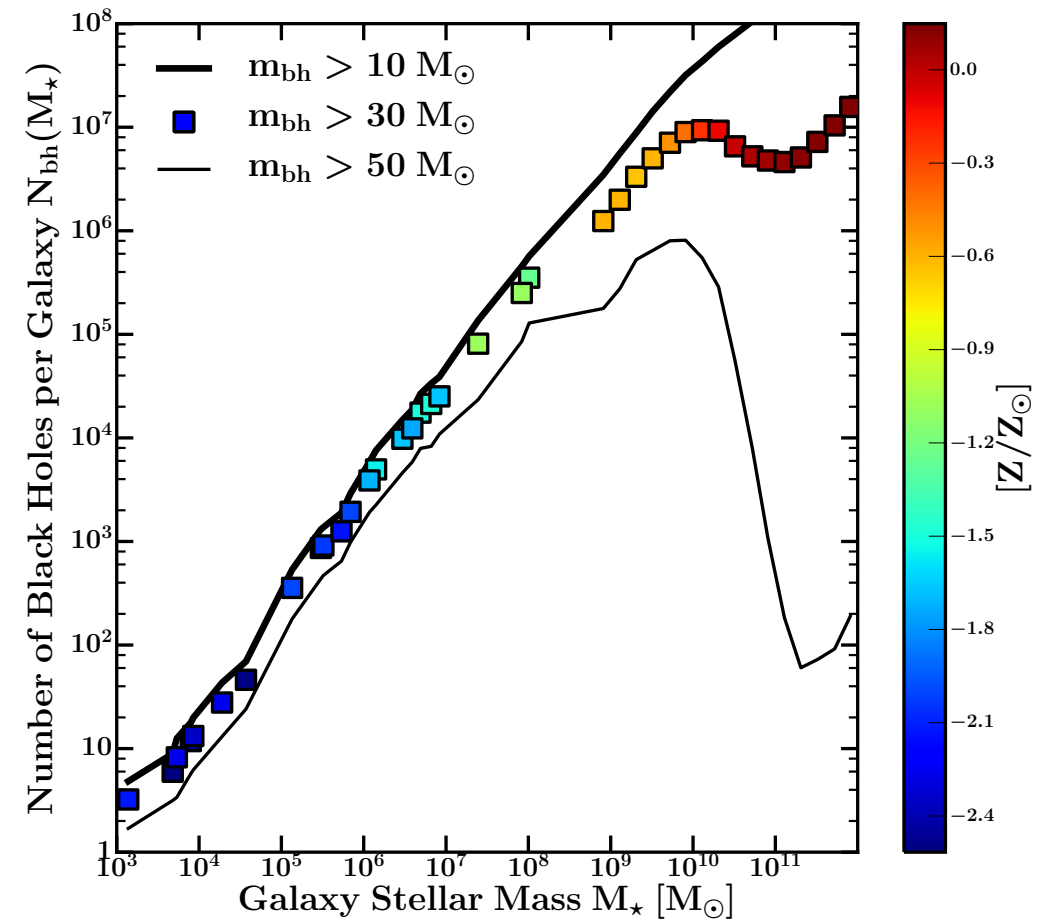
**Figure 2.** The number of remnant black holes per galaxy as a function of galaxy stellar mass, $N_{\rm bh}(M_\star)$, for black holes of mass mass $m_{\rm bh} > 10, 30,$ or $50 M_\odot$. The squares (corresponding to $30 M_\odot$ black holes) are color coded by the median galaxy metallicity. We see that for low metallicities, $N_{\rm bh} \propto M_\star$ in all cases. For the most massive black holes (30, 50 $M_\odot$), the relation breaks when galaxies become too metal rich to produce remnants in proportion to their total stellar mass – these black holes form only in the low-$Z$ tail of the distribution. At the highest stellar masses, the relations begin to rise again, when the relation between $M_\star$ and $Z$ becomes flat.
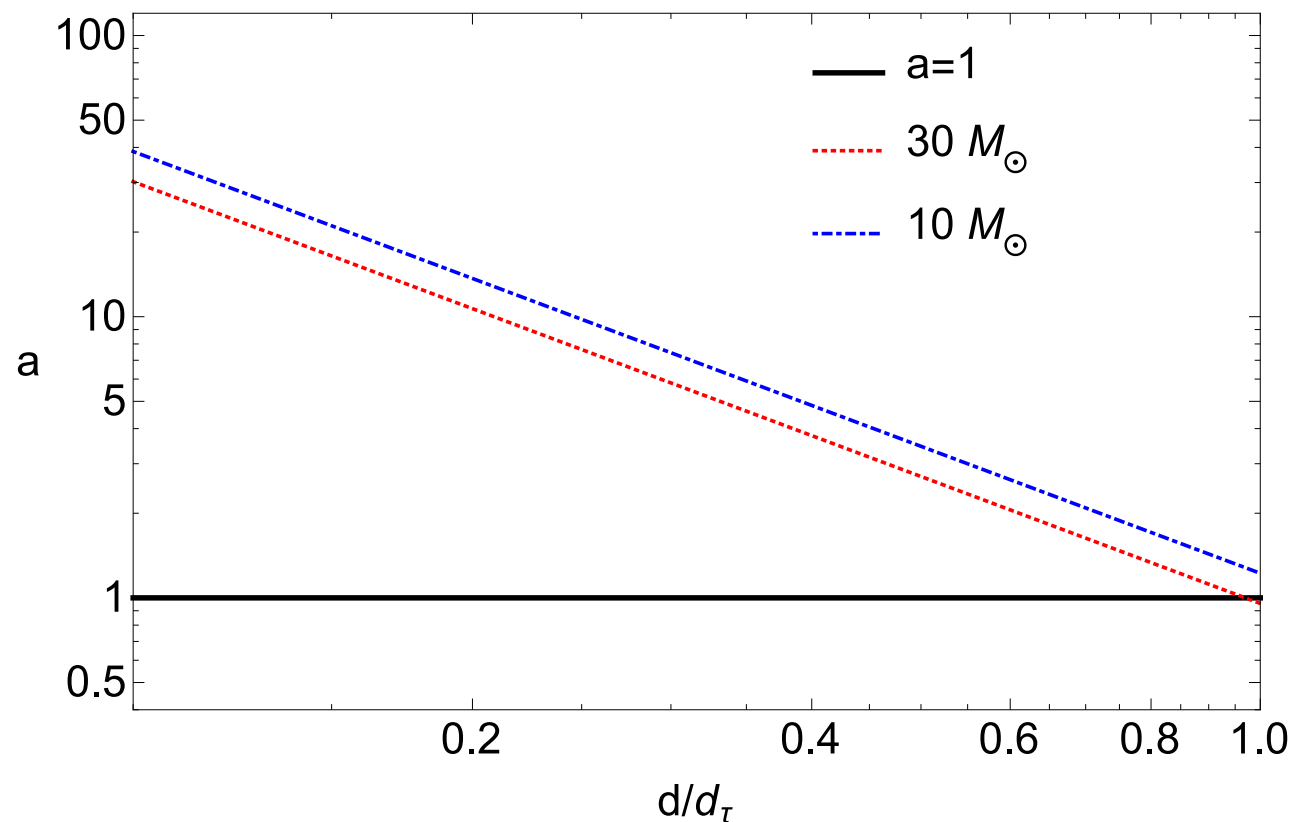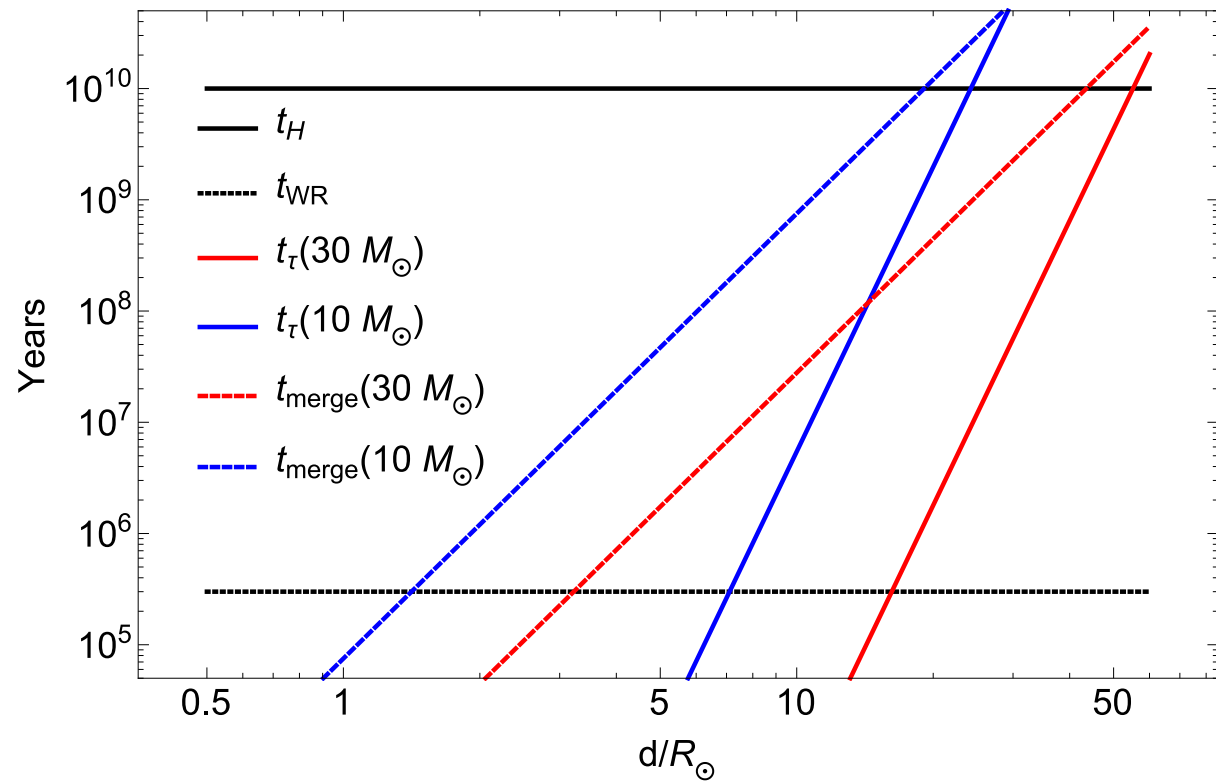
# The "classic" scenario
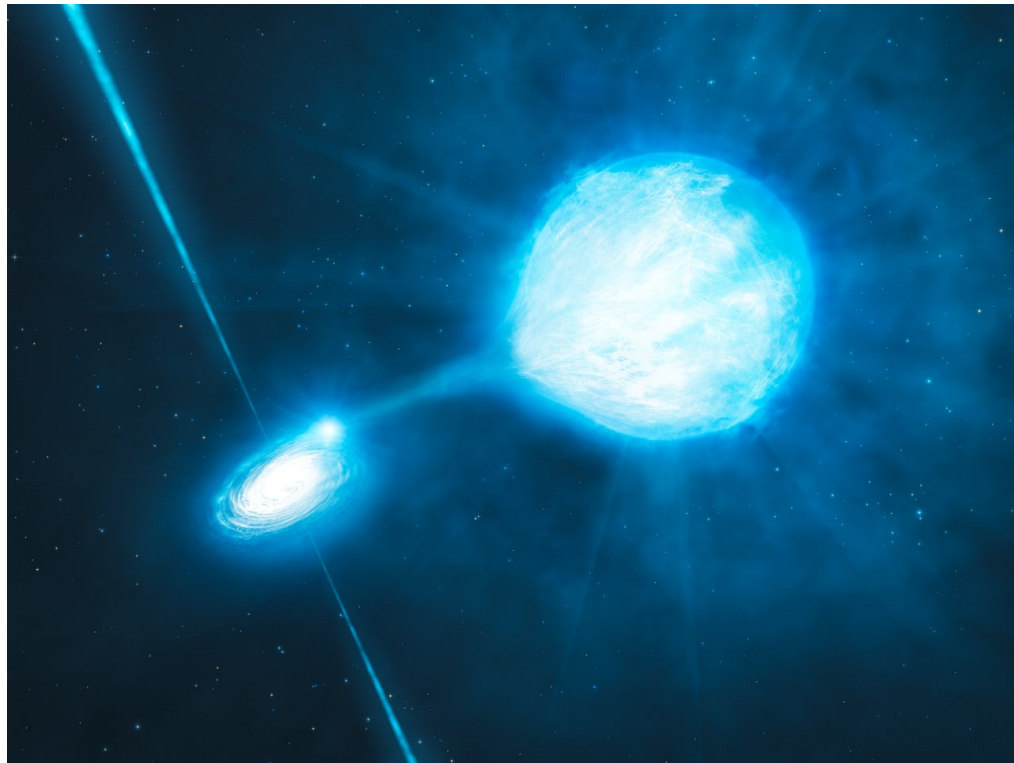


Within the large errors the estimate based on these two systems matches the LIGO rate

Bulik et al. ApJ 730:140 (2011)

|  | BH | WR Star | Period | D | $t_{merge}$ | Chirp Mass |
|---|---|---|---|---|---|---|
| IC 10 X1 | 23 M⊙ | 32 M⊙ | 1.4 days | 20 R⊙ | 3 Gyrs | 15-26 M⊙ |
| NGC 300 X1 | 20 M⊙ | 26 M⊙ | 1.4 days | 22 R⊙ | 3 Gyrs | 11-15 M⊙ |

LIGO Chirp masses from 9 M⊙(GW151226) to 28 M⊙(GW150914)

# Tides on the WR star



$$t_{\mathrm{merge}} = \frac{5}{512}\frac{c^5}{G^3 M^3}\frac{2q^2}{1+q}d^4.$$

$$
\begin{aligned}
a &= \frac{cJ}{GM^2} = \frac{cr_g^2 R^2}{GM}\left(\frac{1+q}{2q}\right)^{1/2}\left(\frac{2GM}{d^3}\right)^{1/2}\frac{\Omega}{\omega}\\
&\equiv a_{\mathrm{sync}}\frac{\Omega}{\omega},
\end{aligned}
$$

$$\dot{a} = \frac{a_{\mathrm{sync}}}{t_\tau}\left(1 - \frac{a}{a_{\mathrm{sync}}}\right)^{8/3} - \frac{a}{t_{\mathrm{wind}}},$$

$$t_\tau \approx 10^7 q^{-1/8}\left(\frac{1+q}{2q}\right)^{31/24}\left(\frac{t_{\mathrm{merge}}}{1\,\mathrm{Gyr}}\right)^{17/8}\,\mathrm{yr}.$$

$$t_{\mathrm{merge}} \lesssim 10^8 \text{ years} \quad (\text{for } t_\tau < \text{ lifetime})$$



| M | $d_\tau$ | $d_{\mathrm{merge}}$ |
|---|---|---|
| 10 $M_\odot$ | 7 $R_\odot$ | 19 $R_\odot$ |
| 20 $M_\odot$ | 12 $R_\odot$ | 32 $R_\odot$ |
| 30 $M_\odot$ | 16 $R_\odot$ | 44 $R_\odot$ |

**Table 1.** Separations corresponding to $t_\tau = 3\times 10^5$ yrs ($d_\tau$) and $t_{\mathrm{merge}} = 10^{10}$ yrs ($d_{\mathrm{merge}}$) for binaries composed of a WR and a BH of equal mass ($M$).

Kushnir, MZ, Kollmeier & Waldman 1605.03893,
MZ, Kushnir, Kollmeier 1702.00885